UNIVERSITA' DEGLI STUDI DI GENOVA
Dipartimento di Medicina Interna e Specialità Mediche (DIMI)

Dottorato di Ricerca in
"MEDICINA TRASLAZIONALE IN ONCOLOGIA ED EMATOLOGIA" (XXX ciclo)

Curriculum
"Genetica Oncologica e Patologia Molecolare"
Coordinatore: Prof. Alberto Ballestrero

Prognostic value of specific chromosome imbalances, mutation profile, and BAP1 expression in uveal melanoma

Relatore:
Prof. Silvia Viaggi

Candidata
Dott.ssa SERENA PATRONE

TABLE OF CONTENTS

Introduction

Materials and Methods

Uveal Melanoma

Uveal melanoma (UM) is the most frequent primary intraocular malignant tumor in adults and represents ~85% of ocular melanomas (OM) and ~5% of all melanomas (Singh et al, 2011). The mean age at the diagnosis is 60 year and its incidence in the past 30 years remained stable, with 5 new cases per million every year (Singh et al, 2011). The incidence rate in Europe ranges between less than two and more than eight per million population (Virgili et al, 2007).

To date, no environmental risk factor has been established, but a correlation between UM and different patient characteristics have been investigated.

The gender has been a debated and controversy topic. Bishop (Bishop et al, 2014) found a significantly lower incidence of UM in women than in men, evidence observed also in other work (McLaughlin et al, 2005). Other studies didn't demonstrate statistically significant differences in survival rate (Zloto et al, 2013; Nichols et al, 2016). A correlation between UM and ethnicity has been suggested from epidemiological studies: a major incidence rate of UM was observed in white Caucasian populations compared to Chinese, Korean, and Japanese populations (Nichols et al, 2016). Iris color, a phenotype correlated with ethnicity and geographical origin, is another characteristic evaluated in several studies. In a meta-analysis, Weis (Weis et al, 2006) showed a statistically significant relationship between light eye color and higher risk of UM.

UM is a cancer arising from melanocytes localized in the uveal tract, a pigment vascular layer situated in the eye between sclera and retina (Figure 1).

Figure 1. Structure of the eye with components of the uvea (iris, ciliary body and choroid)

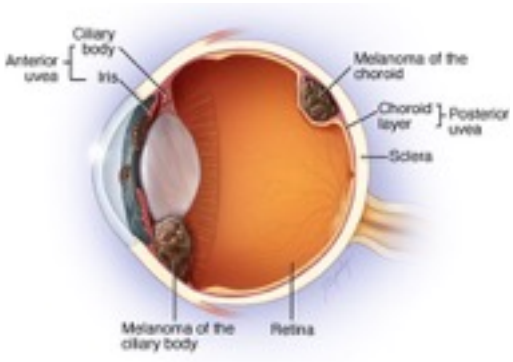

Melanoblast cells, derived from neural crest, are the precursors of uveal melanocytes. Approximately 85-90% of UM involve choroid, 7% ciliary body and 2% the iris (Chang et al, 1998).

Cytological classification is an important prognostic factor. Callender, in 1931 (Callender et al, 1931), first classified UM in six groups, with different prognosis according to the cell type: spindle type A, spindle type B, fascicular, epithelioid, mixed and necrotic. More recently, in a large retrospective study, McLean modified this classification and defined three cell types and relative melanomas, with different prognosis: spindle, epithelioid and mixed cells (McLean et al, 1983). Other clinical prognostic factors in UM include age, tumor size, extra ocular extension, tumor stage according to AJCC classification, mitotic activity, tumor infiltrating macrophages and lymphocytes, and specific chromosomal aberrations and gene expression profile (GEP). In Table 1 are summarized the clinical and histologic factors that have prognostic significance.

Despite the advances in eye-preserving therapies and/or early enucleation, the half of UM cases develops distant metastases, mostly in the liver (Diener-West et al, 2005). Other target sites of metastases are lung, bone, skin, lymph node and, with a rare frequency, central nervous system, kidney, spleen, colon, and pancreas. The uveal tract is highly vascularized, thus the hematogenous spread is the mechanism for metastatic dissemination, but the reason for the hepatic tropism is still not clear. The only confirmed evidence is that in liver of patients with UM, foci of non-proliferative and not vascularized micro metastasis have been identified.

Diagnostic Methods in Uveal Melanoma

The diagnosis of UM is based on clinical examination through ophthalmoscopy exam. Ancillary tests, such as color funds photography, fundus fluorescein angiography (FFA), ultrasonography (USG), indocyanine green angiography (ICGA), optical coherence topography (OCT) and fundus auto-fluorescence (FAF) are also used to help and to confirm the diagnosis. It was estimated that in 28-37% of UM cases there is a delay in UM diagnosis, due to the lack of detection during the first examination, especially in patients with a blind eye or with a dense cataract (Tarlan et al, 2016; Chattopadhyay et al, 2016). Many patients present distortion or loss of vision without pain, flashing, or flickering of light caused by retinal detachment. On the other hand, some patients are asymptomatic and the tumor is identified on routine ophthalmologic visit.

Clinical, histological and pathological features of uveal melanoma

- **Size of tumor**

The macroscopic pathological characteristics of UM depend on size and tumor localization. The Collaborative Ocular Melanoma Study Group (COMS report n °4,1997) has classified in small, medium and large the UM based on the tumor thickness: small tumors if major size is thicker than 10 mm, medium tumors if major size is 11-15 mm, and large tumors if major size exceeds 15mm. The classical appearance of UM is a brown, dome-shaped mass, but also may appear as mushroom- shaped or diffuse type. Considering the pigmentation, about 55% of tumors are pigmented, 15% are not pigmented, and 30% contains both pigmented and non-pigmented areas. It has been estimated that the risk of metastasis increases of 5% with each 1 mm increase tumor thickness.

Usually, small UM presents flat or dome-shaped type because sclera prevents the extra-scleral growth. According to its location, UM may occlude the choroid capillaries, and, with its enlargement, breaks Brunch's membrane and forms its pathognomonic mushroom shape (Ophthalmic Pathology, an Atlas-Textbook; McLean et al, 1983). Invasive tumors might also affect the lens. Scleral infiltration is estimated in 30% of UM (Figure 2). The American Joint Committee on Cancer (AJCC) (Edge et al, 2010) classified the tumor size in T categories (T1-T4), the lymph-node involvement in N categories (NX, N0, N1), and the presence of metastases in M categories (MX, M0, M1a, M1b, M1c). For

Figure 2. Posterior Uvea

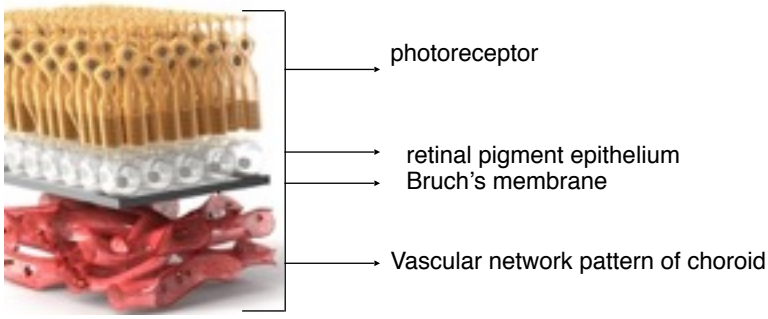

posterior UM, AJCC divided each T category in subgroups reflecting ciliary body involvement and extra-scleral extension: subgroups a, b, c, d, and e. Several studies (Simpson ER, et al 2015; Shields et al 2013) have shown the usefulness of this tumor classification to predict prognosis with an estimated survival rate of 100% for patients with T1 tumors, 90% for patients with T2 tumors, 50% with T3, T3a or T4 tumors.

The rate of UM progression was estimated as 15% for T1 tumors, 25% for T2 tumors, 50% for T3 tumors and 63% for T4 tumors (Edge et al, 2010).

• **Cytology and histopathology**

Among the histologic prognostic factors, UM cell type is an important feature correlated to bad prognosis. Callender first classified UM histologically in 1931 in six groups with different prognosis according to the cell type: spindle type A, spindle type B, fascicular, epithelioid, mixed and necrotic (Callender et al, 1931). This original classification was later modified in 1983 by Mclean (McLean et al, 1983). Two main cell types were described: spindle and epithelioid cells. Spindle cells show a cohesive pattern, plasma membrane not very evident, low cytoplasm with a fibrillary or granular appearance. In addition Callender (Callender et al, 1931) identified two subgroups of spindle cells based on nuclei morphology. The spindle cells subgroup A show elongated nuclei, nucleoli not evident and homogeneous chromatin. Instead, the spindle cells subgroup B shows round nuclei, less homogeneous chromatin and visible eosinophilic nucleoli.

Compared with spindle cells, the epithelioid cells are larger and more pleomorphic, showing a clear plasma membrane, extracellular space, large and round/oval nuclei, plentiful cytoplasm. In these cells, nuclear membrane is irregular, with introflexions and extroflexions. The chromatin is not

homogeneous and often it is localized to the periphery of the nucleus. Large and eosinophilic nucleoli are often present. Epithelioid cells show a high mitotic rate, greater than mitotic rate observed in spindle cells. The mitotic/proliferative index is important due to its correlation with a worst prognosis.

UM with epithelioid cell type are strongly associated with high metastasis and high mortality rates, whereas UM with spindle cells type are usually associated to a good prognosis. A limitation of Callender's classification is the too simplified classification.

Indeed, in UM, a spectrum between the spindle and epithelioid cell type exists and many tumors show a mixed cellular population. In addition, this classification is not very reproducible and standardized. Callender (Callender et al,1931) did not defined the percentage of epithelioid cells to define a UM as a mixed. COMS, through the analysis of 1527 UM samples, defined as epithelioid the tumors with a minimum percentage of 50% epithelioid cells. According to this classification, about 86% UM were with mixed cells and only 5% and 9% belonged to epithelioid-type and spindle-type, respectively (Edge et al, 2010).

• **Infiltrating cells**

Another prognostic feature in UM is the presence of infiltrating cells. McLean first suggested the importance of immune response in cancer progression (McLean et al, 1983). Later, de la Cruz (de la Cruz et al, 1990) studied the prognostic significance of infiltrating cells in UM: conversely to other cancer types, the researcher observed a correlation between infiltrating cells in lesion and reduced patient survival (de la Cruz et al, 1990; Vit et al,1983; Folberg et al, 1993).

• **Tumor vascularization**

Tumors require a blood supply to sustain their growth. Taking into account that cancer microcirculation plays a central role in the hematogenous dissemination of cancer cells, great attention has been directed on tumor angiogenesis, that tumors recruit both from the existing circulation and new angiogenesis (Folkman et al,1995).

In 2000, Folberg (Folberg et al, 2000) described in UM nine different patterns of vascularization: back-to-back closed loops, arcs (incompletely closed loops), arcs with branching, networks (networks were defined arbitrarily as at least three back-to-back closed PAS-positive loops), straight channels, straight

channels that cross-link, parallel, normal. PAS-positive loops and networks were also detected in hepatic metastases and in all secondary metastatic sites.

Folberg observed a higher survival rate if network, parallel and loops patterns were not present (Folberg et al, 2000). The histological detection of closed PAS-positive loops was associated with the presence of other histological features predictive of metastases: the presence of epithelioid melanoma cells by the modified Callender classification and mitotic figures.

Table 1. Clinical and histologic factors with prognostic significance

Clinical factors	Histologic factors
Patient age	Epithelioid cell type
Tumor thickness	High mitotic rate
Ciliary body involvement	Closed-loop vascular periodic acid-shift staining
Extraocular extension	Mean diameter of 10 largest nucleoli
Diffuse growth pattern	degree of pigmentation
Optic nerve involvement	inflammation
Large tumor basal diameter	vascular invasion
Ring melanoma	Tumore necrosis

Primary UM Treatment

The anatomical evidence of a tumor contained in the scleral shell and the absence of lymph vessels in the eye globe, justified for many years enucleation as the only therapeutic option. Nevertheless, McLean (McLean et al, 1995) reported a mortality peak during the first two years after enucleation, maybe due to tumor cells dissemination during the surgery. In the last 30 years, many conservative approaches have been developed, and now UM patients can be treated preserving anatomical and (often) functional integrity of affected eye.

Among the available eye-conserving therapies, there are photocoagulation, transpupillary thermotherapy and radiotherapy (Chattopadhyay et al, 2016).

- **Photocoagulation** is a method used in the past to treat small choroidal melanoma; today, tumors smaller than 3mm are treated with transpupillary thermotherapy (TTT).
- **Transpupillary thermotherapy** (TTT) or Laser therapy is a diode laser-based method used to treat melanomas smaller than 4 mm.
- **Radiotherapy** is the most common eye-conserving approach used by ocular oncologist. There are more possibilities for radiotherapy, including the application of radioactive plaques (brachytherapy), the external beam therapy (hadrontherapy or stereotactic radiotherapy), the gamma-knife. The brachytherapy is the most diffused radiotherapy approach and permits a high irradiation of the tumor without damaging the other tissues. It is performed by attaching the radioactive plaque to the tumor base surface (Figure 3). This plaque can emit gamma-ray by different radioactive source (^{125}Iodine or ^{106}Ruthenium). The plaque remains in this position until the whole radiation dose is emitted, in general 4-7 days for a total dose of 100 Gy. This method is used to treat UM < 9 mm thickness in case of iodine, and < 5mm thickness in case of Ruthenium as radioactive source. The hadrontherapy is the irradiation of a tumor with charged particles and permits the irradiation at a desired depth. This method is used to treat tumors until a 16 mm diameter and 8 mm of thickness. This type of radiotherapy is used to treat tumors up to 14 mm with a basal diameter up to 28 mm. The gamma knife therapy requires a complex equipment and adverse effects have been reported, i.e. radiation retinopathies and neo-vascular glaucomas (Tarlan et al, 2016).

Compared with the other eye-conserving primary treatments, proton beam is associated with the lowest overall risk of local tumor recurrence in UM.

Figure 3. Episcleral Plaque brachitherapy

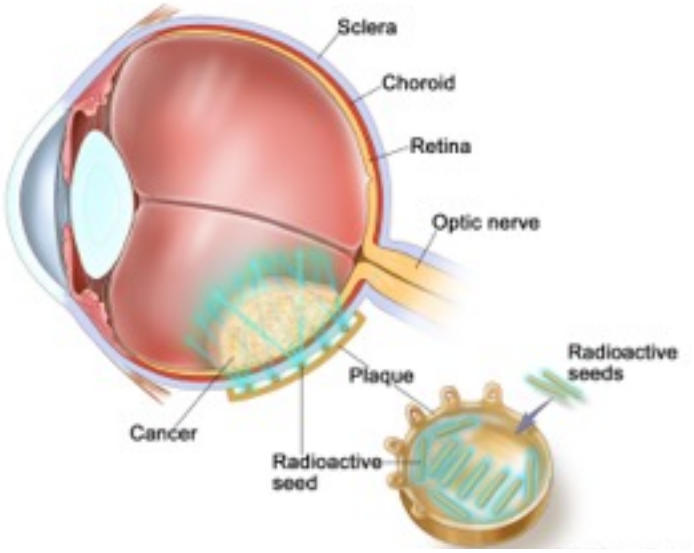

Nowadays, the enucleation is reserved for cases with the worst visual prognosis, such as patients with large uveal melanoma, with choroidal melanoma surrounding optic nerve or presenting hemorrhage. Local resection is an alternative treatment choice for patients with choroidal melanoma, which spares the eye and allows a detailed histopathological and cytogenetic analysis (Tarlan et al, 2016).

Metastatic disease and Adjuvant therapies

Despite successful local treatment, 25% and 34% of UM patients develop metastases within 5 and 10 years, respectively (Diener-West M, et al 2005). Liver is the first site of metastasis of UM (93%), followed by lungs (24%), and bones (16%) (Diener-West M, et al 2005). After metastastatic progression, survival time depends on metastasis type and localization, and, until now, there are no approved adjuvant therapies for UM. Several adjutant trials have been conducted in attempt to prevent metastatic disease in UM, but none of these demonstrated an increase of overall survival or benefit (Chattopadhyay et al, 2016).

• Liver-directed therapy

Since the liver is the first site of metastasis in UM, local treatments such as surgical resection, hepatic arterial infusion, hepatic artery embolization, and radio frequency ablation have been used.

Surgical resection of liver metastasis could increase patient's survival, but it is limited to single metastasis (Mariani et al, 2009).

A trial with 22 patients to test the hepatic arterial infusion of fotemustine showed an improving in progression free survival but it did not reach statistical significance (Ophtalmic Oncology Task Force, 2016). Isolated hepatic perfusion is another therapeutic option to treat metastatic, UM but it is an invasive operative procedure. More commonly used is chemoembolization, a treatment which combines hepatic artery embolization and infusion of chemotherapeutic agents, but also this therapeutic strategy did not showed significant benefits.

• Targeted therapy and Immunotherapy

Targeted therapies based on activated mitogen-activated protein kinase (MAPK) pathway by mutated Gnaq and Gna11 have been tested in several clinical trials but to date they did not provide meaningful responses in metastatic UM (Chattopadhyay et al,2016). Selumetinib, a MEK inhibitor, initially has shown promising clinical outcomes (Carvajal et al, 2014) but phase II trials did not confirmed the results.

Similarly to MAP kinase-targeted therapies, immune checkpoint blockade therapy through monoclonal antibodies directed to immunomodulatory receptors or ligands are objects of studies, but they show only limited activity in metastatic UM. Ipiluminab, a human antibody against CTLA-4, showed in a phase III study an increase in overall survival in melanoma patients, but until now only few data are available. Currently,the combination between ipiluminab and Nivolumab, a monoclonal human antibody against PD-1, is object of study (Chattopadhyay et al, 2016).

Cytogenetic of uveal melanoma

It is known that aneuploidy and chromosomal abnormalities were observed in many types of cancer. Since the detection of PH chromosome (Rowley et al, 1973), many specific cytogenetic changes have been identified and described in a variety of malignancies, and, overall, an high degree of aneuploidy and chromosomal aberrations were found in solid tumor, with a complex change in karyotype (Papadopoulos et al, 2002).

UM is different because it exhibits a relatively low degree of aneuploidy compared to skin melanoma and other cancers and it shows specific recurrent cytogenetic alterations involving the short arm of chromosome 1, and chromosomes 3, 6 and 8. The evidence of a low degree of chromosomal abnormalities, led to believe that these recurrent cytogenetic changes are more important to tumor progression rather than random events (Papadopoulos et al, 2002). By using standard karyotyping, fluorescence in situ hybridization, and comparative genomic hybridization techniques, non-random chromosomal aberrations occurring on chromosomes 3, 6 and 8 were detected (Prescher et al, 1992; McNamara et al, 1997; Bastian et al, 1998; Tschentscher et al, 2000; Hughes et al, 2005; Cross et al, 2006). More recently, many other alternative analysis methods were used to identify chromosomal alterations, such as microsatellite analysis (MSA), multiplex ligation-dependent probe amplification (MLPA), genome-wide single- nucleotide polymorphism array (Prescher et al, 1996; Parella et al, 2003; Hausler et al,2005; Damato et al, 2007; Damato et al, 2012) (Table 2). In these studies, it was reported that the risk of metastatic disease can be predicted by the presence of monosomy 3 and 8q gain.

Chromosome 3 monosomy is the most frequent cytogenetic aberration: in most cases one entire copy of chromosome 3 is lost, but partial deletions are possible. It was reported that preferential deletions include 3p25-25 and 3p11-14 chromosome bands and 3q arm (Chattopadhyay et al, 2016; Parella et al, 2003). Several studies have been performed with the purpose to identify tumor suppressor genes, whose inactivation due to partial deletion or chromosome 3 monosomy could correlate with a higher metastatic risk (Scholes et al, 2003; Killic et al, 2005). A relationship was found when Harbour et al (Harbour et al, 2012) reported in UM cases the presence of somatic mutations on BRCA1 Associated Protein 1 (BAP1) gene.

In a small percentage of UM (5-8%), chromosome 3 isodisomy is present: it occurs when a cell loses one of the chromosome 3 and there is a duplication of the remaining copy. The association of this chromosomal alteration and metastatic risk was demonstrated (Onken et al, 2007).

Loss of 8p occurs in about 25% of UM and gain of 8q occurs in almost 40% of UM. Chromosome 8q gain statistically associated to metastasis and it is also shown to be an independent predictor of survival (Sisley et al, 1997; Harbour et al, 2012). As for monosomy 3, gain of 8q correlates with ciliary body involvement (Sisley et al, 2000). Monosomy 3 and 8q gain often occur together (Aalto et al, 2001).

Chromosome 8q contains many potential oncogenes such as ASAP1, NBN, DDEF1, that are over-expressed in UM with poor prognosis (Ehlers et al, 2008). In addition, the 8q23-24 region, containing the oncogene MYC, it has been described (Parella et al, 2001) as amplified in about 30% of UM. In 8p, a potential tumor supressor gene, LZTS1, was reported (Onken et al, 2008a).

Other studies showed that often 8q gain occurs together with 8p loss, suggesting an isochromosome formation (Prescher et al, 1996).

Chromosome 1p alterations frequently occur in neural crest derived tumors, and are associated to advanced cancer or metastatic disease. In a small case series (29 subjects), Aalto (Aalto et al, 2001) reported a correlation between 1p loss and UM-related patient survival. Results from large UM patients' cohorts did not confirm 1p loss as an independent prognostic factor. These studies suggested instead that monosomy chromosome 3 together with 1p loss may correlate with poor prognosis (Kilik et al, 2005; Trolet et al, 2009; Cassoux et al, 2014).

Chromosome 6 anomalies (6p gain and/or 6q loss) are observed in about 25% of UM cases. Both 6p gain and 6q loss may occur in the same tumor, suggesting the formation of isochromosome 6p (Aalto et al, 2001; Harbour et al, 2012).

Since 6p gain was associated to good prognosis and low risk of metastasis, several authors supposed a protective effect of this chromosomal abnormality against metastatic progression (Prescher et al,1996; Damato et al, 2009). This aberration tends to occur in absence of monosomy 3, indicating a mutually exclusive pattern with this predictor of metastasis.

Loss of 6q, present in about 30% of UM, was associated with a poor prognosis (Elhers et al, 2008).

Table 2. Most commonly used techniques for genetic typing of UM

Techniques	Molecular basis	Quantitative dosage analysis	Degree of automation	Cost	Remarks
Karyotipe	Large gain, loss or alteration of chromosome	+	+	+	Low-resolution copy number variation, it cannot use with FFPE samples
FISH	Gain or loss of small number of chromosome segments labelled with specific probes	+	+	++	Low-resolution copy number variation, it can use with FFPE samples
CGH	Gain or loss of large number of chromosome segments labelled with specific probes	++	++	+++	C-CGH: low resolution;A-CGH high resolution copy number variation. Both can use with FFPE samples
MSA	Loss of heterozygosity of a small number of highly polymorphic DNA segments	++	++	+	Low-resolution copy number variation or LOH, it can use with FFPE samples
SNP	Loss of heterozygosity of a moderately polymorphic DNA segments	+	+++	++	High-resolution copy number variation or LOH, it can use with FFPE samples
MLPA	Gain or loss of multiple chromosome segments	+++	+++	++	High-resolution copy number variation. 50 targets in one reaction. It can use with FFPE samples
UM-GEP (PCR based)	Simultaneous measurement of mRNA expression of multiple genes	Not applicable	+++	++++	Gene expression. Fresh samples preferred

Abbreviations: CGH, comparative genomic hybridisation; MSA, microsatellite analysis; MLPA multiplex ligation- dependent probe amplification; FFPE, formalin-fixed paraffin embedded material; FISH, fluorescence in situ hybridization; LOH, loss of heterozygosity; SNP, single-nucleotide polymorphism; UM-GEP, uveal melanoma gene expression profiling (Coupland et al,2012).

Gene Expression Profile

Data of gene expression profiles in UM samples were reported in different studies (Tschentscher et al, 2003; Onken et al, 2005; Onken et al, 2006; Onken et al, 2006; van Gils et al, 2008).

In 2012, a prospective multicenter study assessed the prognostic accuracy of a 15-gene gene expression profile assay for UM (Tschentscher et al, 2003; Onken et al, 2004; Van Gils et al, 2008; Onken et al, 2006). Based on gene expression profile (GEP) analysis, these authors showed that UM are clustered into two classes strongly correlated with metastatic risk: class 1 UM have a low risk of metastasis and class 2 UM have a high risk of metastasis.

Genes mainly implicated in this classification were involved in cell communication, development, cell growth, cell motility, cell death and immune response (Onken et al, 2005; Onken et al, 2008). Using bioinformatic analyses, genes that were up-regulated and down-regulated in class 1 versus class 2 UM were compared. Other studies showed that the genes expressed in class 1 UM were similar to those in normal uveal melanocytes and cells committed to the neural crest lineage, whereas the genes expressed in class 2 UM were similar to those in primitive stem-like cells

Class 1 tumors were UM characterized by chromosome 3 disomy, chromosome 6p gain and a low risk of metastasis.

In a later study (Harbour et al, 2010) , it has been reported that a depletion of Bap1 protein in UM class 1 culture cells induces a change to epithelial-like phenotype and also a change in a GEP similar to class 2. This evidence suggested the role of Bap1 in maintaining the melanocyte phenotype and in malignant progression.

Among class 1 UM, PRAME mRNA expression was identified as the most significant independent biomarker of metastasis risk (Field et al, 2016). PRAME mRNA expression was reported in association with larger tumor diameter, SF3B1 mutations and chromosome copy number changes such as gain of 1q, 6p, 8q, 9q, loss of 6q and 11q.

PRAME expression is a marker of poor prognosis in many cancers and recently was found as a biomarker for differentiating benign nevi from melanoma (Epping et al, 2006; Clarke et al, 2015). PRAME may promote tumor progression by inhibiting differentiation, growth arrest, and apoptosis induced by

Figure 4. **Molecular hypothesis of tumor progression in uveal melanoma and role of PRAME mRNA increased expression** (Field et al,2016).

Figure 5. Flow diagram that show how prognostic and predictive testing in uveal melanoma can guide patient care.

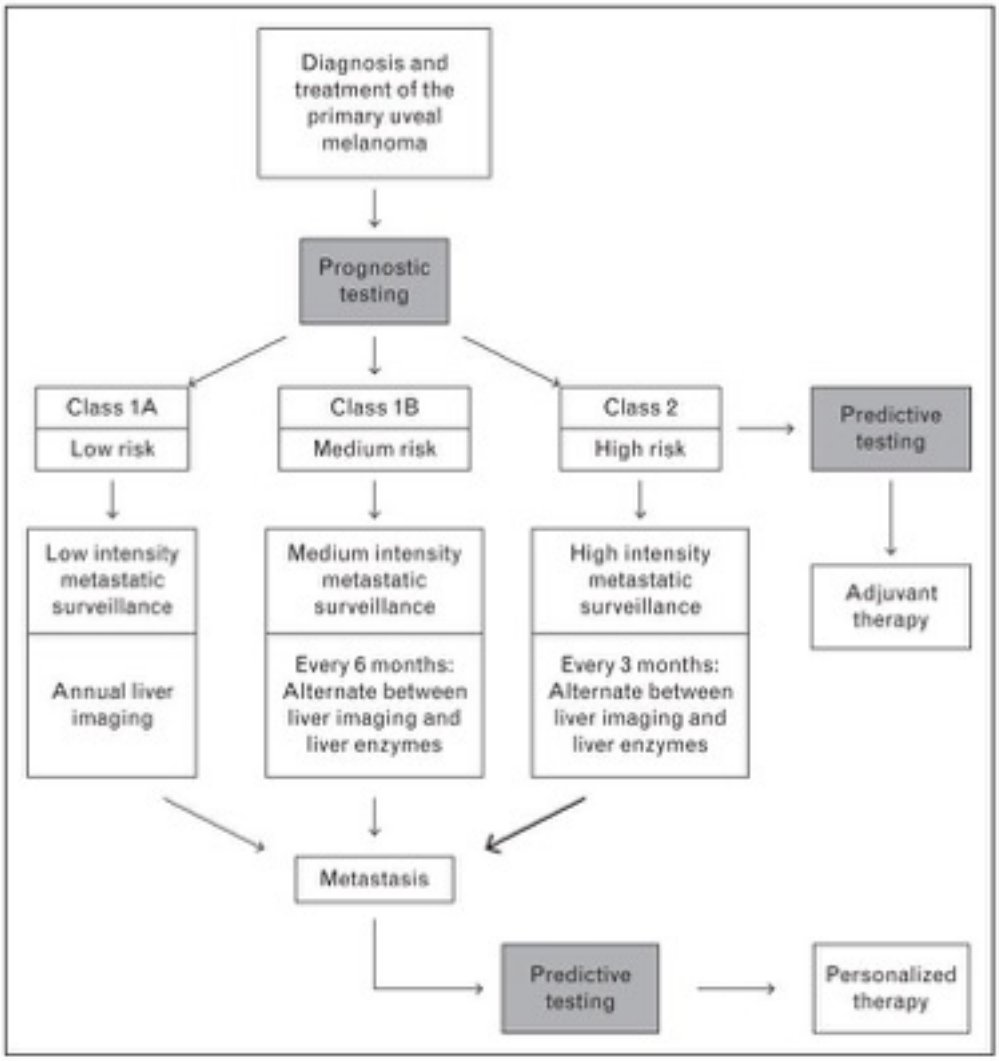

retinoic acid signaling (Epping et al, 2006). More specifically, an increased PRAME mRNA expression in class 1 UM is associated with transcriptional up-regulation of key genes (many contained in chromosome 1q an 6p) involved in chromosome maintenance and stability (Figure 4).

In class 2 UM has been observed a down-regulation of genes involved in melanocytes differentiation, in lineage specification in neural crest cells, genes regulator of Wnt signaling (i.e. EDNRB and CTNNB1), and genes encoding in melanin biosynthesis (i.e. DCT, SILV, and TYR). Conversely, genes involved in epithelial adhesion (i.e. CDH1), in basal membrane synthesis (i.e. TPBG, LAMC1, and COL18A1), and basal membrane interaction (MAFC1, and SPARC) have been observed up-regulated (Onken et al, 2006).

More recently, it has been suggested that this dichotomous model may be too simple and the concept of UM clonal heterogeneity was introduced (Harbour et al, 2012). Indeed, Damato et al (Damato et al, 2010) identified in a large UM series a wide difference in the prevalence of chromosomal abnormalities, suggesting that some alterations may occur earlier than other. Therefore, more clones of malignant melanocytes harboring different chromosomal aberrations could evolve and co-exist within a single UM and one/some of these clones could have the potential to override the others.

The predictive information provided from gene expression profiling are accessible by direct sampling of primary or metastatic tumor tissue or also from DNA of circulating tumor cells. Thus, mutational profiling may provide valuable predictive informations to define the better therapy for each patients and may guide patient care (Figure 5) (Inamdar et al, 2010).

Mutational Profiling

The mitogen-activated protein kinase (MAPK) pathway is commonly altered in many human cancers (Inamdar et al, 2010). In particular, MAPK pathway plays an important role in the development of cutaneous melanoma (CM) through mutations in oncogenes such as RAS and B-RAF or in tumor suppressor genes such as PTEN and CDKN2A. In UM, alterations in MAPK pathway have been reported in GNAQ and GNA11, but mutations in RAS, B-RAF, PTEN or CDKN2A genes were rare (Figure 6) (Janssen et al, 2008; Maat et al, 2008). These findings suggested that other molecular events are involved in UM pathogenesis.

Recent data (Martin et al, 2013; Harbour et al, 2013) showed that UM has relatively few recurring mutations, indicating a low genetic complexity and a low genomic instability than other cancers. Several driver mutations supporting UM initiation, progression and metastasis development have been identified from sequencing of primary tumor samples and confirmed by several studies (Amaro et al, 2017). UM driver mutations have been described in the following genes: GNAQ, GNA11, PLCB4 and CYSLTR2, and metastasis driver mutations in BAP1, SF3B1, and EIF1AX.

Figure 6. MAPK signaling pathway

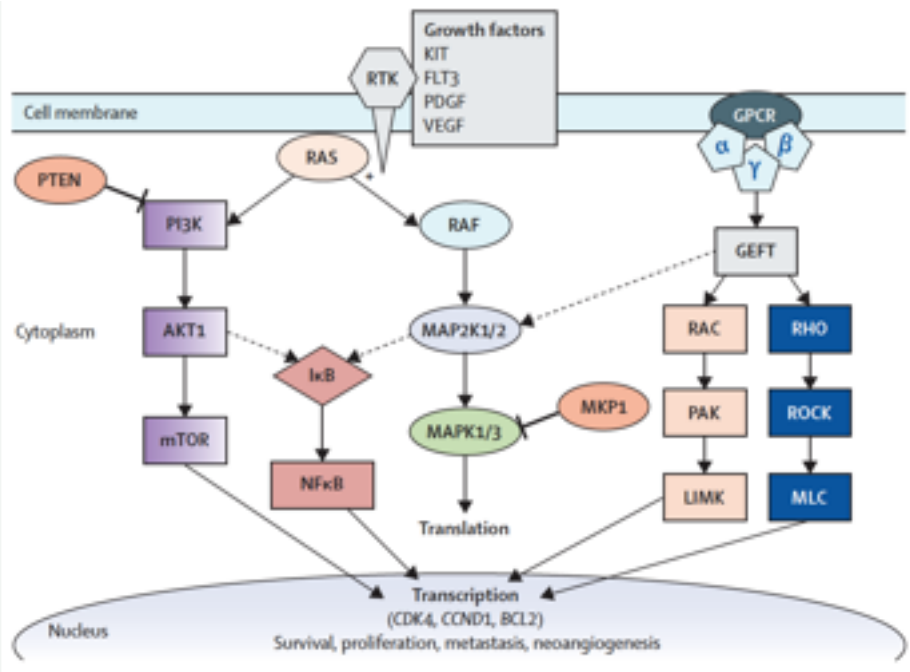

MAP2K1 and MAP2K2 are also known as MEK1 and MEK2, and MAPK1 and MAPK3 are also known as ERK2 and ERK1, respectively. AKT1, protein kinase B. ERK, extracellular-signal-regulated kinase. FLT3, fms-related tyrosine kinase 3. GEFT= RAC/CDC42 exchange factor. GPCR=G protein-coupled receptor. LIMK= LIM domain kinase. MAPK= mitogen-activated protein kinase. MEK= MAPK/ERK kinase. MKP1=MAPK phosphatase 1. MLC= myosin light chain. mTOR=mechanistic target of rapamycin. PAK= p21 protein (CDC42/RAC)-activated kinase. PDGF= platelet-derived growth factor. PI3K= phosphoinositide 3 kinase. PTEN=phosphatase and tensin homologue. RAC=RAS-related C3 botulinum toxin substrate. RAF= rapidly accelerated fibrosarcoma. RAS= rat sarcoma. RHO= RAS homologue. ROCK= Rho-associated, coiled-coil containing protein kinase. RTK= receptor tyrosine kinase. VEGF= vascular endothelial growth factor (Romano et al, 2011).

Guanine Nucleotide-binding Protein subunit α-Q (GNAQ) and Guanine Nucleotide-binding Protein subunit α-11 (GNA11)

GNAQ and GNA11 are two genes localized on 9q21.2 and on 19p13.3, respectively, and both contain 7 exons. Both genes encode for Gα subunits of heterotrimeric Gq protein that activates the G protein signaling cascade via inositol-3-phosfphate, dyalglicerol and cyclic AMP leading to the stimulation of MAP kinases, protein kinase B (Akt) and protein kinase C (PKC). Gnaq protein is a 42142 Da protein and Gna11 is 42123 Da protein. Both proteins contain 359 aminoacids. Heterotrimeric G proteins are membrane bound GTPases that are linked to 7-TM receptors. Each G protein contains an α-, β- and γ-subunit and it is bound to GDP in the 'off' state. Ligand binding causes a receptor conformational change, detaching the G protein and switching it 'on'. Normal activation of Gq leads to a GTPase activity intrinsic to Gα subunits (Figure 7).

The mutations in these two genes are mutually exclusive and they are considered the major driver mutations in UM, indeed they are found in about 80% of UM samples (Onken et al, 2008).

Mutations in GNAQ and GNA11 are found in all stages of UM and benign nevi, and this evidence suggests that GNAQ and GNA11 mutations are an early events in UM tumorigenesis but they are not sufficient for tumor progression (Xu et al, 2014). In UM, mutations in GNAQ and GNA11 genes the mutations are missense mutations at two hotspots, Q209 and R183 (Figure 8).

Figure 7. Schematic of canonical GPCR and heterotrimeric G-protein signaling.

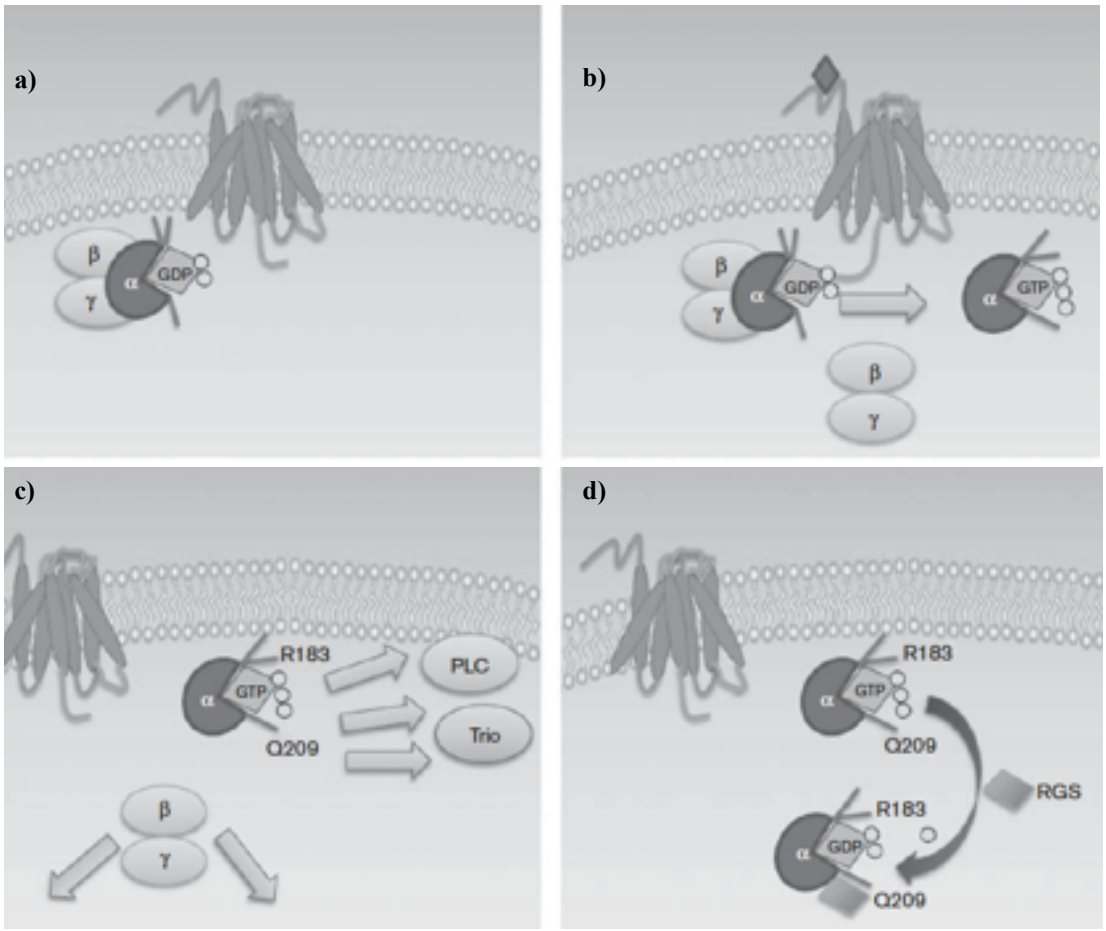

a) In the GDP-bound state, Gα is inactive and bound to Gβγ near the plasma membrane.

b) Upon ligand binding, a conformational change catalyzes GDP exchange for GTP, which alters the conformation of switch I, II, and III regions in red and dissociates Gα from Gβγ.

c) Active Gα and Gβγ signal downstream to multiple effectors.

d) The intrinsic GTPase activity of Gα is accelerated by regulator of G protein signaling (RGS) proteins, which catalyze the hydrolysis of GTP to GDP by the Q209 residue of GNAQ/GNA11. An adjacent R183 residue assists in hydrolysis without RGS binding. This returns the trimer to its membrane-bound, inactive state. GPCR, G-proteincoupled receptor; PLC, phospholipase C. (Shoushtari et al,2014).

There are at least five known variants at residue Q209, but $GNAQ^{Q209L}$ and $GNAQ^{Q209P}$ are the most frequent. Both aminoacidic substitutions disable GTPase activity and lead to constitutive activation of MAP kinase pathway.

Figure 8. Schematic representation of Gnaq and Gna11 protein.

GNAQ and GNA11 genes encode for closely related Gq-α subunits that consist of helical and catalytic GTPase domains.

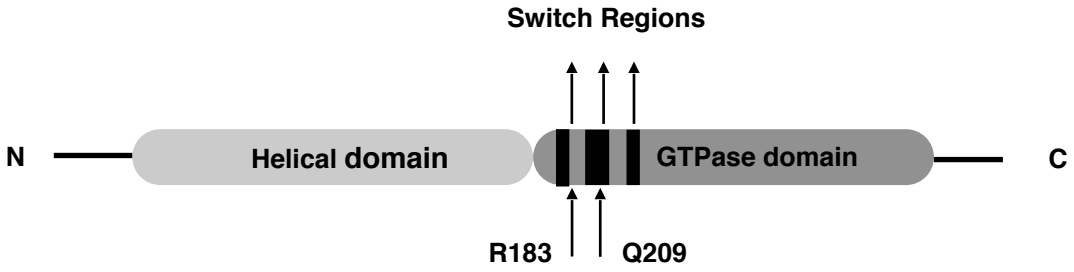

Recently it has been shown that mutations in GNAQ/GNA11 genes activate the transcription factor complex YAP/TAZ in a pathway independent to HIPPO, a regulator of organ size involved in many tumors (Yu et al, 2014; Feng et al, 2014; Feng et al, 2014) (Figure 9). GPCR is involved in cell proliferation and stimulate the activity of transcripional co-activator YAP, a component of Hippo signaling pathway. YAP/TAZ factors are active in proliferating cells, and the cell confluence triggers the activation of LATS1/LATS2 kinase, Hippo pathway inhibitors. O'Hayre (O'Hayre et al, 2014) indicated that mutations in gene encoding Gαq activate YAP by a pathway initiated upon actin polymerzation rather than by the inhibition Hyppo pathway.

Figure 9. Schematic representation of Hippo-dependent and Hippo-independent pathways resulting in YAP activation by the GNAQ and GNA11 oncogene in uveal melanoma (Feng et al, 2014).

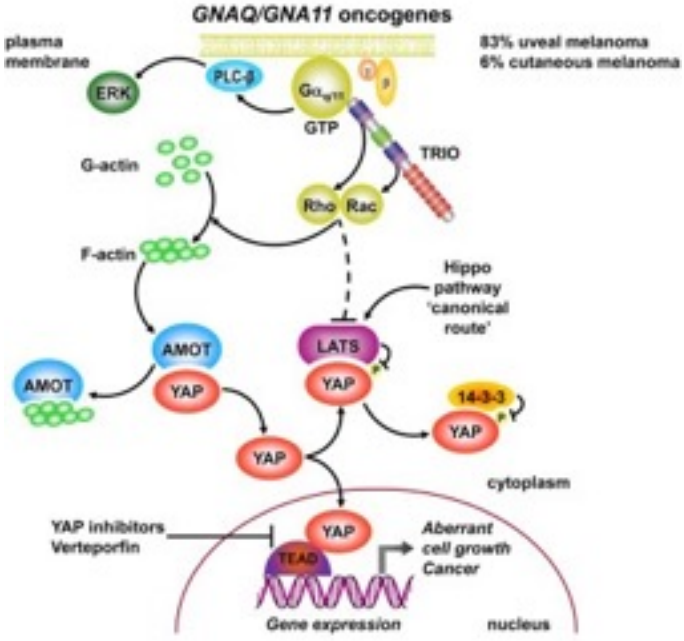

BRCA1- associated protein 1 (BAP1)

BAP1 gene maps on chromosome 3p21.1, consists of 17 exons and codifies for a 90 kDA protein (729 amino acids), a nuclear deubiquitinating enzyme (DUB). Bap1 protein is composed of a N-terminal ubiquitin carboxyl hydrolase domain (UHC), a host cell factor 1 (HCF1), binding domain (HBM) in the middle portion, and a C-terminal domain (CTD) with a coiled- coil motif for interaction with ASXL1/2. Two nuclear localization signals (NLS) and other binding regions are localized in C-terminal (Figure 10).

Figure 10. Schematic representation of BRCA1 -associated protein 1 (BAP1).

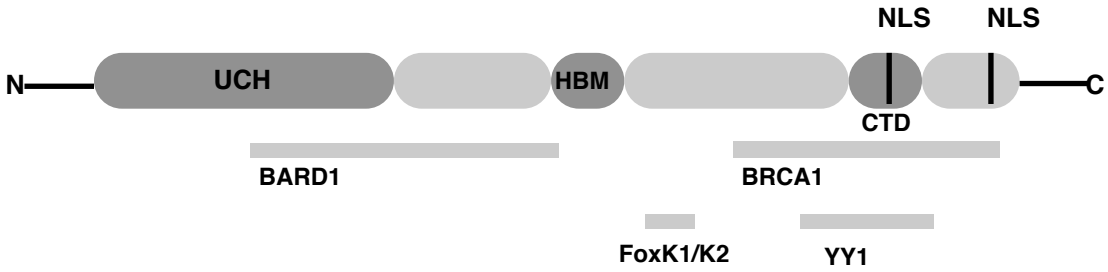

BAP1 include 721 amino acids: ubiquitin carboxyl hydrolase domain (UCH) 1-250, BARD1 binding region 182-365, HBM-HCF1 binding domain 365-385, FoxK1/K2 binding region 477-526, BRCA1 binding region 596-721,c-terminal domain (CDT)-ASXL1/2 binding domain 635-693, Ying Yang (YY1) binding region 642-686, nuclear location signals (NLS) 656-661 and 717-722.

- **Bap1 functions**

Bap1 deubiquitinase activity is involved in key cellular pathways, including cell cycle control, cellular differentiation, transcription regulation and DNA damage repair (Figure 11).

- Bap1 regulates through de-ubiquitination of a lysine, the transcription regulator factor HCF1 activity. Through HCF1, Bap1 modulates chromatin architecture by recruiting histone-modifying complexes, and also by activation of transcription factors members of E2F family. Through E2F factors, Bap1 controls G1/S transition. In case of Bap1 protein loss, an accumulation of HCF1 occurs, promoting transition from G1 to S cell-cycle phase (Figure 11) (Murali et al, 2013).

Figure 11. Schematic representation of BAP1 functions
(Bhattacharya et al,2015)**.**

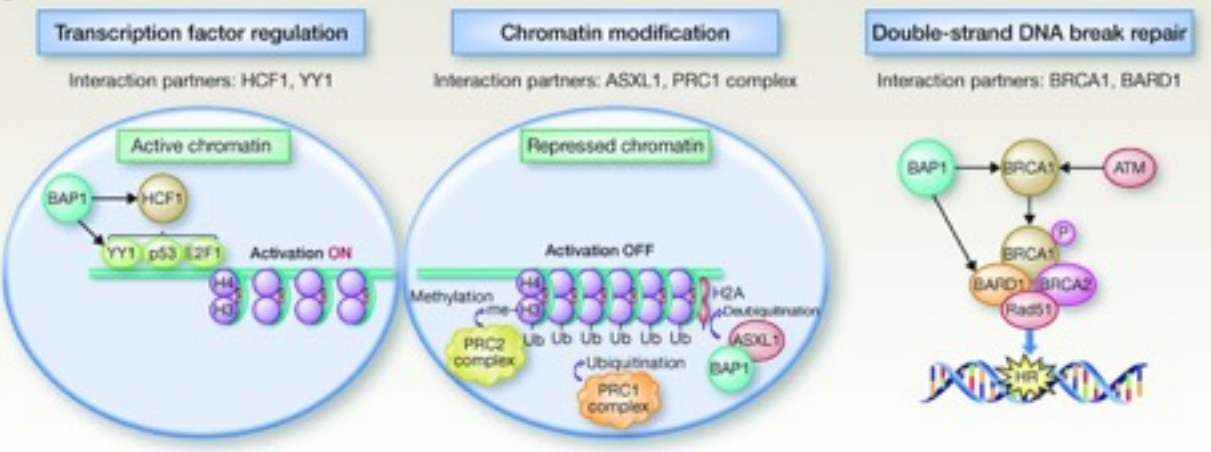

Left: role of BAP1 in transcription factor regulation. HCF1 is a major binding partner of BAP1 by mass spectrum analysis. HCF interacts with specific transcription factors, including OCT1, E2F1, Kox20, Sp1 and GA-binding protein. HCF1 also is associated to many chromatin methyltransferases, chromatin acetyltransferase and deacetylases.

Middle: role of BAP1 in chromatin modifications. The trimethylation of lysine 27 of histone H3 is mediated by the histone methyltransferase EZH1/2, component of polycomb repressive complex 2 (PRC2).

Right: Possible role of BAP1 in DNA repair . BAP1 bind BRCA1 and BARD1,which have important roles in double strand DNA repair process.

Figure 12. Model of BAP1 as a co-regulator of E2F-mediated activation of S phase genes transcription (Pan et al, 2015)**.**

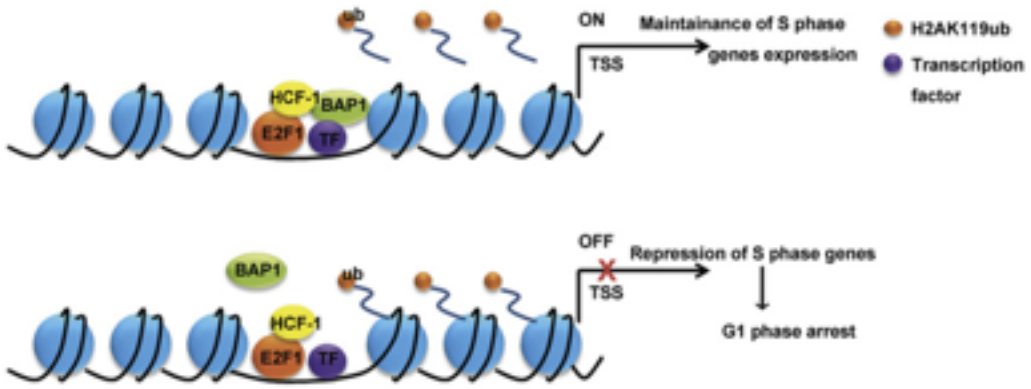

- Bap1 protein forms a ternary complex with HCF1 and transcription factor Ying Yang (YY1), which controls cellular proliferation. This complex is recruited to activate Cytochrome C Oxidase Subunit 7C (COX7C), a component ofmitochondrial respiratory chain. YY1 can works both as inhibitor or as activator of COX7C promoter, depending on the presence/absence of bound toHCF1-BAP1 complex (Daou et al, 2015).
- Bap1 is part of a ternary protein complex interacting with HCF1 and forkhead transcription factors FoxK1/K2. This complex controls cell proliferation and cell cycle. In case of Bap1 loss, it follows an up-regulation of FoxK2 target genes.
- Through the interaction with ASXL1/2, Bap1 forms the polycomb group repressive deubiquitinase complex (PR-DUB) (Pan et al, 2015). This important complex has effect on transcriptional regulators of stem cell pluripotency, embryonic development, self-renewal and cell differentiation. The polycomb-repressive complex works through histones hubiquitination and it follows gene silencing. In case of BAP1 loss, an up-regulation of polycomb target genes occur (Pan et al, 2015). More specifically, mutations targeting BAP1-ASXL1/2 interaction, led to loss of deubiquitination activity with an increased histone H2A ubiquitination, deregulation of cell cycle progression and cellular senescence (Pan et al, 2015) (Figure 17).
- Bap1 is involved in DNA damage signaling and repair through interaction with several proteins such as the BRCA1/BARD1 heterodimer: BAP1 binds and deubiquitinates BARD1 protein and consequently modulates the E3 ligase activity of the same complex (Murali et al, 2013; Daou et al, 2015) (Figure 17).

BAP1 is a tumor suppressor gene, and mutations in both alleles are necessary to inactivate its functions, according to “two hits” Knudson model. BAP1 mutations occur almost exclusively in tumors with monosomy 3 (corresponding to class 2 UM) and they are strongly associated with metastasizing UM. BAP1 mutations rarely occur in UM with disomy 3 (corresponding to class 1 UM), which typically shows mutation in SF3B1 and/or EIF1AX (Harbour et al, 2010).

BAP1 gene mutations are found in many tumors, such as small cell and non-small cell lung cancers, renal cell carcinoma, breast carcinoma and mesothelioma (Peña-Llopis et al, 2012; Ladanyi et al, 2012; Carbone et al, 2013; Murali et al, 2013). Harbour et al 2010 first described inactivating somatic mutations in BAP1 gene in 26 out of 31 (84%) metastasizing UM tumors, suggesting a connection between BAP1 inactivation and UM metastasis, hypothesis reinforced by multiple independent studies (Harbour et al, 2010; Luchini et al, 2016). For BAP1 mutations, all the different mutation types have been reported: deletions, insertions and base substitutions leading to nonsense, frame-shift, missense or synonymous mutations. It is possible to suppose that the different consequences on protein functionality depend on the mutation type and the region involved. For example, frameshift mutations may lead to abnormal mRNAs, subjected to nonsense-mediated decay, protein aggregation (Lykke-Andersen et al, 2015) or truncated proteins with the loss of c-terminal nuclear localization signals (NLS). Instead, missense mutations may lead to inactivation of UCH domain but maintaining protein expression and its nuclear localization. Bap1 has a role in uveal melanocytes as regulator of differentiation, and if Bap1 loss occurs, the cell exhibits stem-like phenotype (O'Shea et al, 2017). However, the role of BAP1 mutations and their oncogenic potential is not fully understood.

Peña-Llopis and colleagues (Peña-Llopis et al, 2012) created a Bap1 protein model on the basis of the related family members Uch-L3 and Uch37, to evaluate the impact of BAP1 missense mutations in a structural context. Among the missense mutations studied, V43G and L112P were predicted to destabilize the protein.

More recently, Bhattacharaya (Bhattacharaya et al, 2015) investigated cellular localization, enzymatic activity and structural changes for four missense mutations (I47F, F81V, A95D, G178V) in Bap1 catalytic domain, to examine the mechanism behind protein structure destabilization. In particular, they observed *in vitro* a BAP1 loss enzymatic activity, decreased protein stability and consequent beta amyloid aggregation. These mutations destabilize BAP1 secondary structure, inducing the hydrophobic core exposure and protein aggregation (Figure 18). In addition, Bhattacharaya observed that BAP1 mutations lead to an up-regulation of heat-shock protein response, specifically

Hsp70 and Hsp90, yet known over-expressed in prostate cancer (Figure 13) (Bhattacharaya et al, 2015).

Figure 13. Schematic model representing the effects of BAP1 functional loss.

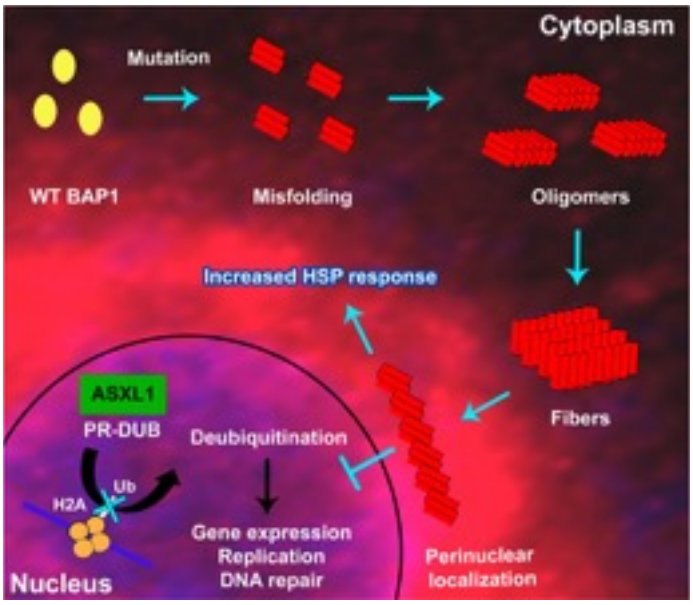

BAP1 wild-type is represented as yellow, BAP1 mutant is represented in red. Mutant BAP1 forms oligomers which induce fibril formation. The consequence aggregation inhibits nuclear localization of BAP1 and PR-DUB complex formation (Bhattacharaya et al,2015).

Until recently, it was thought that nuclear localization was required for all BAP1 functions. Recent experiments, however, showed a novel BAP1 cytoplasmic activity: wt BAP1 localizes at the endoplasmic reticulum, and has a role in promoting apoptosis via Ca2+ mitochondrial changes. Moreover, it was shown that cells from individuals carrying heterozygous germline *BAP1* mutations have a distinctive metabolic signature, consisting in impairment of mitochondrial respiration and increase of aerobic glycolysis leading to Warburg effect (Bononi et al, 2017). Warburg effect protects tumor cells from hypoxia, gives precursor for biosynthesis of many biologic molecules including acid nucleic, promote tumor cells growth through lactate release, and increases the resistance to chemotherapy-induced apoptosis (Cairns et al, 2011; Hsu et al, 2008; Bononi et al, 2017). Metastatic potential and prognosis in UM lacking BAP1 functions could be influenced also by these mechanisms.

Splicing factor 3B subunit 1 (SF3B1)

SF3B1 gene is localized on 2q33.1 chromosome band, contains 25 exons, and codify for a 42142 Da protein.

Sf3b1 is the subunit 1 of the splicing factor 3b, part of splicesoma, a protein complex that processes pre-mRNA into mature mRNA. Together with splicing factor 3a and a 12S RNA unit, forms the U2 small nuclear ribonucleic proteins complex (U2 snRNP). The splicing factor 3b/3a complex binds the pre-mRNA upstream of the intron's branch site in a sequence-independent manner and may anchor the U2 snRNP to the pre-mRNA. Splicing factor 3b is also a component of the minor U12-type spliceosome (Figure 14).

Figure 14. Stepwise assembly of the early splicesome highlighting the known splicing factors that bind to the substrate. In red circle is highlighted Sf3b1 (Fredericks et al, 2015).

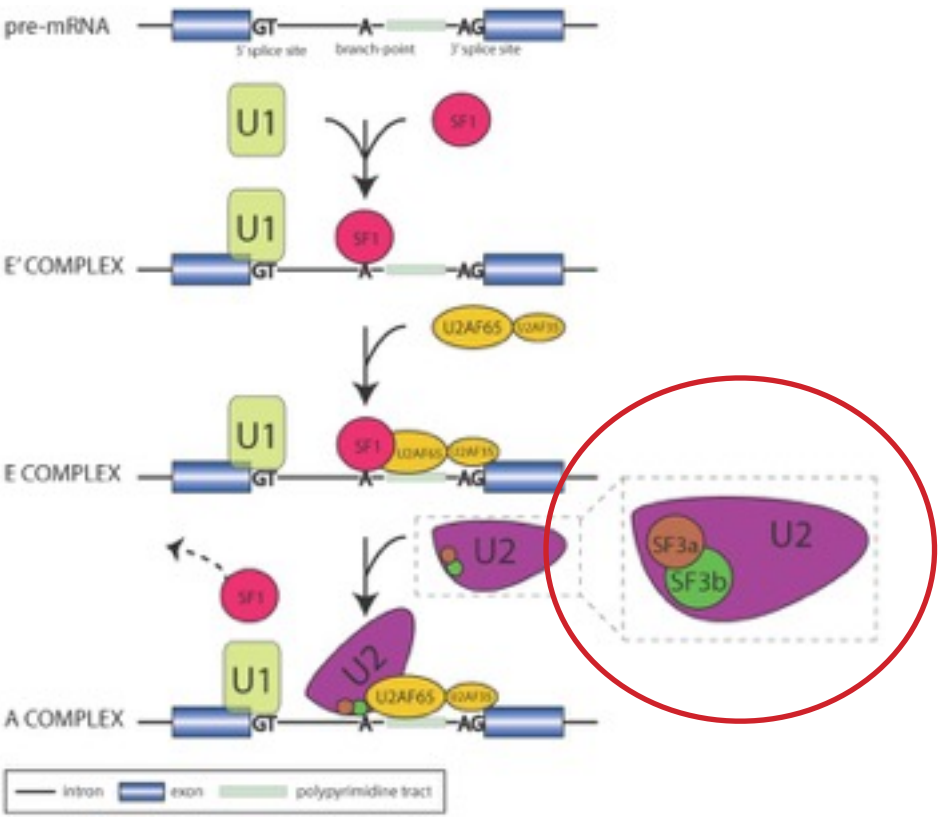

The two thirds carboxy-terminal have 22 non-identical, tandem HEAT repeats that form rod-like, helical structures (Figure 15). Alternative splicing results in several different isoforms.

Figure 15. Schematic representation of SF3B1 protein.

Sf3b1 protein consists of a U2AF2 interaction motif (U), SF3B1 interaction motif (S) and 22 non redundant HEAT domains (HD) . The most common mutation occurs on HD5 at R625.

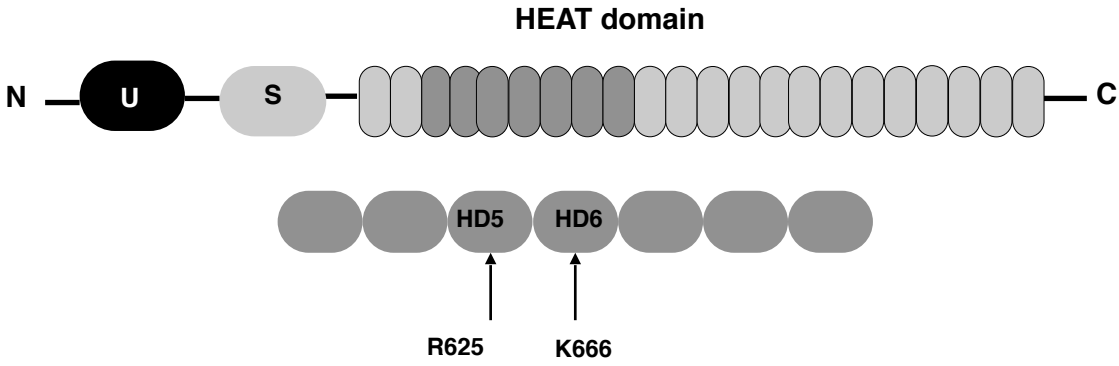

Mutations in SF3B1 were found in about 20% of UM (Alsafadi et al, 2016). SF3B1 is essential in pre-mRNA splicing and it is hypothesized to be involved in cancer through alternative splicing of target genes, which may play a role in tumorigenesis (Golas et al, 2003; Furney et al, 2013). Alsafadi et al (Alsafadi et al, 2016) supposed that mutations in HEAT domains may induce a conformational change of complex U2 and, consequently, an alteration in selectivity for normal splice site. As a result, this conformational change could activate cryptic splices sites (Figure 16).

SF3B1 mutations most frequently lead to arginine-625 residue and less frequently to lysine-666 residue substitution (Figure 15).

SF3B1 mutations are almost mutually exclusive with BAP1 mutations and define a subclass of UM characterized by disomy 3. Initially it has been suggested a protective role of SF3B1 mutations in UM, but some authors proposed an association with the appearance of late metastasis (Tschentscher et al, 2003; Yavuzyigitoglu et al, 2016).

Figure 16. A model for alternative splicing dysregulation induced by SF3B1 hotspot mutations (Alasafadi et al,2016)**.**

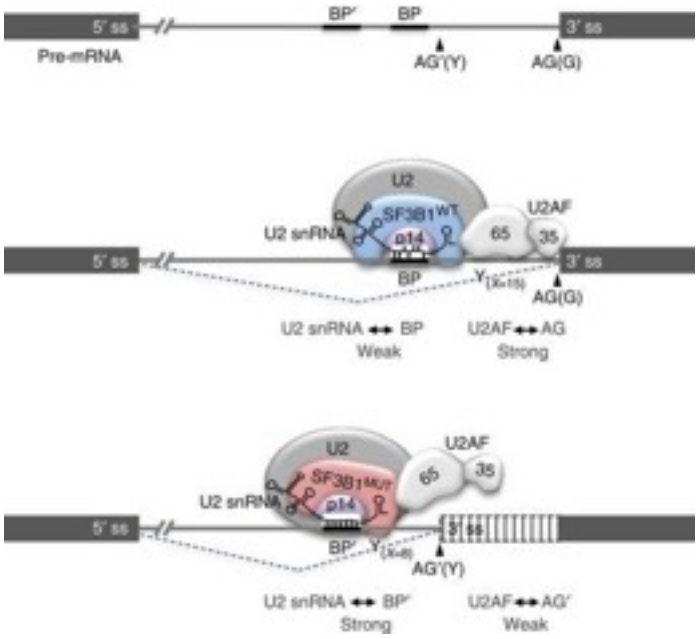

The 3′ss contains a segment, which is rich in pyrimidines (Y), a well-conserved AG dinucleotide and a branchpoint (BP) sequence recognized by the U2 snRNP. The U2 snRNP complex binds to the intron through base-pairing interactions between the BP sequence and the U2 snRNA, and through interactions between intron sequences, SF3B1 and p14. The HEAT repeats of SF3B1 form helical structures that occlude the surface of RNA recognition motif of p14. U2 snRNP containing SF3B1WT recognizes the canonical U2AF-dependant BP. The hotspot mutations of *SF3B1* targeting the HEAT repeats occur on the inner surface of the structure and might induce a conformational change in the U2 snRNP complex altering its selectivity for BPs. U2 snRNP containing SF3B1MUT has more stringent requirement for BP sequences and less for U2AF-dependent sequences, leading to the binding of alternative branchpoints (BP') with high potential of base-pairing with U2 snRNP. AG, canonical 3′ss; AG', alternative 3′ss; *x*, average number of pyrimidines; Y, pyrimidine

Eukaryotic translation initiation factor 1A, X-chromosomal (EIF1AX)

EIF1AX gene is localized in Xp22.12 and encodes for a 164 protein kDA protein (Figure 17). Eif1ax protein is required for binding the 43S complex (40S subunit, eIF2/GTP/Met-tRNAi and eIF3) to the 5' end of capped RNA (Figure 18). With a translation initiation factor activity, it stimulates the transfer of methionyl initiator tRNA (Met-tRNA) to the small ribosomal subunit during translation and it allows the formation of a stable mRNA-ribosome complex.

Mutations in EIF1AX were mainly observed in UM samples with disomy 3 and BAP1 wild type, and they were associated to a low risk of metastatic disease (Ewens et al, 2014).

Identified EIF1AX mutations are missense mutations or deletion and they are heterozygous or hemizygous (in males) mainly occurring in the exon 1 and 2, the amino-terminal portion of the encoded protein. However, in UM, only mutant mRNA transcripts were expressed, suggesting that the wild-type copy of EIF1AX is epigenetically inactivated and, in this case, EIF1AX may act like a recessive gene (Harbour et al, 2014) (Figure 19).

Figure 17. Schematic representation of EIF1AX protein.

Eif1ax protein consists of a N-terminal tail, oligonucleotide binding (OB) fold and C-terminal tail. The mutation to date reported led to to substitutions or loss of one or two amino acid near the amino terminus.

Figure 18. Summary of functional domains in eIF1A and its interactions.
The figure shows N-terminal domain, oligonucleotide-binding domain and C-terminal domain which bind other transcription factors (eIF2,eIF3), 40S ribosome, ternary complex (TC) respectively (Olsen et al, 2003).

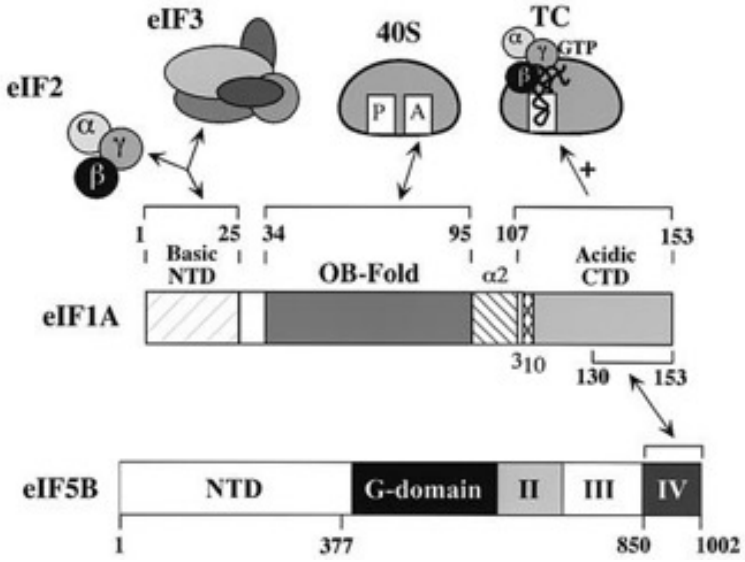

Figure 19. Schematic presentation of cellular functions of proteins commonly mutated uveal melanoma (Harbour et al, 2014)**.**

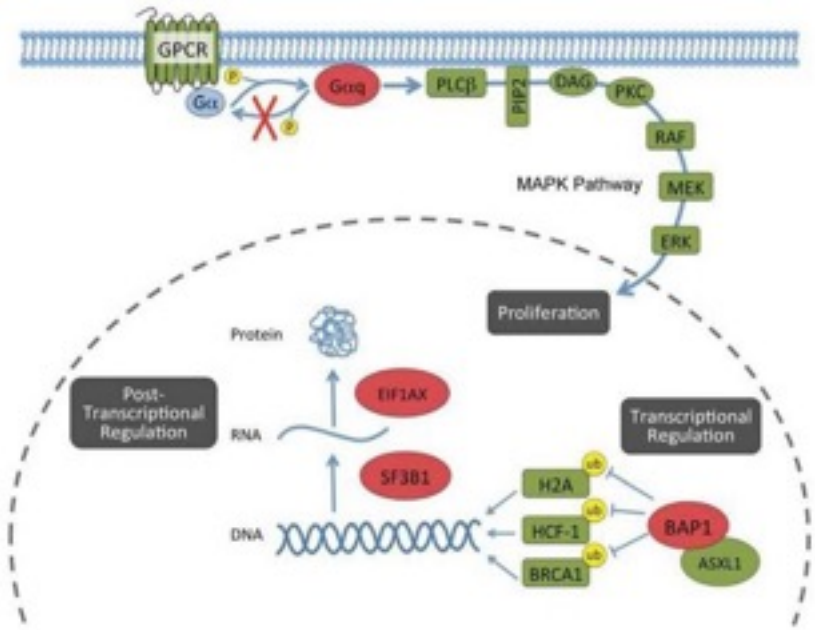

N

Novel identified mutations

Phospholipase C beta 4 (PLCB4)

Through Next Generation Sequencing of UM samples, Johansson et al (Johansson et al, 2016) found in UM samples a recurrent mutation in PLCB4 gene: c.1888G>T p.D630Y (NM_000933). This finding was later confirmed by Moore et al (Moore et al, 2016).

PLCB4 gene maps in 20p12.3-p12.2, and encodes a protein that catalyzes the reaction from phosphatidylinositol 4,5-bisphosphate to inositol 1,4,5-trisphosphate and diacylglycerol.

Four Plcb4 isoforms have been found. Plcb4 protein contains three domain: PI-PLC X-box, between the amino acids 313-463, PI-PLC Y-box, between the amino acids 565-681, and C2, between the amino acids 688-786. Plcb4 protein is part of GPCr signaling pathway, and it is involved in many molecular and biological functions: calcium binding, phosphatidylinositol phospholipase C activity, phospholipase C activity, signal transducer activity. In the retina, Plcb4 plays an important role in intracellular transduction of many extracellular signals.

In UM, both Johansson et al (Johansson et al, 2016) and Moore et al (Moore et al, 2016) identified PLCB4 mutations only in GNAQ and GNA11 wild-type samples, and this finding suggested that PLCB4 mutation are gain-of-function mutations leading to activation of the same pathway activated by GNAQ/GNA11 mutations. As a consequence of these findings, the authors suggested an oncogenic role of PLCB4 mutations in UM with GNAQ and GNA11 wild-type (Johansson et al, 2016; Moore et al, 2016).

Cysteinyl leukotriene receptor 2 (CYSLTR2)

CYSLTR2 gene maps on 13q14.2, and consists of four exons with all introns located in the 5' UTR region of the gene. Moore et al (Moore et al, 2016) analyzed WGS and WES data from 136 UM form multiple cohorts. Using a mutation analysis algorithm to detect hotspot mutations in oncogenes, they identified a hotspot mutation in CYSLTR2 gene. This mutation was observed only in samples lacking mutations in GNAQ, GNA11 or PLCB4, suggesting that they activate the same pathway (Moore et al, 2016).

Mutation L129Q (Moore et al, 2016) is a missense mutation in transmembrane helix 3 (between 124-144 aminoacids) which associates extracellular ligands, intracellular G-alpha subunit, and the other transmembrane helices. L129Q CysLTR2 is constitutively activated, as evidenced by increased calcium mobilization and insensitivity to CysLTR2 agonist leukotriene D4. The missense mutation L129Q has melanocyte lineage-specific effects. *In vivo* experiments also showed that subcutaneously engrafted melan-a cells expressing mutant L129Q CysLTR2 were able to form tumor more rapidly than wild-type cells, suggesting that this novel mutation enhances melanoma tumorigenesis *in vivo*.

Taken together, these findings may indicate an oncogenic role of CysLTR2 in UM through activation of Gα-q signaling.

Multistep carcinogenesis

Hanahan and Weinberg (Hanahan and Weinberg, 2000; Hanahan and Weinberg, 2011) defined the cancer as un uncontrolled, clonal proliferation of cells, which progressively acquire most or all of the 8 “hallmarks" of neoplasia. These hallmarks, which are considered prerequisites necessary for survival, proliferation capacity and invasion of neoplastic cells, are acquired by a multistep process that leads to insensitivity to anti-growth signals, avoiding apoptosis, limitless replicative potential, angiogenesis, sustaining proliferative signaling, reprogramming of energy metabolism, evading immune distruction, tissue invasion and metastasis (Hanahan and Weinberg, 2000; Hanahan and Weinberg, 2011).

Also in UM it is hypothesized that various genetic and epigenetic alterations occur in the development pathway from melanoblasts to UM cells.

UM is a cancer arising from melanocytes localized in the uveal tract. The precursors of the uveal melanocytes are the melanoblast cells, derived from neural crest. Until now, it is not clear whether the melanoma-initiating cells or cancer stem-like cells arise from melanocytes precursor of from melanocytes de-differentiated.

Almost all uveal nevi and UM show mutations in GNAQ or GNA11, suggesting their role in promoting melanocyte proliferation and survival. As already explained activating mutations in PLCB4 and CYSLTR2 genes could have the same role in UM with GNAQ and GNA11 wild type (Moore et al, 2016; Hanahan et al, 2000). Mutations in GNAQ, GNA11 or PLCB4 and CYSLTR2 are necessary for melanocyte cell proliferation but they are not sufficient for malignant transformation to UM. Other mutations and chromosomal aberrations are needed for the progression from uveal nevi to UM (Bauer et al, 2009; van Raamsdonk et al, 2009).

It has been proposed that uveal nevi could progress through one of the two exclusive pathways, characterized by distinct genetic signatures and different metastatic risk. UM with monosomy 3, BAP1 gene mutations, and additional 1p loss and/or 8q gain show a high metastatic risk (class 2 tumor). UM with 6p gain and EIF1AX gene mutations show a low metastatic risk (class 1) (Figure 20).

A metastatic intermediate risk is observed either in class 1 and class 2 UM: class 1 UM harboring SF3B1 mutations and/or increased PRAME mRNA expression show a risk of late metastasis development, and class 2 UM harboring 6p gain show an intermediate risk of progression (Harbour et al, 2010).

Figure 20. Schematic representation of molecular events that occur during progression from uveal melanocyte to metastatic melanoma (Amaro et al, 2017)**.**

The figure shows an hypothesis of multistep UM tumorigenesis based on the current state of knowledge of molecular alterations. UM develops from melanoblasts or melanocytes through mutations in GNAQ ,GNA11 genes or in CYSLTR2, PLCB4 genes. Monosomy chromosome 3, BAP1 mutation and 8q gain are associated to high metastatic risk but the presence of 6p gain may attenuate the metastatic risk. UM harboring SF3B1 mutation shows intermediate risk.

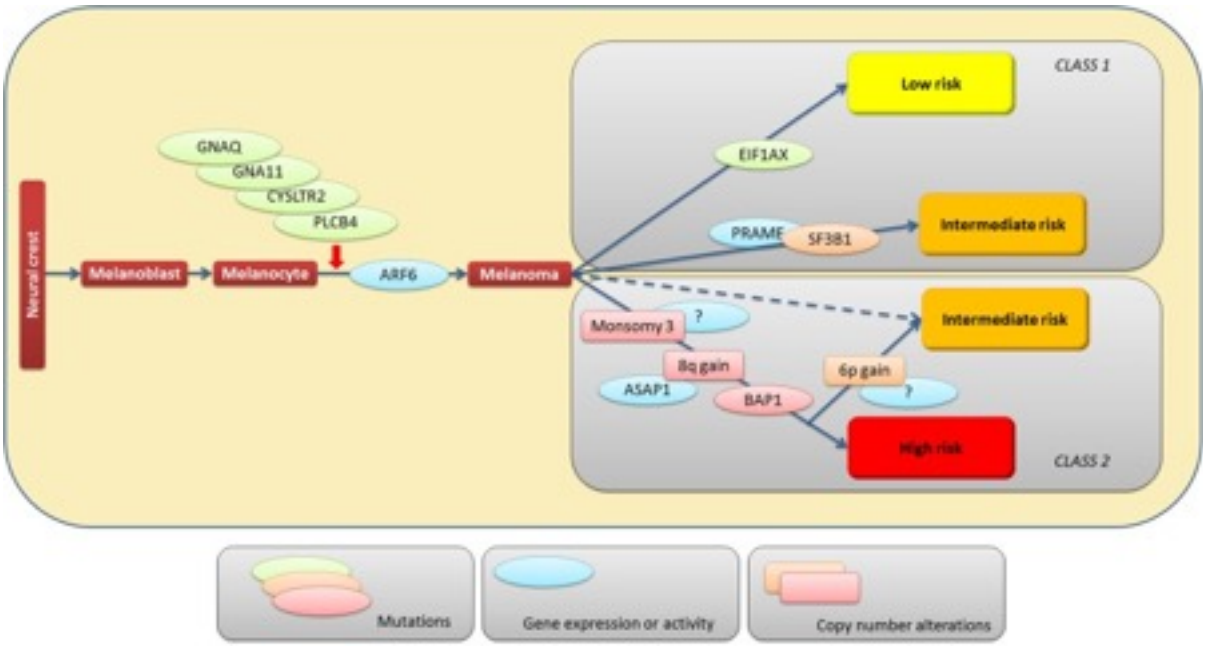

BAP1 germline mutation and BAP1- TPDS

*G*ermline BAP1 mutations were reported in less than 1% of UM patients in the UK (Soura et al, 2016; Aoude et al, 2013), in association with a novel hereditary cancer syndrome, described as *BAP1* tumor predisposition syndrome (*BAP1*-TPDS, #614327 OMIM) or as Cutaneous/Ocular Melanomas, Mealanocytic proliferations and other internal neoplasm. Heterozygous germline BAP1 mutations were instead described in about 20%-30% of subjects with a family history of UM (Popova et al, 2013; Gupta et al, 2015; Turumen et al, 2016).

This tumor predisposition syndrome related to BAP1 is inherited as autosomal dominant character: in carriers harboring heterozygous germline BAP1 mutations, the somatic inactivation of the remaining allele is enough for the development of a malignant phenotype. Indeed, carriers of germline BAP1 mutations have a high-risk of developing of a spectrum of primary tumor types at younger age, including benign melanocytic tumors as well as UM, cutaneous melanoma, malignant mesothelioma, lung adenocarcinoma, meningioma, and renal cell carcinoma (Abdel-Rahman et al, 2011; Testa et al, 2011; Popova et al, 2013; Soura et al, 2016; Rai et al, 2016) (Figure 21).

Other suspected but unconfirmed tumors included in this novel tumors predisposition syndrome are also cholangiocarcinoma, non-small cell lung adenocarcinoma (NSCLC), meningioma, and neuroendocrine carcinoma (Testa et al, 2011; Popova et al, 2013; Rai et al, 2017).

Association between BAP1 germline mutations and development of breast and ovarian cancers has been suspected, but contradictory results are reported in the literature (Coupier et al, 2005; Guénard et al, 2009).

BAP1 tumor predisposition syndrome was phenotypically characterized by Wiesner (Wiesner et al, 2011). The author described specific pink skin lesions, classified as atypical Spitz tumors (ASTs), in two unrelated families harboring BAP1 germline mutations and with a concomitant loss of wild type allele in these skin lesions (Figure 22). The ASTs are a heterogeneous group of melanocytic tumors with both histological features of benign Spitz nevi, characterized by large melanocytes with high mitotic activity and uncommon BRAF mutations, and malignant melanoma. Wiesner et al and Njauw et al (Wiesner et al, 2011; Njauw et al, 2012) described these novel lesions as

nevus-like lesions, round, dome-shaped and ranging in color from orange to red, large epithelioid BAP1 immunohistochemistry negative cells, virtually no mitotic activity, frequent BRAFV600 mutations in melanocytes cells (Wiesner et al, 2011; Njauw et al, 2012).

Due to the differences with benign Spitz nevi, Carbone et al proposed the name BAP1-mutated atypical intradermal tumors (MBAITs) to classify these novel lesions (Carbone et al, 2012).

Also malignant mesothelioma in patients without occupational exposure to asbestos, UM, ovarian cancer, breast cancer, renal cell carcinoma, squamous cell carcinoma, basal cell carcinoma, and pancreatic cancer have been diagnosed in different family members (Wiesner et al, 2011; Abdel-Rahman et al, 2011). Recently, Kadariya et al (Kadariya et al, 2017) performed in vivo studies to determine if heterozygous germline truncating mutation BAP1 in mice predisposes to tumor formation.

Figure 21. BAP1 tumor syndrome phenotype (Soura et al, 2016)**.**

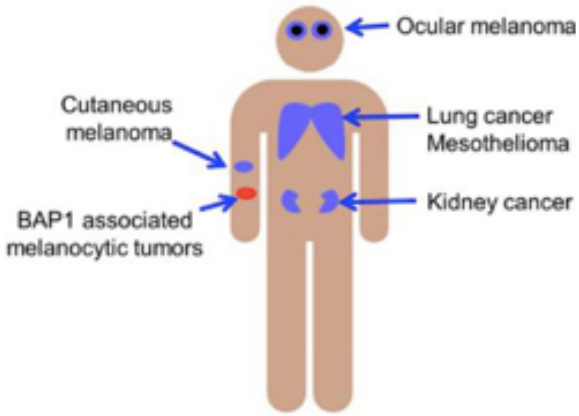

Patients with the BAP1 tumor syndrome are at risk for cutaneous melanoma, MBAITs, ocular melanoma, mesothelioma, lung cancer and renal cell cancer.

Figure 22: MBAITs (Soura et al, 2016)**.**

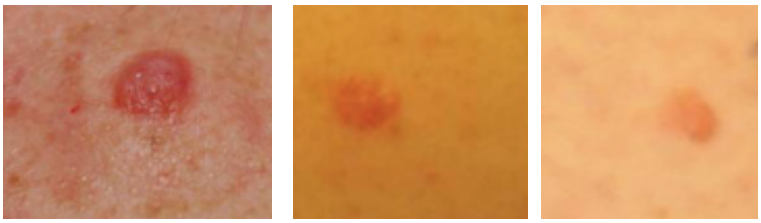

Typical melanocytic BAP1-mutated atypical intradermal tumors (MBAITs). These lesions are generally round, dome-shaped and orange to red color.

They observed that inactivating BAP1 mutations in mouse models induced an increase incidence of ovarian cancer, lung adenocarcinoma, mammary gland carcinoma, spindle cells tumor of skin, and MMs. It has to note that cancer spectrum observed in mice differs from of human tumors, indeed UM, CM, and RCC were not described in mice.

UM is the most frequent cancer diagnosed in patients with BAP1-TPDS (31%), and it is the cancer with the earliest age of diagnosis (Rai et al, 2016). Malignant mesothelioma and cutaneous melanoma are the second and the third most frequent cancers identified in BAP1-TPDS (Rai et al, 2016; Wiesner et al, 2011).

Current knowledge suggests that the presence of germline BAP1 mutations in patients with CM, UM, and RCC are associated with more aggressive cancers. Moreover, Abdel Rahman et al (Abdel-Rahman et al, 2011) reported UM with larger diameters, major involvement of ciliar body and increased risk of metastasis in patients carrying BAP1 germline mutation.

In contrast, patients with germline BAP1 mutations developing malignant mesothelioma (MM) showed a significantly longer survival rate than the other patients with BAP1-TPDS developing the other type of cancers (Rai et al, 2017).

Based on literature data, the penetrance of BAP1-TPDS appears high, but it must be considered that the number of families reported is limited, and also the natural history and the frequencies of BAP1-associated tumors are incomplete. In a recent review (Rai et al, 2017), 57 families and 174 individuals with BAP1-TPDS were described: 148 out 174 (85%) carriers of a heterozygous germline BAP1 pathogenic mutation developed a cancer. Moreover, the authors estimated that BAP1 mutations are present in about 22% of families with familial UM, compared to 2-4% of sporadic UM.

In the clinical context, germline BAP1 mutations can be used as a diagnostic tool to identify mutation carriers and patients with BAP1 tumor predisposition syndrome, but significant uncertainty in terms of appropriate cancer surveillance has been highlighted: lifetime risk of developing cancer is not well known, as well as it is not clear if surveillance could lead to detect cancer early enough to improve the outcome of patients (Pilarski et al, 2014; Carbone et al, 2015). Until now, there are no cancer screening guidelines for BAP1 germline carriers (Rai et al, 2016).

An important challenge in cancer surveillance is to provide non-invasive tests, and also the detections of symptoms as soon as possible (more difficult for RCC and MM). Pilarski (Pilarski et al, 2014) proposed a cancer screening plan with full-body skin examination, eye examination, abdominal ultrasound examination and abdominal MRI to identify possible primary tumors early (ATS, CM, UM, MMe, RCC).

In addition, if a germline BAP1 mutation is identified, it could be important to extend the genetic status analysis to the other family members in order to identify possible other carriers. Because BAP1-TPDS is inherited in an autosomal dominant manner, genetic counseling to inform the BAP1 germline mutation carriers about the nature, the inheritance, and the implications of this tumor predisposition syndrome could be appropriate.

Aim of the research project

Almost half of the patients with UM develop distant metastases. The poor outcome of UM patients with metastatic disease derives from the absence of proven effective adjuvant therapies. Predictive information on the clinical outcome of UM patients could provide the basis to determine an individualized, targeted therapeutic strategy for each UM patient. To reach this goal, it is important to have an accurate prediction system to assess the individual patient's metastatic risk. To address this issue, in this study we evaluated genetic features of a UM series, and analyzed their associations with metastatic progression.

At first, we carried out a multiplex ligation-dependent probe amplification (MLPA) to identify chromosomal imbalances involving chromosomes 1p, 3, 6, and 8. To confirm chromosome 3 status, we used microsatellite analysis (MSA), that could identify samples with isodisomy 3, not identifiable with MLPA analysis.

Because of their importance in UM tumorigenesis, we performed mutational analysis of GNAQ, GNA11, PLCB4, CYSLTR2, BAP1, EIF1AX, and SF3B1.

In particular, the well-established prognostic indicator BAP1 was investigated: we sequenced all the 17 BAP1 exons, and, to better understand the relationship between BAP1 mutational status and its functional activity, we carried out BAP1 immunohistochemistry (IHC). The contemporary use of the two methodologies to study BAP1 has given us the opportunity to compare the validity of BAP1 IHC compared to Sanger sequencing. In addition, we used RNAscope® in situ hybridization, to verify the presence/absence of BAP1 mRNA transcripts in selected UM samples.

Univariate associations between studied parameters and metastatic disease were performed, and associations between mutations and distant progression free survival (DPFS) were studied. In addition, to evaluate if germline BAP1 mutations occur in our UM and their potential contribution in UM developing, we performed BAP1 mutational analysis in DNA extracted from blood of 27 UM patients.

Materials and Methods

Patients and specimens

A total of 63 tissue samples were obtained from primary uveal melanoma after enucleation surgery at E.O. Galliera Hospital during the time period from 2012 to 2016. The clinical data collected were: patient age at time of enucleation, sex, pathological TNM stages, histological cell type, time from enucleation to occurrence of metastasis (months), and the follow-up (months). Written informed consent was obtained for all patients.

Tissue sampling and histopathological analysis

Tumor sampling was performed immediately after enucleation by trans-scleral fine-needle aspiration biopsy (FNAB) or by trans-scleral incisional biopsy. After marking the tumor boundary using trans-pupillary transillumination, FNAB was performed with a 25-gauge needle attached to a 10-ml syringe using manual aspiration with a biopsy gun. Trans-scleral incisional biopsy was performed creating a partial lamellar scleral flap, then incising the inner scleral lamella and sampling the tumor with the Essen biopsy forceps (Dutch Ophthalmic Research Center, Zuidland, The Netherlands). In any case UM biopsies were then placed in RNA*later*™ (Ambion, Monza, Italy) and the eyes were formalin fixed and paraffin embedded (FFPE). For histopathologic examination, 2 μm-thick FFPE sections were stained with the conventional hematoxylin and eosin stain. Cell type was assigned according to the modified Callendar classification system (Callender et al,1931).

DNA extraction

DNA was extracted from fresh UM samples (biopsies) conserved in RNA later (Ambion, Monza, Italy) or from archival formalin-fixed, paraffin embedded (FFPE) block using respectively QIAamp DNA MINI Kit (Qiagen,Hilden, Germany) and QIAamp DNA FFPE MINI kit (Qiagen, Hilden, Germany). DNA from blood samples was extracted with QIAsymphony SP instrument (QIA), a fully integrated system that can automate perform DNA purification from a wide range of samples with minimum input volume of 200 µl.

- DNA from biopsy was isolated in accordance with manufacturer's instructions: the sample was resuspended in 180 µl of ATL buffer (lysis buffer) and 20µl of Proteinase K and it was heated to 56°C until the complete lysis of tissue. 200µl Buffer AL was added to the lysate and it was incubated at 70°C for 10 minutes. The lysate, with 200µl of ethanol 100%, was placed in a spin column and centrifuged. Two steps with wash buffer were followed and lastly the DNA was eluted with Buffer AE.
- DNA form FFPE sample was isolated in accordance with manufacturer's instructions: two 10 um-thick section was cut from paraffin block and subjected to de-paraffinization using xylene. After centrifugation, the pellet was resuspended in a mixture containing 180µl lysis buffer and 20µl of Proteinase K and heated to 56°C until the complete lysis of tissue. An incubation at 90°C for 10 minutes followed. The next steps are similar to the DNA extraction from fresh samples.

• **DNA Quantification and Quality Assessment**

DNA concentration and purify were estimated measuring the absorbance at 280 and 260 nm with NanoDrop ND-1000 spectrophotometer (NanoDrop, Minneapolis, MN).

If DNA quality resulted not optimal, we used Amicon Ultra-0.5 mL Centrifugal Filters to clean up the DNA before its use (Merck-Millipore).

Indeed, the ratio of absorbance at 260 and 280 nm is used to assess the purity of DNA. A 260/280 ratio of ~1.8 is generally accepted as "pure" DNA.

The 260/230 ratio is a secondary measure of DNA purity. A ratio in the range of 1.8-2.2 values is accepted as “pure” DNA. Ratio considerably lower may indicate presence of co-purified contaminants.

Multiplex Ligation-dependent Probe Amplification or MLPA

MLPA is a method developed by MRC-Holland based on the semi-quantitative polymerase chain reaction principle. MLPA technique can be applied for detecting copy number changes in genomic DNA and, in particular, it is possible to detect DNA copy number changes in up to 40 sequences in a single reaction.

MLPA advantages are the possibility to use a few DNA amount with good results, short execution time (24-48h) and no special equipment is required except for a thermal cycler and a capillary electrophoresis sequencer. In addition, it is possible to analyze in a unique reaction many target sites.
MLPA probes consist of two oligonucleotides, each containing a specific PCR primer sequence (PCR primer sequence X and PCR primer sequence Y) and a sequence complementary to the target, known as the hybridization sequence. The two probes hybridize adjacent to each other (23.1). If the probes correctly hybridize to the target sequence they are ligated by a ligase enzyme (Figure 23.2). The PCR primers exponentially amplify the ligated probes (Figure 23.3). One of the primers is labeled with a fluorescent dye to visualize the amplification product.

- **MLPA procedure**

SALSA® MLPA® probemix P027-C1 and P417-B2 BAP1 (MRC-Holland) were used in association with MLPA reagents kit to identify chromosomal imbalances in UM samples (P027-C1) and deletions/duplications of one or more sequences in the BAP1 gene (P417-B2 BAP1).
SALSA® MLPA® probemix P027-C1 Uveal Melanoma probe mix contains 38 probes: 7 probes on chromosome 1p, 15 probes on chromosome 3p and 4 probes on chromosome 3q, 4 probes on chromosome 6p and 2 probes on chromosome 6q, 4 probes on chromosome 8p and 2 probes on chromosome 8q. In addition SALSA P027-C1 contains 12 reference probes detecting sequences that could be stable in UM (chromosomes 2, 4, 10, 11, 12, 13, 14,

15, and 18). Table 3 and Figure 23 show the salsa MLPA probes of probemix P027-C1 and their cytogenetic localization.

SALSA® MLPA® probemix P417-B2 BAP1 contains one probe for each exon of BAP1 gene. In addition, 10 flanking probes for BAP1 gene and 15 reference probes are included in this probemix to facilitate the determination of the extent of a copy number change. Reference probes are included to detect autosomal chromosomal locations which are relatively stable both in melanocytic tumours. Table 4 and Figure 24 show P417-B2 BAP1 probes and their cytogenetic localization.

Figure 23. Schematic representation of MLPA procedure.

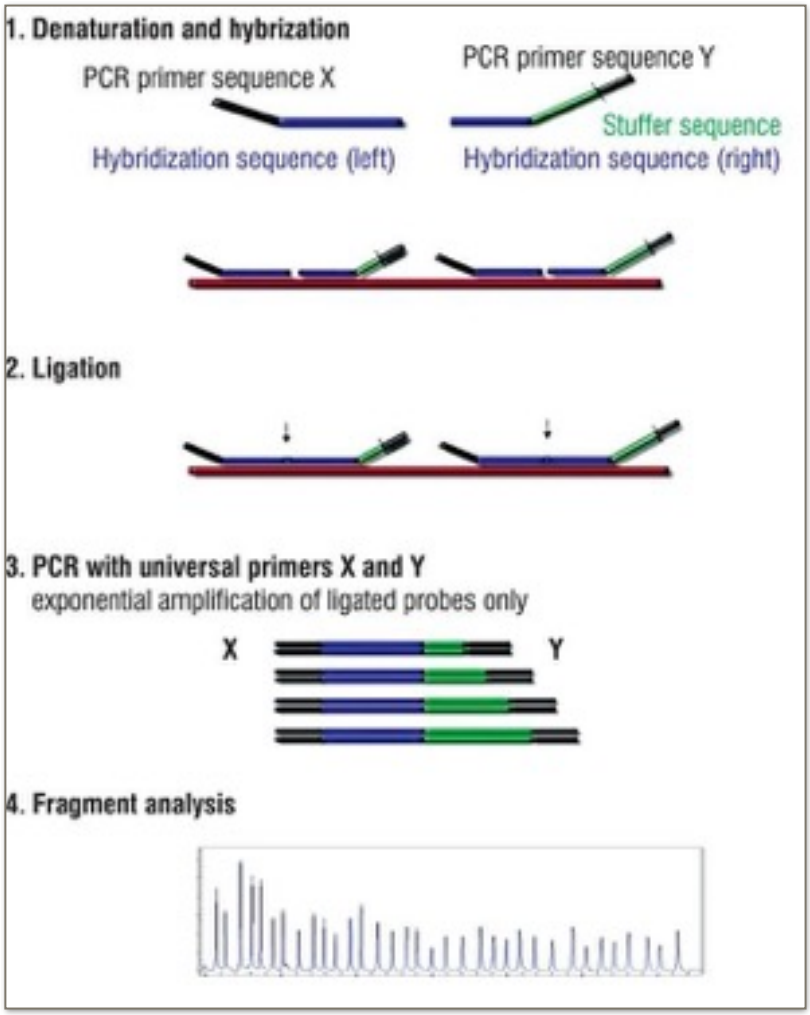

We performed the MLPA procedure as follows:

- Denaturation: 100 ng of DNA sample were diluted with TE to 5 μl and it was heated at 98°C for 5-30 min in a thermal cycler (Veriti 96 well, Applied Biosyjstem) and then cooled at 25°C;
- Hybridization: 3 μl of Hybr-probe mix (1.5 μl salsa probe and 1.5 μl MLPA buffer) was added to the sample, heated for 1 min at 95°C, and then incubated at 60°C for a minimum of 16 h and maximum of 20 h;
- Ligation: it was performed by diluting sample to 40 μl with Lig-mix containing 25 μl water, 3 μl ligase-65 BufferA and 3 μl ligase-Buffer B. The sample was incubated at 54°C for 15 min, and then heated to 98°C for 5 min to allow ligase enzyme inactivation.
- Amplification: the amplification of ligation products was performed using a pair of universal primers complementary to PCR primer sequence X and PCR primer sequence Y. The sample was diluted with 10 μl of Pol-mix (0.5 μl salsa PCR primers, 7,.5 μl salsa polymerase and 0.5 μl water) and the MLPA reaction took place in the thermal cycler with the following conditions: x35 (95°C 30'', 60°C 30'', 72°C 1'), x1 (72°C 30') .

After amplification 0.85μl of PCR products were mixed with injection mixture containing 18 μl of highly deionized HI-DI formamide (Applied Biosystem, ABI, Foster City, CA) and 0.4 μl internal line size standard ROX-500 (GeneScan-500 ROXSize Standard, ABI). The PCR products, suchly diluted, were separated by electrophoresis on ABI Prism 3130xl Genetic Analyzer and analyzed by Coffalyser.net

Table 3. SALSA® MLPA® probemix P027-C1 arranged according to chromosomal position

Length (nt)	SALSA MLPA probe	Gene (exon)	Chromosomal position
196	04888-L04272	MFN2	1p36.22
274 «	04148-L03503	NBL1	1p36.13
355	02267-L01425	PTAFR	1p35.3
220	13671-L17892	GJB3	1p34.3
418	03964-L03351	MUTYH	1p34.1
241 ±	03601-L19174	RPE65	1p31.2
136	02867-L02334	NOTCH2	1p12
207	14147-L17987	CHL1	3p26.3
283 ‡	15895-L18089	BRK1	3p25.3
391	13322-L14735	VHL, ex 2	3p25.3
445	15899-L18091	VHL, ex 3	3p25.3
259	06900-L06480	PPARG	3p25.2
474 ±	06118-L05573	XPC	3p25.1
190	15896-L17989	MIR128-2	3p22.3
139	15288-L20037	MLH1	3p22.2
454	16407-L18832	CTNNB1	3p22.1
364	15897-L18094	RBM5	3p21.31
483	16644-L19176	BAP1, ex 9	3p21.1
226	16643-L20039	BAP1, ex 4	3p21.1
178 ±	02292-L02212	FHIT, ex 5	3p14.2
337	02290-L01781	FHIT, ex 4	3p14.2
409	04603-L03256	ROBO1	3p12.3
328 ±	05297-L04685	PROS1	3q11.1
247	05708-L19175	CASR	3q21.1
201	00487-L00069	MME	3q25.2
344 ±	03271-L02708	OPA1	3q29
382	10252-L11363	ECI2	6p25.2
463	10253-L18092	DCDC2	6p22.3
427	00585-L18090	CDKN1A	6p21.2
160 « ±	02611-L02082	RUNX2	6p21.1

Table 3. SALSA® MLPA® probemix P027-C1 arranged according to chromosomal position

Length (nt)	SALSA MLPA probe	Gene (exon)	Chromosomal position
266	04745-L19276	CTGF	6q23.2
233	02798-L20038	IGF2R	6q25.3
310	02552-L19178	LZTS1	8p21.3
318 ±	04239-L03575	NRG1	8p12
184 ±	16641-L19172	RP1	8q12.1
165	15894-L16789	MYC, ex 1	8q24.21
154	00580-L00145	MYC, ex 3	8q24.21
299	16241-L18499	ASAP1	8q24.21

Table 4 SALSA® MLPA® probemix P417-B2 BAP1 arranged according to chromosomal location

Length (nt)	SALSA MLPA probe	Gene/exon	location/ ligation site
telomeric			
385	16176-L21699	MLH1	3p22.2
364	15897-L18094	RBM5	3p21.31
184	12125-L21391	RASSF1	3p21.31
214	03206-L13082	ZMYND10	3p21.31
BAP1 at 3p21.1			
		STOP codon	2415-2417 (Exon 17)
332	17414-L21123	Exon 17	2580-2581
281	21244-L29701	Exon 16	2214-2215
190	17404-L21113	Exon 15	2139-2140
263	17409-L21118	Exon 14	2111-2112
244	17407-L21116	Exon 13	1814-1815
308	17413-L21122	Exon 12	1388-1389
179	17403-L21112	Exon 11	1342-1343
285	17411-L21120	Exon 10	1057-1058
268	17398-L19176	Exon 9	923-924

Table 4 SALSA® MLPA® probemix P417-B2 BAP1 arranged according to chromosomal location

Length (nt)	SALSA MLPA probe	Gene/exon	location/ ligation site
299	17412-L21397	Exon 8	879-880
149	17400-L21109	Exon 7	710-711
257	17408-L21394	Exon 6	610-611
208	17405-L21114	Exon 5	483-484
227	16643-L19177	Exon 4	441-442
173	17402-L21111	Exon 3	321-322
159	17401-L21110	Exon 2	285-284
232	17406-L21392	Exon 1	238-237
		START codon	228-231 (Exon1)
221	07223-L21127	HESX1	3p14.3
317	04710-L01787	FHIT	3p14.2
346	10794-L11434	MITF	3p13
274	06439-L05965	ROBO1	3p12.3
202	05292-L21125	PROS1	3q11.1
378	14836-L21403	CPOX	3q12.1
telomeric			

Microsatellite analysis

Microsarellite analysis (MSA) utilizes short, highly polymorphic repeated sequences within the chromosome. The number of repetitions aimed at a specific microsatellite often varies between the maternal and paternal allele.

We performed this technique to identify samples with isodisomy of chromosome 3, not identifiable with only MLPA analysis. Through microsatellite analysis we determined allelic imbalance (AI), loss of heterizigosity (LOH) or retention of heterozygosity (ROH) at specific loci by comparing the intensity of amplification products between the UM sample and the corresponding normal control.
MSA on chromosome 3 required many tests in order to choose the best microsatellite panel. We used 12 polymorphic microsatellite repeats on chromosome 3 divided according to the lengths and the labels (VIC, FAM or NED) in three microsatellite panels for DNA extracted from fresh samples, two panels for DNA extracted from FFPE samples, and amplified in multiplex PCR. Table 5 and Table 6 show the list of microsatellite repeats, their chromosomal localization, size and micro satellite primers. Figure 25 shows both localization of MLPA probes and microsatellite loci on chromosome 3.

- **Microsatellite procedure**

Microsatellite analysis was performed using 25 ng of genomic DNA extracted from tumor an blood sample in a 25 μl reaction mix: 10x Platinum® PCR Supermix, 1.5 mM $MgCl_2$, 200 μM M dNTPs, 0.4 μM each primer pair and 2U Taq Platinum (Invitrogen– Life Technologies Corporation, Italy).
After an initial cycle of denaturation at 95°C for 12 min, amplification was obtained by 10 x (15s, 94°C; 15s 56°C; 30s 72°C), 20 x (15s 89°C; 15s 56°C; 30s 72°C); 30m 72°C. PCR products were quantified and analyzed using the ABI 3130XL (Applied Biosystems-Life Technologies Corporation, Milan, Italy) and Genemapper™ software (Applied Biosystems, Foster City, CA, USA) respectively. A comparison of the peak area of DNA from UM biopsy specimens and normal DNA from matched blood samples allowed the determination of allele ratio in tumour.

Table 5. Microsatellite panels for fresh samples

Panel	Locus	Map	Size	Forward primer	Reverse primer
Panel 1	D3S1292 (VIC)	3q21-q22	142-166	TGGCTTCATCAC CAGACC	CAGATTCAAGAGG CACTCCA
	D3S1265 (VIC)	3q29	212-236	GAAGCAGGAGAA TCACGGA	CGTTCTGTGTGTT GCTAGTATGT
	D3S3681 (NED)	3p12.3	210-246	GTGAGAACCATT TGGGGCAG	GGCGAGCTATCTG TCAGGG
	D3S1271 (NED)	3q12.3	146-158	TGATTGGAGGTG GTAGAGG	AGCTATCATGTAGA AAAGCAGC
Panel 2	D3S1304 (VIC)	3p26	253-269	TTCGCTCTTTGAT AGGC	ATTTCATTTGTAATT TACTAGCAG
	D3S3521 (FAM)	3p21.3	227-287	CAGTAAGTCCAT GCCAGGG	GCAGCAGTTACCT TGGAGTG
	D3S3686 (FAM)	3q26.3	108-134	AGGGTATTTCATT CCCATTG	CCAGGTTACGCCA AGTG
	D3S1558 (FAM)	3p13.32	152-166	GGGTGCTATCATT TTAACC	CCTTAATGTGCTCA TGGAAG
	D3S3668 (NED)	3q25	235-257	CTTTTGGGAATTA AAAACTTCAGG	GTCAGTAAAACATG GAAATATGAGC
	D3S1597 (NED)	3p25.3	162-180	AGTACAAATACAC ACAAATGTCTC	GCAAATCGTTCATT GCT
Panel 3	D3S3697 (VIC)	3p14.1	190-225	TAGCCCCCTGCT GTCA	CTGGCCCAGGTTG GAA
	D3S3630 (FAM)	3p26	172-188	AAGGGATAAGCT GCAAATCA	ACCAAATACAATTC ATGAGACCTGA

Table 6. Microsatellite panels for FFPE samples

Panel	Locus	Map	Size	Forward primer	Reverse primer
Panel A	D3S3697 (VIC)	3p14.1	190-225	TAGCCCCCTGCT GTCA	CTGGCCCAGGTTG GAA
	D3S3686 (FAM)	3q26.3	108-134	AGGGTATTTCATT CCCATTG	CCAGGTTACGCCA AGTG
	D3S1558 (FAM)	3p13.32	152-166	GGGTGCTATCATT TTAACC	CCTTAATGTGCTCA TGGAAG
	D3S1597 (NED)	3p25.3	162-180	AGTACAAATACAC ACAAATGTCTC	GCAAATCGTTCATT GCT
Panel D	D3S1292 VIC	3q21-q22	142-166	TGGCTTCATCAC CAGACC	CAGATTCAAGAGG CACTCCA
	D3S3697 VIC	3p14.1	190-225	TAGCCCCCTGCT GTCA	CTGGCCCAGGTTG GAA
	D3S3630 FAM	3p26	172-188	AAGGGATAAGCT GCAAATCA	ACCAAATACAATTC ATGAGACCTGA
	D3S1271 NED	3q12.3	146-158	TGATTGGAGGTG GTAGAGG	AGCTATCATGTAGA AAAGCAGC

Figure 24. Localization of MLPA probes and micro satellite loci on chromosome 3

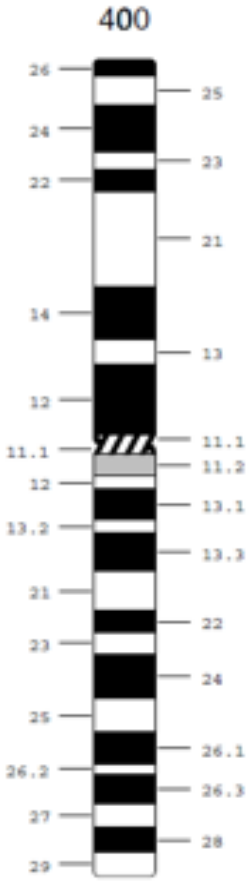

Chromosome 3	Microsatellite loci	MLPA probes
	D3S630 3p26; D3S1304 3p26	CHL1 3p26.3
	D3S1597 3p25-p22	BRK1; VHL ex 2; VHL ex3 3p25.3
		PPARG 3p25.2 XPC 3p25.1
		MIR128-2 3p22.3 MLH1 3p22.2 CTNNB1 3p22.1
	D3S3521 3p21.3	BAP1 ex 9; BAP1 ex 4 3p21.1
		RBM5 3p21.31
	D3S3697 3p14.1	
		FHIT ex 5; FHIT ex 4 3p14.2
	D3S3681 3p12.3	ROBO1 3p12.3
	D3S1271 3q12.3	PROS1 3q11.1
	D3S1558 3q13.32	
	D3S1292 3q21-q22	
		CASR 3q21.1
	D3S3668 3q25	
	D3S3686 3q26.3	MME 3q25.2
		OPA1 3q29

Immunohistochemical staining

The immunohistochemistry assay was performed at the Pathology Unit, E.O. Galliera. A representative block containing the largest amount of viable tumour was selected from each case, from which unstained 2 μm sections were prepared and submitted for assessment of BAP1 expression by immunohistochemistry (IHC)

Immunohistochemistry was performed with an automated IHC staining system (Ventana BenchMark ULTRA, Ventana Medical Systems) according to the manufacturer's instructions and using red chromogen. After deparaffinization of paraffin-embedded blocks, heat–induced antigen retrieval was performed and the section were incubated with a mouse monoclonal antibody raised against amino acids 430-729 of human BAP1 (C-4 clone sc-28383, 1:50 dilution, Santa Cruz Biotechnology, inc. USA). This was followed by incubation with haematoxylin II. Endothelial cells vascular of UM were used as positive controls for BAP1 expression.
Immunohistochemistry scoring: staining BAP1 expression was scored as diffuse (nuclear staining present in >90% of tumor cells) or absent (nuclear staining present in <10% of tumor cells).

Sodium bisulfite modification and Pyrosequencing Assay

Genomic DNA (500 ng) extracted from UM frozen or FFPE tissues was chemically modified with the Epitect Bisulfite kit (Qiagen, Milan, Italy) following the manufacturer instructions. The PCR and sequencing primers for BAP1 were designed with the Pyrosequencing Assay Design Software (Biotage, Uppsala, SW)) to recognize some CpG sites in the CpG island in the TSS defined as Area 1 (Ibragimova et al, 2013). The PCR primers sequences were: BAP1 Forward: 5'-Bio-GAGGGAGGGTTTGGATATG-3'; BAP1 Reverese: 5'-ATCCCCTCCTCACCTAAA-3'. The sequence of the sequencing primer was: BAP1 Sequencing primer: 5'-CCCCTCCTCACCTAAA-3'. The PCR reactions were performed using IMMOLASE™ DNA Polymerase (Bioline, Aurogene, Rome) according to according to the manufacturer instructions (95°C for 10 min followed by a three steps PCR (annealing temperature 62°C) for 45 cicles. The setup of the primers design was checked utilizing commercial bisulfite modified

DNA derived by chemically methylated and un-methylated samples (EpiTect PCR Control DNA Set, Qiagen, Milan). The resulting amplicons were subjected to pyrosequencing analysis with a SPQ 96MA instrument (Qiagen). The sequencing reactions were performed with the Pyro Gold reagent kit SPQ 96MA, according to the manufacturer instructions. The analysis was conducted with the Pyro Q-CpG software (version 1.0.9)

Mutational analysis

Polimerase Chain Reaction (PCR)

PCRs was generally carried out using 25 ng of genomic DNA on 25 μl reaction mix containing 10x Platinum PCR supermix, 1.5 mM MgCl2, 1.25 mM dNTPs, 10mM primers and 0,5U Taq Platinum (Invitrogen-Life Technologies Corporation, Monza, Italy) on a Verity 96 well thermal cycler. Thermal cycling conditions were: x1 (95°C 5 min), x35 (95°C 30s 58°C 30s 72°C 30s) x1 (72°C 7min). All PCR primers were designed with the universal M13 sequence at 5'-end: universal forward primer 5'-GTTGTAAAACGACGGCCAGT-3' and M13 reverse primer 5'-GTGTGAAATTGTTATCCGCT-3'.

A challenge was encountered in PCR primers design. We designed additional primers specific for amplification from FFPE samples because the extraction procedure usually leads to DNA fragmentation. We tested every primers pairs on control DNA extracted from blood and FFPE tissue control sample with different annealing temperature and magnesium concentration to choose the best PCR conditions. For some genes we increased the initial denaturation time and/or we added additive such as DMSO to reduce the secondary structure's development.

- **GNAQ and GNA11 PCR**

GNAQ and GNA11 mutations occur at the two known hotspots: exon 5 c.626 A>T Q209L or A>C Q209P, and exon 4 c.548 G>A R183Q. We designed two couples of PCR primers for exon 4 and exon 5 (GNAQ isoform NM_ 002072.3, GNA11 isoform NM_002067.2) (Table 7).

PCRs was carried out with 25 ng of genomic DNA on 25 μl reaction mix containing 10x Platinum PCR supermix,1.5 mM MgCl2, 1.25 mM dNTPs, 10mM

primers and 0,5U Taq Platinum (Invitrogen-Life Technologies Corporation, Monza, Italy) on a Verity 96 well thermal cycler. Thermal cycling conditions were: x1 (95°C 5 min), x35 (95°C 30s 58°C 30s 72°C 30s) x1 (72°C 7min). The PCR reaction mix also contained DMSO to reduce secondary structures development.

Table 7. GNAQ and GNA11 primers

Gene/Exon	Name	Primer sequence (5'→3')	Amplicon Size
GNAQ, exon 4	GNAQ 4F	GTGTCACTGACATTCTCATTGTG	231 Bp
	GNAQ 4R	GAGTTTACCAAATGTACTCAAGGC	
GNAQ, exon 5	GNAQ 5F	AATTGACTTGGATGATCATCGTC	233 Bp
	GNAQ 5R	TTGATCATATTCACTAAGCGCTAC	
GNA11, exon 4	GNA11 4F	AGCCGGCCTGAGCAC	212 Bp
	GNA11 4R	CAAATGAGCCTCTCAGTGCC	
GNA11, exon 5	GNA11 5F	CAGGTGGCTGAGTCCTGG	173 Bp
	GNA11 5R	TTGGCAGGTGGGGAAG	

- **BAP1 PCR**

A set of 16 couples of primers to perform the amplification in DNA extracted from fresh samples were used. A problem occurring with DNA extraction form FFPE samples is its possibly fragmentation due to the same extraction procedure, thus we designed additional FFPE primers to cover the length of longer exons. All primers used for fresh and FFPPE samples and the size of amplicons are summarized in Table 8.

PCRs was generally carried out with 25 ng of genomic DNA on 25 μl reaction mix containing 10x Platinum PCR supermix, 1.5 mM MgCl2, 1.25 mM dNTPs, 10 mM primers and 0.5U Taq Platinum (Invitrogen-Life Technologies Corporation, Monza, Italy) on a Verity 96 well thermal cycler. Thermal cycling conditions were: x1 (95°C 5 min), x35 (95°C 30s 58°C 30s 72°C 30s) x1 (72°C 7min) for all out the exon 2 which it works at 60°C of annealing temperature.

Table 8. BAP1 PCR primers

Exon	Name	Primer sequence (5'→3')	Amplicon Size
1	BAP1 1F	GAGGGCCTGGACATGGC	145 Bp
	BAP1 1R	GTCAGGCAGGCGCGTC	
2	BAP1 2F	ACGCGCCTGCCTGAC	138 Bp
	BAP1 2R	TTGAGTGAGGGCGCAGG	
3	BAP1 3F	GGGCTGTCCTTCCCTACTG	160 Bp
	BAP1 3R	CCTGTTCTCTGGGACCTTCC	
4	BAP1 4F	TGGCTGATCTGGCTCTGC	213 Bp
	BAP1 4R	CATGGCAGCATCCCACC	
5	BAP1 5F	TGACTGACCTGCTCTGGATC	200 Bp
	BAP1 5R	AGTGGCCCTCAGGGTCAG	
6	BAP1 6F_FFPE	TTTGCCTTCCACCCATAGT	169 Bp
	BAP1 6R_FFPE	CTCCCACCCCACATCAG	
7	BAP1 7F_FFPE	TTTGGGCCCTGACTCT	208 Bp
	BAP1 7R_FFPE	AGAGACACCCAACAGGC	
6-7	BAP1 6.7F	TCCACCCATAGTCCTACCTGAG	260 Bp
	BAP1 6.7R	GCTCCCTAGGAGGTAGGCAG	
8	BAP1 8F	CCTGGCCTGCCCAAAC	194 Bp
	BAP1 8R	TCCCAAAGTAGGTACAGCTCCAG	
9	BAP1 9F	CTCAACCTGATGGCGGG	234 Bp
	BAP1 9R	AATGCAGGGAGGGTTGG	
10	BAP1 10F_FFPE	CTTTCTCCTCTGAGCCCTGG	256 Bp
	BAP1 10R_FFPE	AGACATTAGCGGGTGGCTC	
	BAP1 10F	AAGGTAGAAGCCCGGGTCTAC	275 Bp
	BAP1 10R	TGTTTAGGCCTCCCATGTCAG	
11	BAP1 11.1F_FFPE	GGAGGTCCTGCCTGTGTTC	186 Bp
	BAP1 11.1R_FFPE	CTAGAAAGGCCGGCAGC	
	BAP1 11.2F_FFPE	GGTGAAGCCTCCAGGCAG	142 Bp
	BAP1 11.2R_FFPE	GCAGCCTCTCAAGAGAATCAAGT	
	BAP1 11F	GGAAGTGCTGGTTCACAGG	388 Bp
	BAP1 11R	AGCTTGACCCAGCCATG	
	BAP1 12F_FFPE	CAGCACTTGTTTGTAACTGCC	

Table 8. BAP1 PCR primers

Exon	Name	Primer sequence (5'→3')	Amplicon Size
12	BAP1 12R_FFPE	ACCTAGAACCTGGTAGCCTTAGA	207 Bp
	BAP1 12F	TAGGCTCAGCCTGGGCC	253 Bp
	BAP1 12R	GAGATATTCAGGATGGGATCCG	
13	BAP1 13.1F_FFPE	TGGTCACCTGGCCCG	163 Bp
	BAP1 13.1R_FFPE	AAGACGTTGATGGTGTTGGG	
	BAP1 13.2F_FFPE	GCCAGGGGCATTGAGC	222 Bp
	BAP1 13.2R_FFPE	GGGTGAGGGGTGCGAG	
	BAP1 13.3F_FFPE	ATTCCTCTGTCCATCAAGACTAGC	177 Bp
	BAP1 13.3R_FFPE	ATAGGCGAGCGCAGTGG	
	BAP1 13.3bisF_FFPE	CCCCAGCAATGAGAGTACAGAC	159 Bp
	BAP1 13.3bisR_FFPE	AACACGCAGCAGGCTGTC	
	BAP1 13.4F_FFPE	CTCCCACATCTCCAAGGTG	197 Bp
	BAP1 13.4R_FFPE	GGGTGCACCAAGTGGC	
	BAP1 13aF	TACTGCTGGGTATGGTCACCT	335 Bp
	BAP1 13aR	CACCTTGGAGATGTGGGAG	
	BAP1 13bF	AGCAATGAGAGTACAGACACGG	345 Bp
	BAP1 13bR	GGACACTTTGTGGTCACTTGG	
14	BAP1 14.1F_FFPE	CACTCTGATGATTTTCTTGTGACC	135 Bp
	BAP1 14.1R_FFPE	CTGCTGTCCGTGGCTTC	
	BAP1 14.2F_FFPE	ATCAGACCAATCCAAGGCAG	191 Bp
	BAP1 14.1F_FFPE	AGCTCAGGCCTTACCCTCTG	
	BAP1 14F	CCAAGTGACCACAAAGTGTCC	300 Bp
	BAP1 14R	AAGAACTTGGCACCTGGGC	
15	BAP1 15F_FFPE	GTGGGGCTTTGTTGCTG	198 Bp
	BAP1 15R_FFPE	GGGAGAGGCCAGATGAGG	
16	BAP1 16F-FFPE	AGATTGGCTCCAGTGCTCTC	168 Bp
	BAP1 16R-FFPE	AAGGACACGGCCCTCAG	
15-16	BAP1 15.16F	TAGCTGCCTATTGCTCGTGG	406 Bp
	BAP1 15.16R	GAAGGACACGGCCCTCAG	
17	BAP1 17F_FFPE	GCCAGCACCTGCTCAAG	233 Bp
	BAP1 17R_FFPE	ACACGGCAAGAGTGGGC	233 Bp

Table 8. BAP1 PCR primers			
Exon	**Name**	**Primer sequence (5'→3')**	**Amplicon Size**
17	BAP1 17F	CCTCAGCTCCTGGCCTG	311 Bp
	BAP1 17R	AGGGAAGGACCCTGGTGA	

- **EIF1AX PCR**

EIF1AX mutations occur on exon 1 and 2. To perform the amplification in DNA extracted from fresh samples, we designed two couples of PCR primers for exon 1 and exon 2 (isoform NM_001412.3). We also designed additional FFPE primers to perform the amplification in DNA extracted from FFPE samples. The primers used and the sizes of amplicons are summarized in Table 9.

Exon 2 PCR was carried out with 25 ng of genomic DNA on 25 μl reaction mix containing 10x Platinum PCR supermix, 2 mM MgCl2, 1.25 mM dNTPs, 10mM primers and 0,5U Taq Platinum (Invitrogen-Life Technologies Corporation, Monza, Italy) on a Verity 96 well thermal cycler. Thermal cycling conditions were: x1 (95°C 5 min), x35 (95°C 30s 54°C 30s 72°C 30s) x1 (72°C 7min). Exon 1 PCR conditions were slightly modified with a reaction mix containing 1.5 mM $MgCl_2$ and with 54°C of annealing temperature. For both the exons, the PCR reaction mix contained DMSO to reduce secondary structures development.

Table 9. EIF1AX primers			
Gene/Exon	**Name**	**Primer sequence (5'→3')**	**Amplicon Size**
EIF1AX, exon 1	EIF1AX 1F_FFPE	CGCTACCCGGAAAGAAGTC	146 Bp
	EIF1AX 1R_FFPE	CTGGGTGACCTGCAATCTAC	
	EIF1AX 1F	GAAAAGCGACGCAAAGAGTC	320 Bp
	EIF1AX 1R	CTGGGTGACCTGCAATCTAC	
EIF1AX, exon 2	EIF1AX 2F_FFPE	TTACAGATAATTAATGTCATTTAC CTCC	225 Bp
	EIF1AX 2R_FFPE	ATGGGCAAGACGCTGTC	
	EIF1AX 2F	GGGTAGGGAGGTGATAATGTG	406 Bp
	EIF1AX 2R	CTGTAATCGTGCCACCACAC	

- **SF3B1 PCR**

The mutation hotspots in SF3B1 occur on exon 15 (R625 and K666), primers used and the sizes of amplicons are summarized in Table 10.

PCR was carried out using 25 ng of genomic DNA on 25 μl reaction mix containing 10x Platinum PCR supermix, 1.5 mM $MgCl_2$, 1.25 mM dNTPs, 10mM primers and 0,5U Taq Platinum (Invitrogen-Life Technologies Corporation, Monza, Italy) on a Verity 96 well thermal cycler. Thermal cycling conditions were: x1 (95°C 5 min), x35 (95°C 30s 60°C 30s)x1 (72°C 7min). The PCR reaction mix also contained DMSO to reduce secondary structures development.

Table 10. SF3B1 primers

Gene/Exon	Name	Primer sequence (5'→3')	Amplicon Size
SF3B1 exon 15	SF3B1 15F	TGATTATGGAAAGAAATG GTTGAAG	191 Bp
	SF3B1 15Rint	CATGTTCAATGATTTCAA CTAAACTTC	
SF3B1 exon 15	SF3B1 15intF	TCCGTAACACAACAGCTA GAGC	217 Bp
	SF3B1 15Ru	CAACTTACCATGTTCAAT GATTTCAAC	

- **PLCB4 PCR**

The mutation hotspot in PLCB4 occurs on exon 20 (pD630Y) (isoform NM_00933). We designed one couple of primers to amplify only this exon (Table 11).

PCR was carried out with 25 ng of genomic DNA on 25 μl reaction mix containing 10x Platinum PCR supermix, 1.5 mM MgCl2, 1.25 mM dNTPs, 10mM primers and 0,5U Taq Platinum (Invitrogen-Life Technologies Corporation, Monza, Italy) on a Verity 96 well thermal cycler. Thermal cycling conditions were: x1 (95°C 5 min), x35 (95°C 30s 58°C 30s 72°C 30s) x1 (72°C 7min). The PCR reaction mix contained DMSO to reduce secondary structures development.

Table 11. PLCB4 primers			
Gene/Exon	**Name**	**Primer sequence (5'→3')**	**Amplicon Size**
PLCB4 exon 20	PLCB4 F	CAAACGGCAAATGAGTCGC	185 Bp
	PLCB4 R	CAACTGATGGGAAGTGCTGG	

- **CYSLTR2 PCR**

The mutation hotspot in CYSLTR2 occurs on exon 6 (p.L129Q) (isoform NM_020377.3) (Table 12). PCRs was carried out using 25 ng of genomic DNA on 25 μl reaction mix containing 10x Platinum PCR supermix, 1.5 mM MgCl2, 1.25 mM dNTPs, 10mM primers and 0,5U Taq Platinum (Invitrogen-Life Technologies Corporation, Monza, Italy) on a Verity 96 well thermal cycler. Thermal cycling conditions were: x1 (95°C 5 min), x35 (95°C 30s 58°C 30s 72°C 30s) x1 (72°C 7min). The PCR reaction mix also contained DMSO to reduce secondary structures development.

Table 12. CYSLTR2 primers			
Gene/Exon	**Name**	**Primer sequence (5'→3')**	**Amplicon Size**
CYSLTR2 exon 6	CYSLTR2 F	GATATTTGGAGACCTGGCCTGCA	199 Bp
	CYSLTR2 R	TGAGGAAGCCATGATAAGG	

- **PTK2B PCR**

In this gene no mutation hotspots were identified. We analyzed the gene region codifying the chinasic domain (exons 19, 20, 21, 22,23 24,25,26 and 36) and the Focal Adhesion Targeting region (FAT) (isoform NM_173174.2).

We designed thirteen pairs of primers to amplify the twelve exons (due to the length, the exon 36 was divided in two amplicons). All PCR primers are summarized in Table 13.

PCR was carried out with 25 ng of genomic DNA on 25 μl reaction mix containing 10x Platinum PCR supermix, 1.5 mM MgCl2, 1.25 mM dNTPs, 10mM primers and 0,5U Taq Platinum (Invitrogen-Life Technologies Corporation, Monza, Italy) on a Verity 96 well thermal cycler. To perform the

reaction for amplicons 20, 21, 27, 34, 36.1, thermal cycling conditions were: x1 (95°C 5 min), x35 (95°C 30s 58°C 30s 72°C 30s) x1 (72°C 7min), for amplicons 19, 22, 23, 24, 25, 26, 35 were x1 (95°C 5 min), x35 (95°C 30s 60°C 30s 72°C 30s) x1 (72°C 7min) and for amplicons 36.2 were x1 (95°C 5 min), x35 (95°C 30s 62°C 30s 72°C 30s) x1 (72°C 7min). The PCR reaction mix also contained DMSO to reduce secondary structures development.

Table 13. PTK2B primers

Gene/Exon	Name	Primer sequence (5'→3')	Amplicon Size
PTK2B exon 19	exon 19 F	GCATCTTGTCCACGGCTG	210 Bp
	exon 19 R	GTCTAGCACGAAGGGAGGAT	
PTK2B exon 20	exon 20 F	TAGAGCCTGCAGACACTCAG	212 Bp
	exon 20 R	GGAAGAGGAGTGTAAGGGAAGA	
PTK2B exon 21	exon 21 F	GGGTCCTGAACACACTCTTG	175 Bp
	exon 21 R	CCCTCTCTTCCCAGGCTG	
PTK2B exon 22	exon 22 F	GCTCCACCTGTCCCTCTT	197 Bp
	exon 22 R	CTGTGCTCTGAATGCCCC	
PTK2B exon 23	exon 23 F	GTCCCCTGGCTCCATACTG	196 Bp
	exon 23 R	CCACTCCCTCCACCCCTA	
PTK2B exon 24	exon 24 F	TTCCATCTGTCTGTCCATCTCT	264 Bp
	exon 24 R	ACTGTAGACTTCCTTCTTCTGGA	
PTK2B exon 25	exon 25 F	CAGGCTAAGGGTCTTCAGAAAG	210 Bp
	exon 25 R	CACCTTTTCATGCCCTCCC	
PTK2B exon 26	exon 26 F	CCTGACGCTCCCTTACACC	250 Bp
	exon 26 R	ACAGCCCACACTCCATGC	
PTK2B exon 27	exon 27 F	GCGTCTCACTTTGACCTAGTTT	208 Bp
	exon 27 R	TGGCTTTGCTTTGACTCACA	
PTK2B exon 34	exon 34 F	AAGAATCATTCCGTGCCCC	265 Bp
	exon 34 R	CAGTCCCCTTTCCTTCCAG	
	exon 35 F	GCCATCCTGCCCCTTTCTC	

Table 13. PTK2B primers

Gene/Exon	Name	Primer sequence (5'→3')	Amplicon Size
PTK2B exon 35	exon 35R	CTATGGTGCTGTCTGGAATGGG	137 Bp
PTK2B exon 36	exon 36.1 F	GGCCTCTCAACCTGTCCTG	170 Bp
	exon 36.2 R	GGGTGTGTGAAGCCGTCA	
	exon 36.2 F	CAGAACGCCGTGACCTCC	179 Bp
	exon 36.2 R	GGAAGACGCAGGCAGGTG	

Sequencing reaction

The PCR fragments were sequenced with direct Sanger sequencing and it was performed in 10 μl reaction mix containing BigDye® Terminator with dNTPs and a small amount of all four dideoxynucleotides labeled with fluorophores, 5X sequencing Buffer (BigDye™ Terminator v1.1 Cycle Sequencing Kit ABI PRISM®, Applied Biosyjstem) 10mM universal M13 primers on a Verity 96 well thermal cycler. Thermal cycling conditions were: 1X(95°C 1min) 20X (95°C 30sec, 60°C 3min) 1X(10°C 10min). In some difficult cases we used an higher denaturation temperature (96°C instead 95°). Sequencing data were analyzed with ABI PRISM® SeqScape® Software. SeqScape® is a software for sequencing and genetic analysis who help for variant identification and permits basecalling, sequence assembly, alignment and comparison for comparative sequencing analysis, simultaneous viewing of multiple sequences and electropherogram.

RNAscope® In Situ Hybridization Assay

The RNAscope® Assays (Advanced Cell Diagnostic ACD) is a gene expression analysis by RNA In Situ Hybridization. In situ hybridization (ISH) is a powerful research tool that can provide mechanism of gene expression changes in a specific cell population. Initially, probes containing radio labeled nucleotides were used to detect mRNA transcripts. However, the recents techniques use alternative methods of detection, such as probes labeled with digoxigenina, biotin, enzymes or fluorophores. Among some of the more recent ISH methods there is RNAscope®, a novel in situ mRNA analysis technology available also for FFPE Tissues. The ability to detect single mRNA transcripts using standard microscopy techniques is the biggest advantage of this method. This method is based on probes designed to be highly specific to the target and all steps are standardized with a reproducible protocol. We used the RNAscope protocol pretreatment specific for FFPE samples and the RNAscope® 2.5HD Reagent Kit-RED. In addition to BAP1 specific probe, we used probe PPIB as positive control probe and dapB as negative control probe. After the assay, we visualized the stained tissue sections under a standard bright field microscope

and we evaluated target probe signal. A positive signal is a pink punctate dots in cells. RNAscope® 2.5HD Reagent Kit-RED contains FAST RED dye, it is a chromogenic staining and permits high contrast.

• **RNAscope® In Situ Hybridization Assay Workflow**

Deparaffinization was performed in according to the RNA scope pretreatment protocol specific for FFPE tissue samples: 2x(10min) in histoclear and after 2x (4min) in ethanol 100%. After deparaffinization, the assay can be divided in four general steps summarized in figure 25:

- STEP 1- Permeabilization: the slides are before baked 1h at 60°C, after deparaffinized. It follows three pretreatment with the RNA-scope Pretreatment Kit to unmask target RNA and permeabilize cells. The pretreatment kit contains hydrogen peroxide to block the activity of endogenous peroxidase enzyme, target retrieval reagent and protease reagent to allow a better access to RNA target. With the IMMEDGE™ Hydrophobic barrier pen we designed a square around each section.
- STEP 2- Hybridization: RNAscope Probes pool hybridize to our RNA target of interested. The hybridization probe step is performed baking the slides 2h at 40°C. The probes has a particular double Z design and ~20 double Z are specifically designed for detecting the RNA target. Every probe pool contains a tag that permit the visualization under the microscope. In order to substantially improve the signal-to-noise ratio, this assay employs this specific probe design that permit a tandem hybridization to the target sequence (Figure 26). Each probes consists in three elements (Figure 27): a spacer sequence that links the two components of the probe, the upper region of the Z is a 14-base tail sequence, the two tails from a double Z probe pair forms a 18-25 base binding site for the pre-amplifier. Thus special double z probe design provides hybridization also against partial target RNA.
- STEP 3-Amplification**:** this step consist of six sequential hybridization of amplifiers and label probes (from AMP1 to AMP6) with the purpose to amplify the probe hybridization signal.

All the amplification are performed in the HybEZ Humidity Control Tray. The amplifications are performed as follows:

1. AMP1: 30 min at 40°C;
2. AMP2*:* 15 min at 40°C;
3. AMP3*:* 30 min at 40°C;
4. AMP4*:* 15 min at 40°C;
5. AMP5*:* 1h min at room temperature;
6. AMP6*:* 15 min at room temperature;

After the amplifications, it follows the signal detection and the counterstain**:** the slides are incubated 10 min at room temperature with a mix containing 1:60 Fast RED-B /Fast RED-A, rinsed with tap water and stained with 50% Hematoxylin staining solution for 2 min at room temperature. Lastly the slides were baked up to 45 min at 60°C and mounted with ECOmount with a previous quickly step in ethanol.

- STEP 4- visualization and evaluation the sample*:* each dot signal represents a single test target RNA molecule and can be visualized with a microscope.

Figure 25. Schematic presentation of RNAscope assay workflow (Wang et al, 2012)

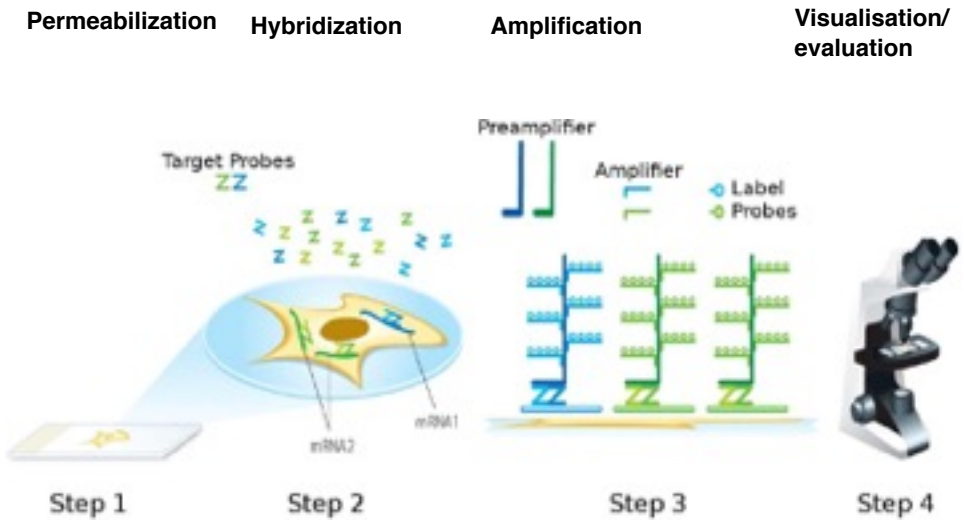

Step 1: tissue is fixed and permeabilized to allow for target probe access;

Step 2: target RNA-specific “double Z” probes are hybridized in pairs;

Step 3: multiple signal amplification molecules are hybridized. Each labeled probe is conjugated to a different fluorophore or enzyme;

Step 4: detection signal.

Figure 26. Probe tandem hybridization (Wang et al, 2012)

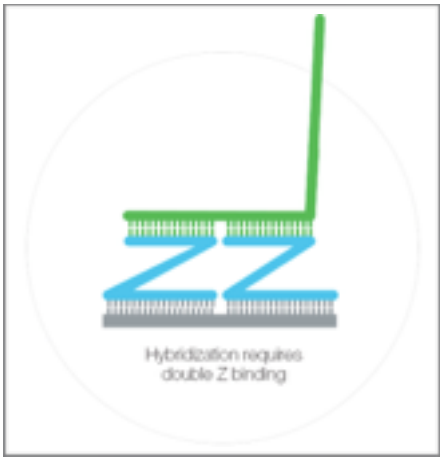

A pair of target double Z probes, each possessing a different type of tail sequences, hybridize contiguously to the target region. The two tail sequences are the hybridization site for the pre-amplifier.

Figure 27. Schematic presentation of double Z probes (Wang et al, 2012)

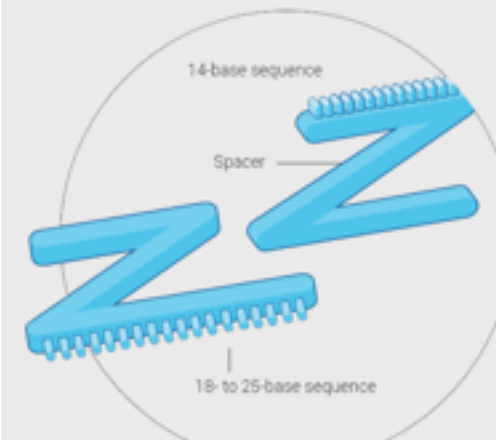

the upper region of the Z is a 14-base tail sequence;
spacer sequence that links the two components of the probe;
18 to 25 base binding sequence for the pre-amplifier.

RESULTS

Patients

Tissue samples were obtained from 63 primary UM after enucleation surgery at E.O. Galliera Hospital, Genoa, Italy, between December 2005 and June 2016. Written informed consent was obtained from all patients.

Among the 63 patients, 40 (63%) were men and 23 (37%) were women, with a median age at the time of eye enucleation of 64 years (range 28-89 years) and median follow-up time of 3 years (interquartile range, IQR: 2-6 years). Thirty-five out of 63 (56 %) patients had developed UM metastases to the liver (mean time to metastasis 25.7 months; range 0–97 months), and 13 out 60 (21,7%) died for UM metastatic progression during the follow up period. UM 34 and UM46 died for other causes. The pathological TNM stages showed stage 4c in 1case (1,8%), 4b in 6 cases (10,7%), 4a in 16 cases (28%), 4 in 5 cases (9%), 3b in 1 case (1,8%), 3a in 18 cases (32%), 3 in 1 case (1,8%), 2c in 1 case (1,8%), 2a in 6 cases (10,7%), 2 in 1 case(1,8%). The ciliary body was involved in 5/63 UM (8%) and the only choroid in 58/63 (92%) cases. The histological examination showed spindle cells in 1 case (1,6%), mixed cells in 13 cases (20,7%), epithelioid cells in 49 cases (77,7%). Extrinsecation was found in 9 out of 56 cases (16%) and for 6 cases the data is not available.

All patients' clinical data, UM histological cell type, pathological T stages, time to metastasis and follow up are summarized in Table 14.

Table 14. Patients, tumor characteristics, and follow up

Id	Age at Diagnosis (Y)	Sex	T	Cell Type	MT	Time To MT (months)	Follow up (months)	Dead
UM01	64	M	T4A	M	yes	38	38	yes
UM02	62	M	T2A	F	yes	30	30	no
UM03	69	M	T4	M	yes	24	24	yes
UM04	73	F	T2A	M	yes	93	93	no
UM05	74	M	T4C	E	yes	47	47	yes
UM06	71	F	UN	M	no	0	148	no
UM07	80	M	T4B	E	yes	29	29	yes
UM08	60	M	T2C	E	yes	97	100	no
UM09	75	F	T4A	E	yes	26	31	no
UM10	69	M	T3A	E	no	0	13	no
UM11	62	M	T4	E	yes	6	6	no
UM12	78	F	T4A	E	no	0	51	no
UM13	47	M	T3B	E	yes	25	25	yes
UM14	57	F	T4A	E	yes	14	14	UN
UM15	48	M	T3A	E	no	0	33	no
UM16	77	M	T4B	E	yes	3	3	yes
UM17	64	M	T3A	E	yes	7	21	no
UM18	85	M	UN	E	no	0	0	no
UM19	53	M	T2A	E	yes	6	13	no
UM20	78	M	T3A	E	no	0	3	no
UM21	74	M	T4	E	yes	27	27	yes
UM22	67	M	T4B	E	yes	17	17	yes
UM23	47	M	T2A	E	no	0	11	no
UM24	47	M	T3	E	no	0	41	no
UM25	40	M	T4B	E	no	0	25	no
UM26	86	M	T4A	E	yes	12	19	yes
UM27	74	M	T3A	M	UN	UN	UN	UN

Table 14. Patients, tumor characteristics, and follow up

Id	Age at Diagnosis (Y)	Sex	T	Cell Type	MT	Time To MT (months)	Follow up (months)	Dead
UM28	49	F	T3A	M	yes	25	25	no
UM29	41	M	T3A	E	no	0	28	no
UM30	81	M	UN	E	yes	40	43	no
UM31	78	F	T4A	E	no	0	28	no
UM32	63	F	T4A	E	no	0	42	no
UM33	51	F	T3A	E	yes	0	0	no
UM34	74	F	T2A	M	yes	64	64	yes
UM35	28	F	UN	M	UN	UN	UN	no
UM36	66	M	T3A	M	no	0	22	no
UM37	79	M	T3A	M	yes	17	20	yes
UM38	71	M	UN	E	yes	25	39	yes
UM39	66	F	T3A	E	no	0	21	no
UM40	66	F	T4	E	yes	6	19	no
UM41	59	M	T4A	E	no	25	25	no
UM42	83	F	T3A	E	no	0	36	no
UM43	30	M	T3A	E	no	0	23	no
UM44	75	F	UN	M	yes	11	11	no
UM45	28	F	T3A	E	yes	13	28	no
UM46	89	F	T4B	E	no	0	23	yes
UM47	47	M	T2	E	no	0	52	no
UM48	58	M	T4A	E	yes	7	7	no
UM49	41	M	T3A	E	yes	26	39	no
UM50	64	F	T4A	E	yes	6	23	no
UM51	59	M	T3A	M	no	0	8	no
UM52	35	F	T3A	E	no	0	1	no
UM53	64	F	T4A	M	no	0	22	no
UM54	71	F	T4	E	yes	22	22	no

Table 14. Patients, tumor characteristics, and follow up

Id	Age at Diagnosis (Y)	Sex	T	Cell Type	MT	Time To MT (months)	Follow up (months)	Dead
UM55	28	M	T4A	E	no	0	22	no
UM56	68	F	T4A	E	no	0	43	no
UM57	64	M	T4A	E	no	0	35	no
UM58	78	M	T4A	E	yes	0	0	UN
UM59	40	F	T4A	E	yes	26	38	no
UM60	52	M	T3A	E	yes	0	36	no
UM61	66	M	T2A	E	no	0	73	no
UM62	51	M	UN	E	yes	23	27	no
UM63	84	M	T4B	E	yes	30	34	no

Abbreviations: M, male; F, female, T, tumor stage, E, epithelioid cell; S, spindle cell; M, mixed epithelioid and spindle cells; UN, unknown.

Chromosome imbalances results (MLPA and MSA)

The presence of chromosomal imbalances involving chromosome 1p, 3, 6 and 8 in our cohort of UM samples were evaluated by MLPA analysis. MLPA was successfully carried in 60/63 (95%) UM samples but failed in UM14, UM38 and UM62. The distribution of losses on chromosome 1p, 3, 6q, 8p and gains on chromosome 8q, 6p is shown in Figure 28. Forty out of 60 (67%) samples harbored monosomy 3, 5/60 (8%) a partial monosomy 3 (Figure 29), 13/60 (22%) the loss of the short arm of chromosome 1 (1p-), 17/60 (28%) 6p gain, and 41/60 (70%) 8q gain. Partial 8q gain was found only in sample UM49, whereas a partial 6p gain was found in 6 samples. MLPA showed a concomitant loss of all probes on chromosome 6q and 8p with gain 6p and 8q suggesting an the formation of isochromosomes i(6p) and i(8q), respectively. In particular: a presumptive i(6p) was identified in 7 UM samples, of which 3 with monosomy 3 and 4 with disomy 3; a presumptive i(8q) was identified in 12 UM samples all with monosomy 3 (Figure 28 and Figure 30). In two samples with monosomy 3 (UM20 and UM41), MLPA showed both the presumptive isochromosome i(6p) and i(8q). A third sample, UM 16, MLPA showed the formation of i(8q) with loss 6q and partial 6p gain (Figure 28 and Figure 31). In UM17, in addition to 1p loss, 6p gain, 6q loss, 8q gain, MLPA showed the losses of control probes in EDAR 2p12.3, GNRHR 4q13.2, ATP7B 13q14.3, RNMT 18p11.21 (Figure 32).

In 57 UM samples, the monosomic/disomic status of chromosome 3 was also confirmed by chromosome 3 MSA. In 4 UM samples (UM2, UM20, UM33, and UM34) with a normal chromosome 3 dosage by MLPA, loss of heterozygosity (LOH) of all informative MSA markers indicated isodisomy of chromosome 3. MSA failed in UM01, UM06, UM10, UM40, UM49, and UM54.

Figure 28. Overview of chromosome imbalances, gene mutations, and metastatic progression in the 63 UM cases.

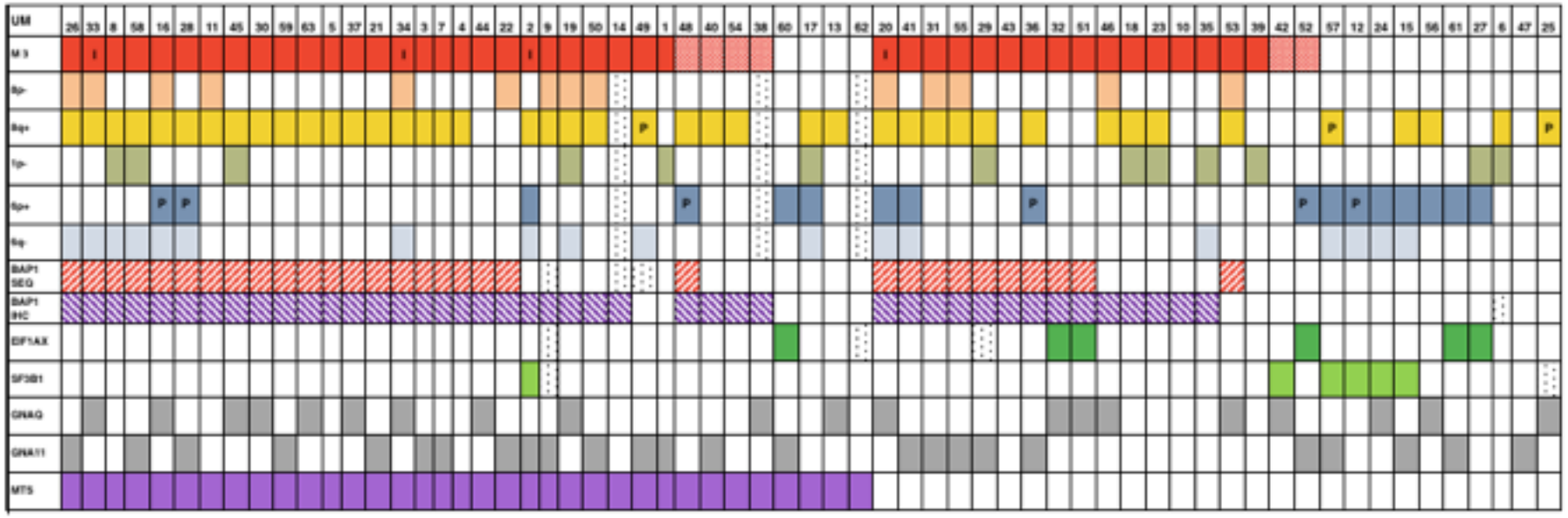

Abbr. I, isodisomy 3; P partial gain or loss.Squares in full colour indicate the presence of the specific imbalance/mutation. Squares in different colored pattern indicate the presence of mutations; color square in BAP1 IHC row indicate negative nuclear BAP1 IHC signal.

Figure 29. UM cases with partial monosomy 3 (pM3) according to MLPA data

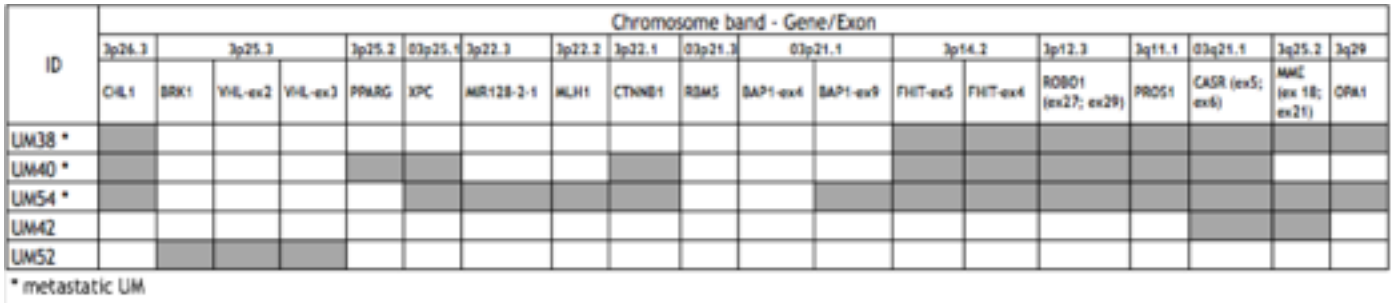

ID	Chromosome band - Gene/Exon																		
	3p26.3	3p25.3			3p25.2	03p25.1	3p22.3	3p22.2	3p22.1	03p21.3	03p21.1		3p14.2		3p12.3	3q11.1	03q21.1	3q25.2	3q29
	CHL1	BRK1	VHL-ex2	VHL-ex3	PPARG	XPC	MIR128-2-1	MLH1	CTNNB1	RBM5	BAP1-ex4	BAP1-ex9	FHIT-ex5	FHIT-ex4	ROBO1 (ex27; ex29)	PRDS1	CASR (ex5; ex6)	MME (ex 18; ex21)	OPA1
UM38 *																			
UM40 *																			
UM54 *																			
UM42																			
UM52																			

* metastatic UM

Squares in full grey color indicate monoallelic deleted probe on short or long arm of chromosome 3

[a], metastatic UM

Figure 30. UM cases identified with gains/losses on chromosome 8 according to MLPA data

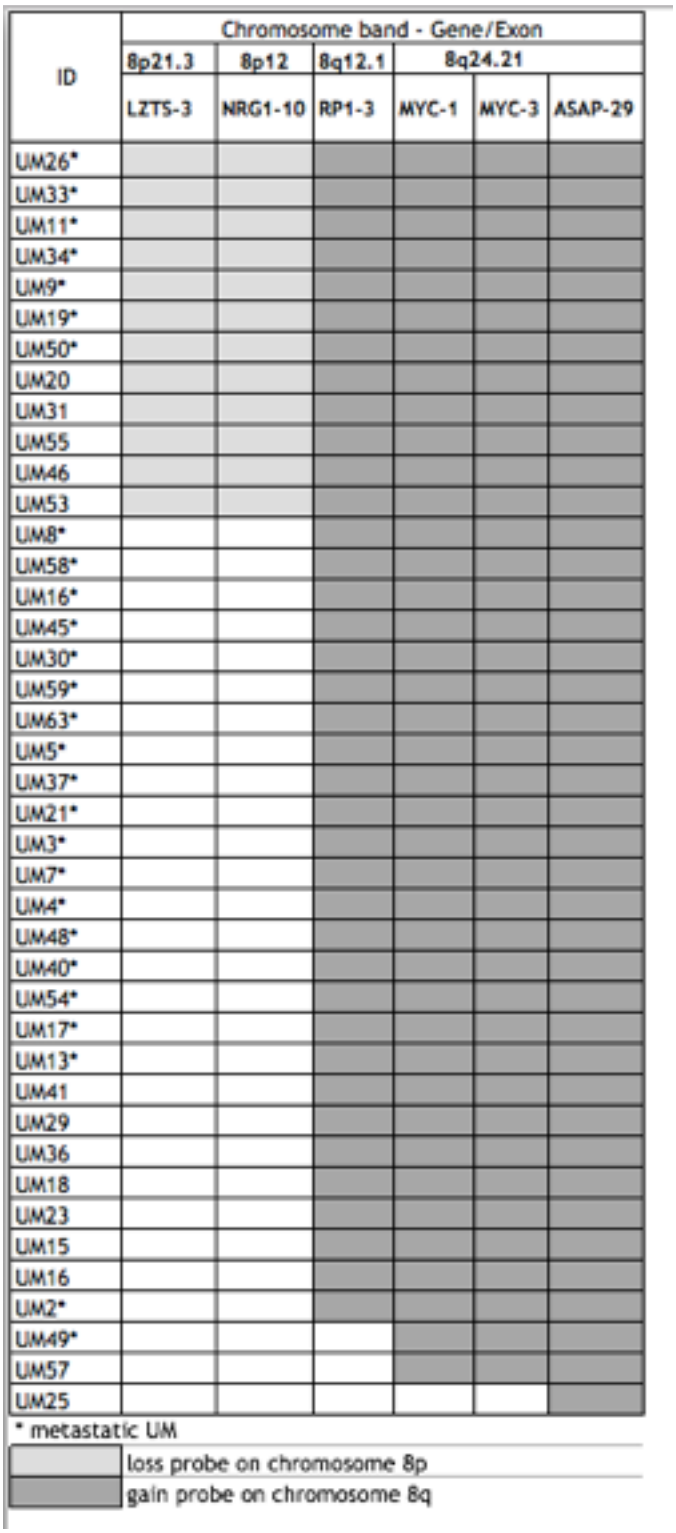

ID	Chromosome band - Gene/Exon					
	8p21.3	8p12	8q12.1	8q24.21		
	LZTS-3	NRG1-10	RP1-3	MYC-1	MYC-3	ASAP-29
UM26*						
UM33*						
UM11*						
UM34*						
UM9*						
UM19*						
UM50*						
UM20						
UM31						
UM55						
UM46						
UM53						
UM8*						
UM58*						
UM16*						
UM45*						
UM30*						
UM59*						
UM63*						
UM5*						
UM37*						
UM21*						
UM3*						
UM7*						
UM4*						
UM48*						
UM40*						
UM54*						
UM17*						
UM13*						
UM41						
UM29						
UM36						
UM18						
UM23						
UM15						
UM16						
UM2*						
UM49*						
UM57						
UM25						

* metastatic UM

loss probe on chromosome 8p

gain probe on chromosome 8q

Square in full grey color indicates deleted exon

Figure 31. UM cases identified with gains/losses on chromosome 6 according to MLPA data

ID	Chromosome band - Gene/Exon					
	6p25.2	6p22.3	6p21.2	6p21.1	6q23.2	6q25.3
	ECI2-11	DCDC2-9	CDKN1A	RUNX2-3	CTGF-5	IGF2R-3
UM2*						
UM17*						
UM20						
UM41						
UM57						
UM24						
UM28*						
UM15						
UM16*						
UM12						
UM26*						
UM33*						
UM8*						
UM58*						
UM34*						
UM19*						
UM49*						
UM35						
UM48						
UM60						
UM36						
UM52						
UM56						
UM61						
UM27						

* metastatic UM

loss probe on chromosome 6q

gain probe on chromosome 6p

Square in full grey color indicates deleted exon

Figure 32. UM17 MLPA results.

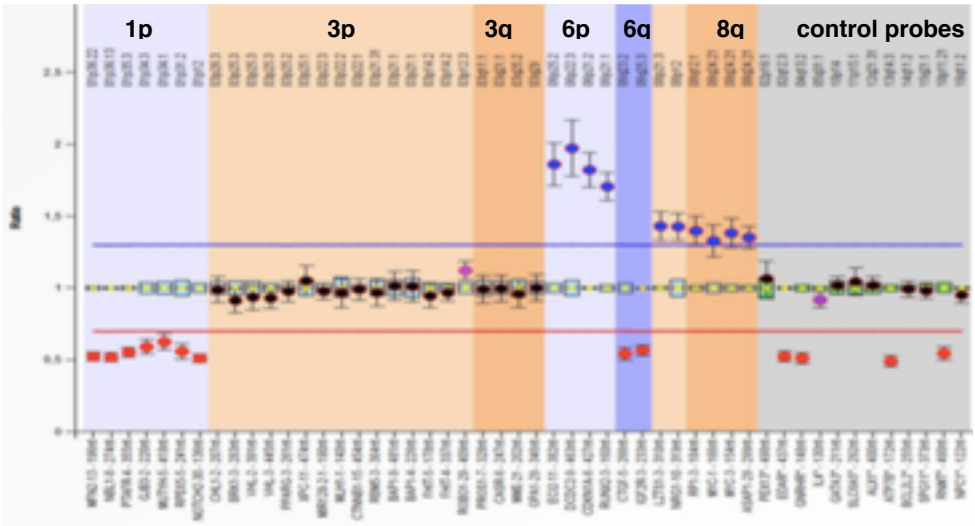

MLPA showed 1p loss, 6p gain, 6q loss, 8q gain and losses of control probes in EDAR 2p12.3, GNRHR 4q13.2, ATP7B 13q14.3, RNMT 18p11.21.

Mutational analysis results

GNAQ and GNA11 mutational analysis

GNAQ and GNA11 sequencing was successful in all 63 UM samples. Altogether, GNAQ and GNA11 mutations were detected in 55/63 samples (71,4%): GNAQ mutations were found in 20 out 63 samples (33%) and GNA11 mutations in 25/63 samples (40%). In GNAQ, all mutations are missense mutations on the two known hotspots Q209 and R183. In Q209,13/20 UM samples (65%) had the mutations c. 626 A>C p.Q209P whereas 6/20 UM samples (30%) had c.626A>T p.Q209L. In R183, 1/20 UM samples (5%) had c.547 C>T p.R183C.

Also in GNA11 all the mutations are missense mutations on the two known hotspots Q209 and R183. In Q209 hotspot, 23/25 UM samples (92%) had c. 626A>T p.Q209L whereas 2/25 (8%) had c.547 C>T p.R183C. Among the 55 GNAQ and GNA11 mutations, 26 (47%) were found in patients with metastatic disease. All the sequencing analysis results are summarized in Table 16.

BAP1 mutational analysis

BAP1 coding regions and splice sites sequencing was successful in 60/63 (95%) of UM samples. In three samples, UM14, UM19 and UM49, the sequencing failed due to poor DNA quality and/or quantity. BAP1 mutations were found in 31/60 UM samples (52%) of which 27 were with monosomy 3, 3 with isodisomy (UM33, UM34, UM20) and 1 (UM48) with partial monosomy 3 (Figure 22 and 23). BAP1 mutations were found in 8/12 (67%) UM samples with presumptive i(8q) and in a 2 out 7 (29%) UM samples with presumptive i(6p) (Figure 22). In 6 UM samples with monosomy 3 (UM16, UM28, UM31, UM36, UM43 and UM48), Sanger sequencing identified BAP1 heterozygous mutations. Thirteen out of 31 (42%) UM had in-frame mutations, consisting in 10 missense mutations and 3 in-frame deletions. To predict the possible impact of the amino acid substitutions due to the different missense mutation on the structure and function of BAP1 protein, Polyphen-2 (genetics.bwh.harvard.edu/pph2/index.shtml) and SIFT (sift.jcvi.org) were used. Out-of-frame mutations were present in 18 out of 31 (58%) UM: 13 samples had frameshift insertions/deletions, 2 samples splice site mutations, 2 samples nonsense mutations, and 1sample a read-through mutation. In 21/31 (67%) samples with BAP1 mutations, were presents metastasis. In Table 16 are summarized BAP1 sequencing results and chromosomal 3 status. Figure 34 shows the distributions of BAP1 mutations in monosomic UM cases.

Table 16. Genetic Analysis of 63 UM studied

ID	Chrom. 3 Status	Gnaq protein	Gna11 protein	exon/ intron	Mutation	BAP1 seq	Bap1 protein	IHC
UM01	pM3	wt	Q209L	wt	wt	wt	wt	pos
UM02	Iso3	wt	Q209L	wt	wt	wt	wt	neg
UM03	M3	wt	Q209L	E14	FS del	c. 1817_1821del	A606Gfs* 35	neg
UM04	M3	wt	wt	E05	del in frame	c.265_300del	N89_L100 del	neg
UM05	M3	wt	wt	E05	missense	c.290T>C	L97P	neg
UM06	D3	wt	wt	E06	syn	c.417G>A	wt (K139K)	-

Table 16. Genetic Analysis of 63 UM studied

ID	Chrom. 3 Status	Gnaq protein	Gna11 protein	exon/ intron	Mutation	BAP1 seq	Bap1 protein	IHC
UM07	M3	wt	Q209L	E17	missense	c.2089T>C	S697P	neg
UM08	M3	wt	wt	E05	del in frame	c.287_307del	L96_N102 del	neg
UM09	M3	wt	Q209L	nd	nd	nd	nd	neg
UM10	M3	wt	wt	wt	wt	wt	wt	neg
UM11	M3	wt	wt	E08	missense	c.638G>C	R213P	neg
UM12	D3	wt	wt	wt	wt	wt	wt	pos
UM13	D3	Q209P	wt	wt	wt	wt	wt	pos
UM14	M3	wt	wt	nd	nd	nd	nd	neg[b]
UM15	D3	wt	Q209L	wt	wt	wt	wt	pos
UM16	M3	Q209L	wt	E6	FS del	c.425del [a]	N142Ifs* 45	neg
UM17	D3	wt	wt	wt	wt	wt	wt	pos
UM18	M3	wt	wt	wt	wt	wt	wt	neg
UM19	M3	Q209P	wt	wt	wt	wt	wt	neg
UM20	Iso3	Q209P	wt	E11	FS del	c. 1074-1081del	A359Rfs *36	neg
UM21	M3	wt	Q209L	E4	missense	c.188C>G	S63C	neg
UM22	M3	wt	Q209L	E04	missense	c.233A>G	N78S	neg
UM23	M3	wt	wt	wt	wt	wt	wt	neg[b]
UM24	D3	Q209P	wt	wt	wt	wt	wt	pos
UM25	D3	Q209L	wt	wt	wt	wt	wt	pos
UM26	M3	wt	Q209L	E04	FS del	c.175_179del	R59Kfs* 8	neg
UM27	D3	wt	wt	wt	wt	wt	wt	pos
UM28	M3	wt	Q209L	E07	missense	c.466C>T [a]	Q156*	neg
UM29	M3	wt	R183C	Ex5	missense	c.335T>G	L112R	neg
UM30	M3	Q209P	wt	E05	del in frame	c.356_358del	T119del	neg
UM31	M3	wt	Q209L	E04	FS del	c.145del [a]	L49Cfs*23	neg
UM32	M3	Q209P	wt	E03	FS del	c.79del	V27Cfs* 45	neg

Table 16. Genetic Analysis of 63 UM studied

ID	Chrom. 3 Status	Gnaq protein	Gna11 protein	exon/ intron	Mutation	BAP1 seq	Bap1 protein	IHC
UM33	Iso3	Q209L	wt	E04	FS del	c.145del	L49Cfs*23	neg
UM34	Iso3	Q209P	wt	E13	FS del	c.1499_1515del	G500Afs*31	neg
UM35	M3	wt	wt	wt	wt	wt	wt	neg
UM36	M3	wt	Q209L	E08	missense syn	c.629T>A [a] c.627C>A [a]	I210N (V209V)	neg
UM37	M3	Q209L	wt	E05 E13	Missense syn	c.283G>C c.1356C>T	A95P (L452L)	neg
UM38	pM3	Q209P	wt	E09 E17	syn syn	c.681C>T [a] c.2163T>C [a]	(R227R) (S721S)	neg
UM39	M3	wt	wt	wt	wt	wt	wt	pos
UM40	pM3	wt	Q209L	wt	wt	wt	wt	neg[b]
UM41	M3	wt	Q209L	E05	FS ins	c.327_328insAG	P110Sfs*4	neg
UM42	pM3	R183Q	wt	wt	wt	wt	wt	pos
UM43	M3	wt	wt	I6	SA	c.438-2A>G [a]	SA	neg
UM44	M3	Q209P	wt	E17	RT	c.2189G>T	*730Lext*205	neg
UM45	M3	Q209P	wt	E09	FS del	c.760_763del	T254Yfs*2	neg
UM46	M3	Q209P	wt	wt	wt	wt	wt	neg
UM47	D3	wt	Q209L	wt	wt	wt	wt	pos
UM48	pM3	wt	wt	E11	FS del	c.967del [a]	A323Pfs*12	neg[b]
UM49	M3	wt	R183C	nd	nd	nd	nd	pos
UM50	M3	wt	Q209L	_	_	wt	wt	neg
UM51	M3	Q209P	wt	E09	FS del	c.681_697del	F228Gfs*9	neg
UM52	D3	wt	Q209L	wt	wt	wt	wt	pos
UM53	M3	Q209P	wt	E05	missense	c.281A>G	H94R	pos
UM54	pM3	wt	wt	I5	var intr NM_004656.3	c.376-4_376-15del [a]	wt	neg

Table 16. Genetic Analysis of 63 UM studied

ID	Chrom. 3 Status	Gnaq protein	Gna11 protein	exon/ intron	Mutation	BAP1 seq	Bap1 protein	IHC
UM55	M3	wt	Q209L	I5	SA	c.375+1G>A	SA	neg
UM56	D3	Q209L	wt	wt	wt	wt	wt	pos
UM57	D3	wt	Q209L	wt	wt	wt	wt	pos
UM58	M3	wt	Q209L	E07	FS del	c.503del	F168Sfs* 19	neg
UM59	M3	wt	Q209L	E01	NS	c.7A>T	K3*	neg
UM60	D3	wt	Q209L	wt	wt	wt	wt	pos
UM61	D3	wt	Q209L	wt	wt	wt	wt	pos
UM62	D3	wt	wt	wt	wt	wt	wt	pos
UM63	M3	Q209L	wt	E07	missense	c.580G>A	G194R	neg

Abbreviations: D, disomy; M, monosomy; pM, partial monosomy; Iso3, isodisomy 3; FS, frameshift; IF, in frame; NS, nonsense; RT, readthrough; syn, synonimous; E, exon; I, intron. Numbering of mutations on the genomic level refers to build GRCh37/hg19 (ensemble/ UCSC).

Figure 34. Distributions of BAP1 mutations in monosomic UM cases

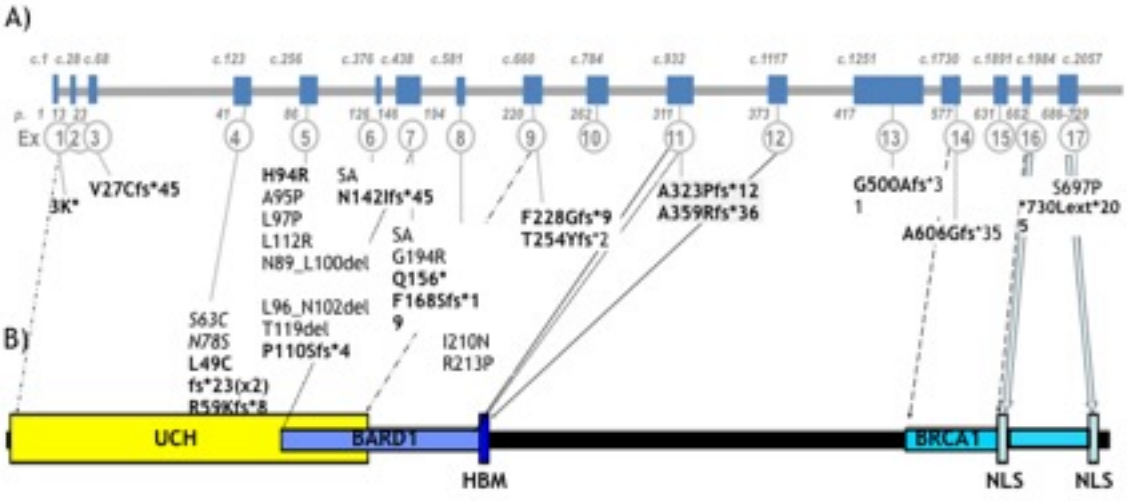

A) Structure of BAP1 gene in 17 exons, and relative mutations distribution (BAP1 - GRCh37(hg19); transcript NM_004656.3): missense and in/del in frame mutations are typed in italic, and frameshift mutations in bold. Splice indicates splice-site mutation.

B) Functional domains and regions of interaction of the 729 aa BAP1 protein, consisting of an Ubiquitin Carboxyl-terminal Hydrolase (UCH, 1-240), a BARD1 binding domain (BARD1, 182-365); an HCF-1-binding domain (HBM, 363-386), a BRCA1 binding domain (BRCA1, 594-722), and two putative Nuclear Localization Signals (NLS, 656-661 and 717-722).

Thirty-one BAP1 mutations were found and 19/31 (61%) mutations were not already reported in any other cancer, thus we submitted these mutations in NCBI GeneBank. Mutations References and GeneBank accession number of submitted BAP1 mutations were summarized in Table 17.

Table 17. Reported and unreported BAP1 mutation

ID	BAP1 seq	BAP1 protein	Reference/NCBI GeneBank accession nr.
UM03	c.1817_1821del	A606Gfs*35	MF947150
UM04	c.265_300del	N89_L100del	MF802277
UM07	c.2089T>C	S697P	MF802270
UM11	c.638G>C	R213P	MF802269
UM16	c.425del	N142Ifs*45	MF802272
UM20	c.1074-1081del	A359Rfs*36	MF947147
UM26	c.175_179del	R59Kfs*8	MF802274
UM30	c.356_358del	T119del	MF802276
UM34	c.1499_1515del	G500Afs*31	MF947149
UM36	c.629T>A c.627C>A	I210N (V209V)	MF802273
UM41	c.327_328insAG	P110Sfs*4	MF947144
UM44	c.2189G>T	*730Lext*205	MF802271
UM45	c.760_763del	T254Yfs*2	MF947145
UM48	c.976del	A323Pfs*12	MF947148
UM51	c.681_697del	F228Gfs*9	MF947146

Table 17. Reported and unreported BAP1 mutation			
ID	**BAP1 seq**	**BAP1 protein**	**Reference/NCBI GeneBank accession nr.**
UM53	c.281A>G	H94R	MF802275)
UM55	c.375+1G>A	SA	MF947151
UM58	c.503del	F168Sfs*19	MF802269
UM59	c.7A>T	K3*	MF588675

EIF1AX and SF3B1 mutational analysis

EIF1AX sequencing was successful in 60/63 (95%) UM samples. Five out of 60 (8%) UM had a missense mutation in EIF1AX gene (Figure 35a and 35b), in either exon 1 (UM32, UM52, UM60) or exon 2 (UM27, UM51). Two out of 5 EIF1AX mutations were found in cases with monosomy 3, BAP1 mutation, and loss of BAP1 nuclear immunostaining. No UM with a mutation in EIF1AX gene contained presumptive i(6p) or i(8q). All the results of EIF1AX sequencing are summarized in Table 18.

SF3B1 sequencing was successful in 61/63 (97%) samples. SF3B1 heterozygous mutations were found in 6/61 (9,8%) samples at the known hotspot R625. In R625 hotspot, 3/6 UM samples (UM02,UM12,UM57) showed c.1873 C>T p.R625C mutation and 3/6 UM samples (UM15, UM24, UM42) showed c.1874 G>A p.R625H mutation (Figure 35b and 35c). Five SF3B1 mutations occurred in non-metastatic UM with BAP1 wild type and positive BAP1 nuclear IHC, and 1/6 in metastatic UM with BAP1 wild type but with negative BAP1 nuclear IHC. Three out five UM with a mutation in SF3B1 harbored a presumptive i(6p) and 1/6 with loss 6q and partial gain 6p. No UM with mutation in SF3B1 harbored a presumptive i(8q). All the results of SF3B1 sequencing are summarized in Table 18.

Figure 35. Sequencing analysis of EIF1AX and SF3B1

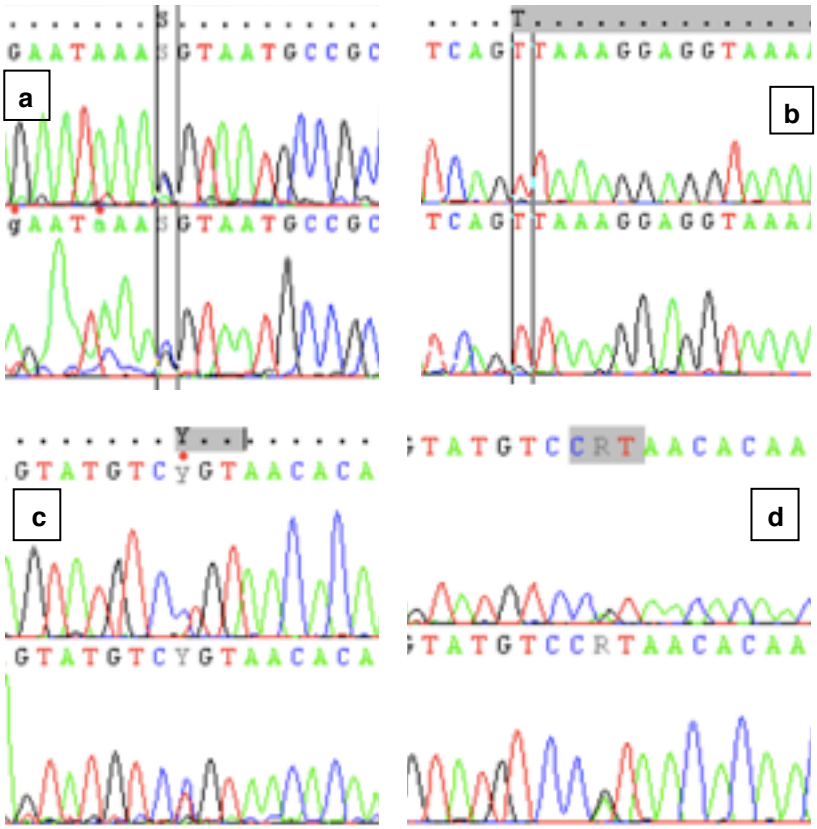

a) UM32, EIF1AX exon 1 c.16 G>C p.G6R, heterozygous;

b) UM52, EIF1AX exon 2 c.17G>T p.G6V, homozygous;

c) UM57, SF3B1 exon 15 c. 1873 C>T p.R625C, heterozygous;

d) UM24, SF3B1 exon 15 c. 1874 G>A p.R625H, heterozygous.

PLCB4, CYSLTR2 and PTK2B mutational analysis

Sanger sequencing of PLCB4, CYSLTR2 and PTK2B genes was performed in 13 UM samples, characterized by GNAQ and GNA11 wt. Due to poor DNA quality and/or quantity PLCB4 sequencing failed in two UM samples (UM05 and UM06), CYSLTR2 in 5 UM, and PTK2B in 7 UM.
In sample UM17 we detected the mutation c.1888 G>T p.D630F in PLCB4 gene. In UM05 and UM06 we identified the mutations c.2807G>A p.R936Q, and c.1625G>T p.S542I in exon 35 and in exon 23 respectively, of PTK2B gene. No mutations were found in CYLSTR2 gene. All sequencing results are summarized in Table 18.

Table 18. EIF1AX, SF3B1, PLCB4 and PTK2B sequencing analysis results

ID	Plcb4 protein	Cysltr2 protein	Ptk2b protein	Eif1ax protein	Sf3b1 protein
UM01	_	_	_	wt	wt
UM02	_	_	_	wt	R625C
UM03	_	_	_	wt	wt
UM04	wt	_	_	wt	wt
UM05	_	wt	R936Q	wt	wt
UM06	_	_	S542I	wt	wt
UM07	_	_	_	wt	wt
UM08	wt	wt	wt	wt	wt
UM09	wt	wt	_	nd	nd
UM10	wt	wt	_	wt	wt
UM11	wt	wt	wt	wt	wt
UM12	wt	wt	wt	wt	R625C
UM13	wt	wt	wt	wt	wt
UM14	_	_	_	wt	wt
UM15	wt	wt	_	wt	R625H
UM16	wt	_	_	wt	wt
UM17	D630F	wt	_	wt	wt
UM18	wt	wt	_	wt	wt

Table 18. EIF1AX, SF3B1, PLCB4 and PTK2B sequencing analysis results					
ID	**Plcb4 protein**	**Cysltr2 protein**	**Ptk2b protein**	**Eif1ax protein**	**Sf3b1 protein**
UM19	_	_	_	wt	wt
UM20	wt	_	_	wt	wt
UM21	wt	wt	_	wt	wt
UM22	wt	_	wt	wt	wt
UM23	_	_	_	wt	wt
UM24	wt	wt	_	wt	R625H
UM25	wt	_	_	wt	nd
UM26	wt	wt	wt	wt	wt
UM27	wt	wt	wt	G15N	wt
UM28	wt	wt	_	wt	wt
UM29	_	_	_	nd	wt
UM30	wt	wt	wt	wt	wt
UM31	wt	wt	_	wt	wt
UM32	wt	wt	wt	G6R	wt
UM33	wt	wt	_	wt	wt
UM34	wt	wt	_	wt	wt
UM35	_	_	_	wt	wt
UM36	wt	wt	_	wt	wt
UM37	wt	wt	_	wt	wt
UM38	_	_	_	wt	wt
UM39	wt	_	wt	wt	wt
UM40	wt	wt	wt	wt	wt
UM41	wt	wt	_	wt	wt
UM42	wt	wt	_	wt	R625H
UM43	wt	wt	wt	wt	wt
UM44	wt	wt	_	wt	wt
UM45	wt	_	_	wt	wt
UM46	wt	wt	_	wt	wt

Table 18. EIF1AX, SF3B1, PLCB4 and PTK2B sequencing analysis results

ID	Plcb4 protein	Cysltr2 protein	Ptk2b protein	Eif1ax protein	Sf3b1 protein
UM47	_	_	wt	wt	wt
UM48	wt	wt	_	wt	wt
UM49	wt	_	_	wt	wt
UM50	wt	_	_	wt	wt
UM51	wt	wt	_	G9N	wt
UM52	wt	wt	wt	G6V	wt
UM53	wt	wt	wt	wt	wt
UM54	wt	wt	_	wt	wt
UM55	wt	wt	wt	wt	wt
UM56	wt	wt	_	wt	wt
UM57	wt	wt	_	wt	R625C
UM58	wt	_	_	wt	wt
UM59	wt	wt	_	wt	wt
UM60	_	_	_	K3E	wt
UM61	wt	wt	_	wt	wt
UM62	wt	_	_	nd	wt
UM63	wt	wt	_	wt	wt

BAP1 germline mutational analysis

BAP1 coding regions and splice sites sequencing was successfully performed in 26 samples of patients with UM (Table 19). Altogether, we found BAP1 germline mutations in 2/26 (8%) samples (UM37, UM41, and UM58). In addition, in UM 37, we identified the heterozygous substitution in exon 13 c. 1356C>T that led to the synonymous mutation L452L , and in UM27 blood sample, the intronic variant c.1729+8 T>C. In UM41, we identified the heterozygous insertion in exon 5 c.327_328insAG that led to frameshift mutation p.P110Sfs*4 (Table 19 and Figure 36). In exon 11 of UM58 we identified the heterozygous substitution c.1012 C>T that led to missense mutation p.P338S. As already reported (Page 15), in UM58 we identified the mutation c.503del p F168Sfs*19 (Table 19 and Figure 36).

Table 19. Germline mutational analysis results of 27 UM studied

ID	Chrom. 3 Status	BAP1 in UM	Germline exon/intron	Germline BAP1 seq	Germline Bap1 protein
UM14	M3	wt	wt	wt	wt
UM58	M3	c.503del F168Sfs*19	E11	c. 1012 C>T	P338S
UM09	M3	wt	wt	wt	wt
UM15	D3	wt	wt	wt	wt
UM17	D3	wt	wt	wt	wt
UM19	M3	wt	wt	wt	wt
UM25	D3	wt	wt	wt	wt
UM28	M3	wt	wt	wt	wt
UM31	M3	c.145del p.L49Cfs*23	wt	wt	wt
UM33	M3	c.145del p.L49Cfs*23	wt	wt	wt
UM35	M3	wt	wt	wt	wt

Table 19. Germline mutational analysis results of 27 UM studied

ID	Chrom. 3 Status	BAP1 in UM	Germline exon/intron	Germline BAP1 seq	Germline Bap1 protein
UM37	M3	c.1356C>T p.L452L; c.283G>C p.A95P	wt	c.1356C>T	L452L
UM39	M3	wt	wt	wt	wt
UM27	D3	c.1729+8T>C[a] rs150945583		c.1729+8T>C [a]	rs150945583
UM43	M3	c.438-2A>G	wt	wt	wt
UM50	M3	wt	wt	wt	wt
UM51	M3	c.681_697del F228Gfs*9	wt	wt	wt
UM52	D3	wt	wt	wt	wt
UM56	D3	wt	wt	wt	wt
UM29	M3	c.335T>G; p.L112R	wt	wt	wt
UM36	M3	c.627C>A p.V209V c.629T>A p.I210N	wt	wt	wt
UM23	M3	wt	wt	wt	wt
UM18	M3	wt	wt	wt	wt
UM20	M3	c.1074_1081del p.A359Rfs*36	wt	wt	wt
UM41	M3	c.327_328insAG p.P110Sfs*4	E5	c.327_328insAG [a]	P110Sfs*4
UM45	M3	c.760_763del p.T254Yfs*2	wt	wt	wt

Figure 36. BAP1 mutational analysis in UM58_S and UM58

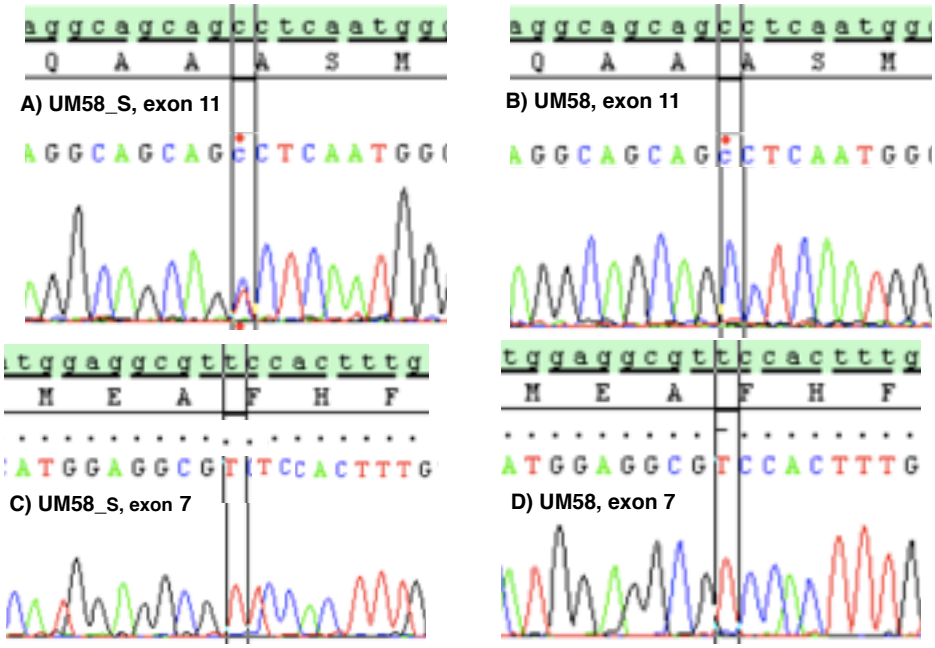

A) UM58_S: exon 11, heterozygous mutation c.1012 C>T p.P338S in UM58 blood;

B) UM58: exon 11, UM58 tumor tissue, wild type;

C) UM58_S: exon 7,wild type;

D) UM58: exon 7, UM58 tumor tissue, homozygous mutation c.503del p.F168fs*19.

BAP1 immunohistochemical assay results

BAP1 IHC was successful in 62/63 UM samples. Nineteen out 62 (31%) samples showed a positive BAP1 nuclear immunostaining (Figure 37a and 37b, respectively) and 43/62 (69%) were IHC negative (Figure 37c). In positive UM samples, BAP1 staining did not show any intratumoral heterogeneity. Among the 43 UM with negative nuclear IHC, 4 UM samples (UM14, UM23, UM40, UM48) showed a cytoplasmic signal (Table 16) and 7 UM (UM16, UM28, UM31, UM36, UM38, UM43, UM48) showed immune-cell infiltration (Figure 37d).

Figure 37. BAP1 IHC in UM FFPE sections.

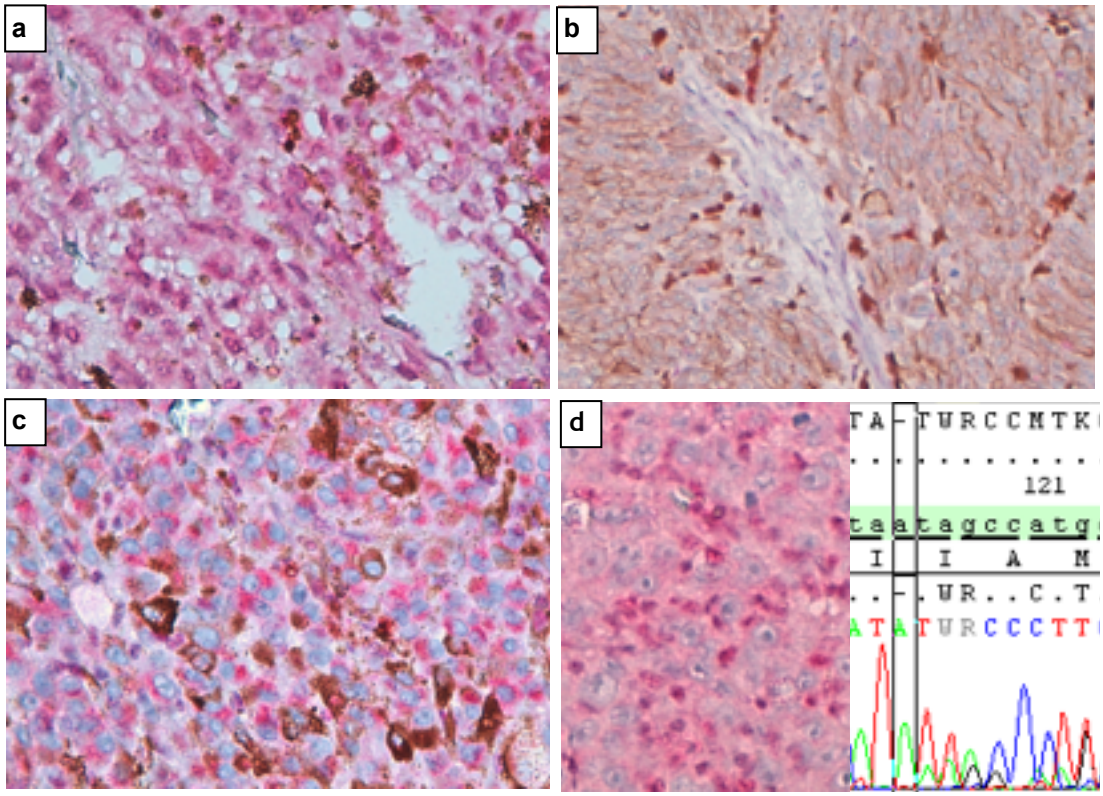

a) BAP1 positive nuclear IHC signal in UM13, characterized by disomy 3 and BAP1 wt

b) Lack of nuclear BAP1 IHC signal in UM32, with monosomy 3 and BAP1 c.79del mutation.

c) Cytoplasmic BAP1 IHC signal in UM40, characterized by a partial monosomy 3 and BAP1 wt.

d) IHC staining of UM16, a case with monosomy 3 and BAP1 c.425del mutation: tumor cells are BAP1 IHC negative, and infiltrating cells show BAP1 positive nuclear IHC signal (left panel); the electropherogram shows a heterozygous deletion (right panel).

In all the cases with negative BAP1 IHC, BAP1nuclear IHC signal in endothelial cells represents the internal positive control.

Promoter methylation analysis

BAP1 promoter methylation analysis was conducted in 3 out 11 UM samples with discrepancy between sequencing BAP1 and BAP1 IHC but no hyper-methylation was detected (Figure 38).

Figure 38. BAP1 promoter methylation analysis

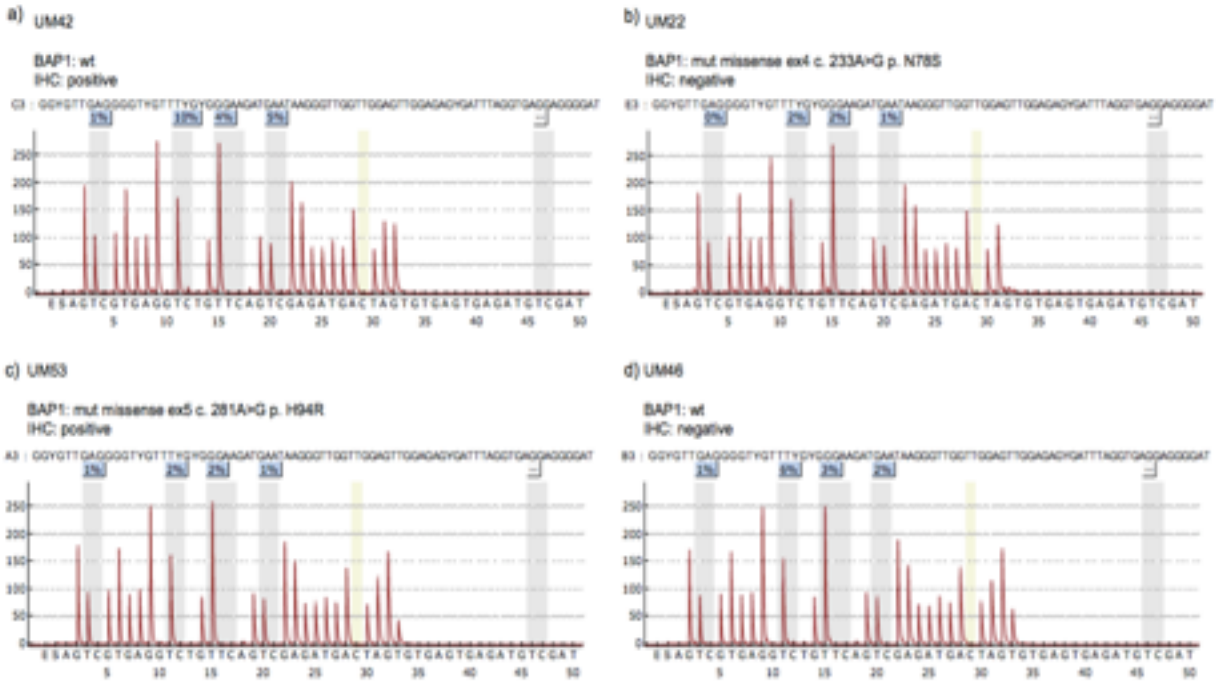

RNAscope in situ hybridization

We performed RNAscope® assay on UM samples with discrepancy between BAP1 sequencing and BAP1 IHC results: sample UM53 harboring the missense mutation H94R but with positive BAP1 nuclear immunostaining and samples UM35, UM50, UM46, UM18, UM10, UM40, and UM54, all resulting BAP1 wild-type but with negative BAP1 nuclear immunostaining.

We initially tested the RNAscope® assay by using HeLa FFPE control slides with negative control probe DapB and positive control probe PPIB, provided with the kit (Figure 39a and Figure 39b). Then we tested the assay conditions with UM FFPE sections: UM25 and UM32 were hybridized with positive control PPIB probe, negative control probe DapB, and BAP1 probe (Figure 39c, d and e).

RNAscope® assay was successful in 7/12 UM samples with with discrepancy between BAP1 sequencing and BAP1 IHC. In 1/12 sample the melanin amount was too high to evaluate the result. In 4/12 samples no FFPE blocks were available.

In Table 20 are summarized the results.

Figure 39. RNAscope assay results on control slides

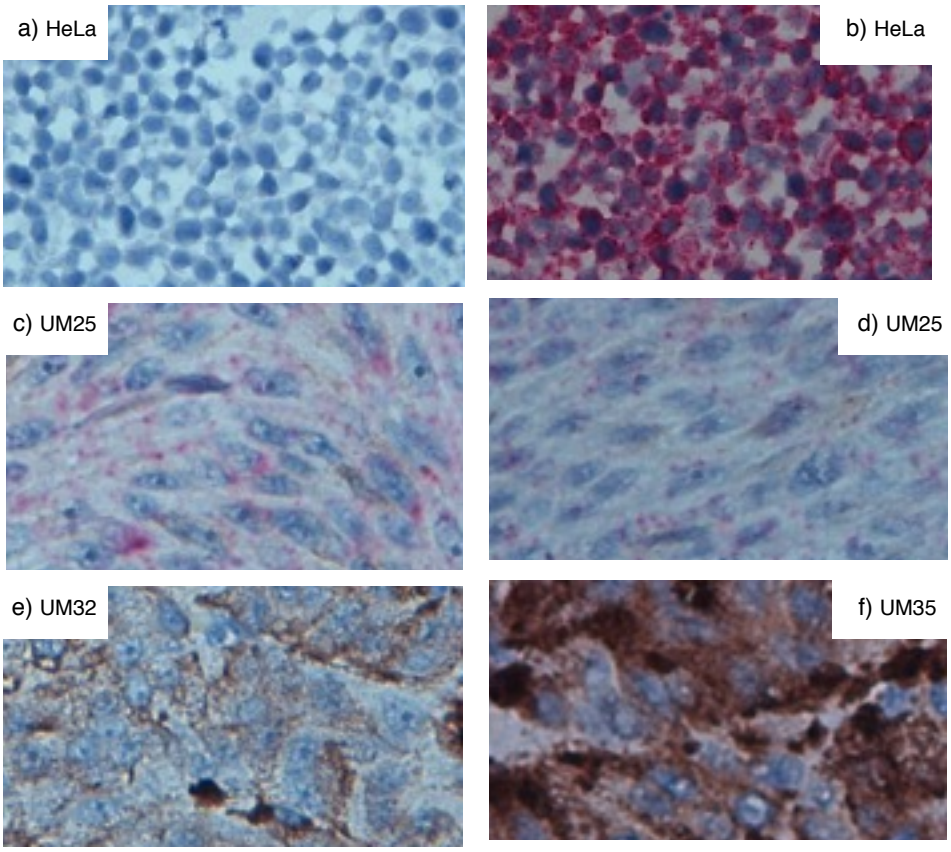

a) HeLa control slide with DapB negative control probe; b) HeLa control slide with PPIB positive control probe; c) UM25 (BAP1 wild-type and positive nuclear BAP1 IHC with PPIB positive control probe; d)UM25 (BAP1 wild-type and positive nuclear BAP1 IHC) performed with BAP1 probe; e) UM32 (missense mutation V27Cfs*45 and negative BAP1 nuclear IHC) performed with BAP1 probe; f) UM35 (BAP1 wild-type and positive nuclear BAP1 IHC) performed with BAP1 probe, plentiful presence of melanin.

All the microphotographs were taken at 40x magnification.

Table 20. RNAscope results

Sample	Chr3	BAP1 sequencing	BAP1 IHC	cytoplasmatic BAP1 signal
UM25 (control sample)	D3	wt	pos	+++
UM53	M3	H94R	pos	++
UM10	M3	wt	neg	++
UM50	M3	wt	neg	++
UM46	M3	wt	neg	+
UM40	pM3	wt	neg	-
UM18	M3	wt	neg	-
UM54	pM3	wt	neg	-
UM35	M3	wt	neg	not evaluable for the presence of melanin
UM02	M3	wt	neg	nd
UM19	M3	wt	neg	nd
UM23	M3	wt	neg	nd
UM38	M3	wt	neg	nd

MLPA P417- BAP1 results

To detect deletions not recognizable with Sanger sequencing, we performed BAP1-MLPA analysis on samples with BAP1 wt and BAP1 negative IHC (UM54, UM46, UM38, UM19, UM10, UM35, UM23, UM50, UM40, UM02, and UM18). MLPA was successfully performed in 7/11 (70%) UM, and we identified deletion of 1 or more BAP1 exon in 4 out of 7 UM samples (Figure 33 and Table 15). UM50, UM23, UM02, and UM18 samples failed, due to the poor quality or quantity of DNA.

Figure 33. UM46 sample, harboring monosomy 3, showed the deletion of exon 5.

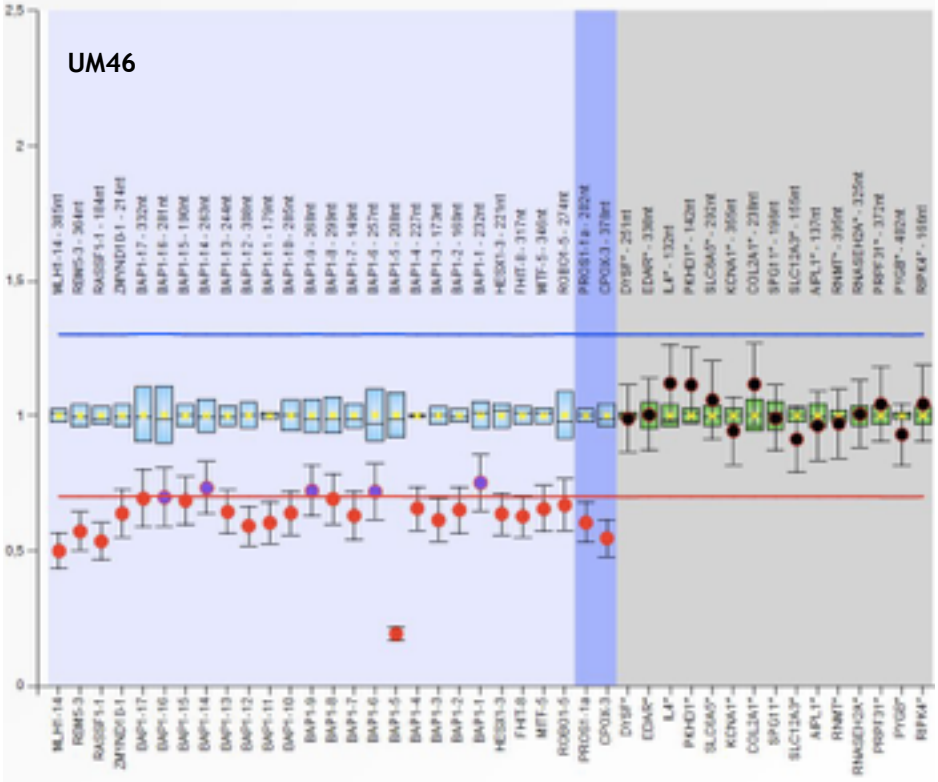

Table 15. P417-BAP1 MLPA results							
BAP1 exon	UM cases						
	UM19	UM54	UM46	UM38	UM40	UM35	UM10
Exon 17							
Exon 16							
Exon 15							
Exon 14							
Exon 13							
Exon 12							
Exon 11							
Exon 10							
Exon 9							
Exon 8							
Exon 7							
Exon 6							
Exon 5							
Exon 4							
Exon 3							
Exon 2							
Exon 1							

Squares in full dark grey color indicate deleted exons with a ratio <0.5.

Associations between mutations and distant progression free survival (DPFS)

Univariate associations between studied parameters and metastatic disease were performed using the Fisher's exact test (Table 20). Significant associations with DPFS were found for monosomy 3 (p=0.008), gain of 8q (p=0.012), BAP1 mutation (p=0.019), and loss of BAP1 protein expression (p=0.005). Conversely, gain of 6p was associated with the absence of liver metastases (p=0.019).

As regards time-to-event analysis, after a median follow-up time of 3 years (interquartile range, IQR: 2-6 years), median DPFS was 2.5 years (IQR: 1.8–7.7 years). Kaplan-Meier DPFS curves and Hazard Ratios adjusted for age, sex and tumor stage, T (Cox regression) showed that the presence of monosomy 3 was significantly associated to DPFS (HR=6.3, 95%CI: 1.5-27.2), as well as 8q gain (HR=3.6, 95%CI: 1.05-12.6), and BAP1 negative IHC (HR=4.3, 95%CI: 1.4-12.8), while the presence of BAP1 mutation was not statistically significant (HR=1.6, 95%CI: 0.7-3.8) (Figure 42).

The presence of monosomy 3 and 8q gain together was associated to metastatic disease (log rank p=0.004) (Figure 43). Since no events were registered in the group without UM specific chromosome imbalances (n=7 subjects), we could not estimate HRs by COX model.

Table 20. Association of clinical and molecular characteristics with metastasis onset.

	No MT	MT	Tot.	two-tailed P value
Sex				
M	17	23	40	P=0.79
F	11	12	23	
Position				
choroid+ciliar body	1	4	5	P=0.36
choroid	28	30	58	

Table 20. Association of clinical and molecular characteristics with metastasis onset.

	No MT	MT	Tot.	two-tailed P value
Extrinsecation				
no	26	21	47	P=0.28
yes	3	6	9	
Cell type				
epithelioid	23	26	49	P=0.55
mixed epithelioid/ fused	8	6	14	
GNAQ				
wt	19	24	43	P>.99
mut	9	11	20	
GNA11				
wt	18	20	38	P=0.61
mut	10	15	25	
BAP1 (Sanger seq)				
wt	19	10	29	P=0.019
mut	10	21	31	
BAP1 IHC				
pos	14	5	19	P=0.005
neg	14	29	43	
SF3B1				
wt	22	33	55	P=0.08
mut	5	1	6	
EIF1AX				
wt	23	32	55	P=0.16
mut	4	1	5	
Chr3 status				
D	12	4	16	P=0.008
M	16	30	46	

Table 20. Association of clinical and molecular characteristics with metastasis onset.				
	No MT	**MT**	**Tot.**	**two-tailed P value**
1p				
wt	22	25	48	P=.76
1p-	7	6	12	
6p				
wt	17	27	46	P=0.019
6p+	12	4	14	
6q				
wt	21	21	42	P=0.57
6q-	7	11	18	
8q				
wt	14	5	19	P=0.012
8q+	15	27	41	

Figure 42. Kaplan-Meier DPFS curves and Hazard Ratios

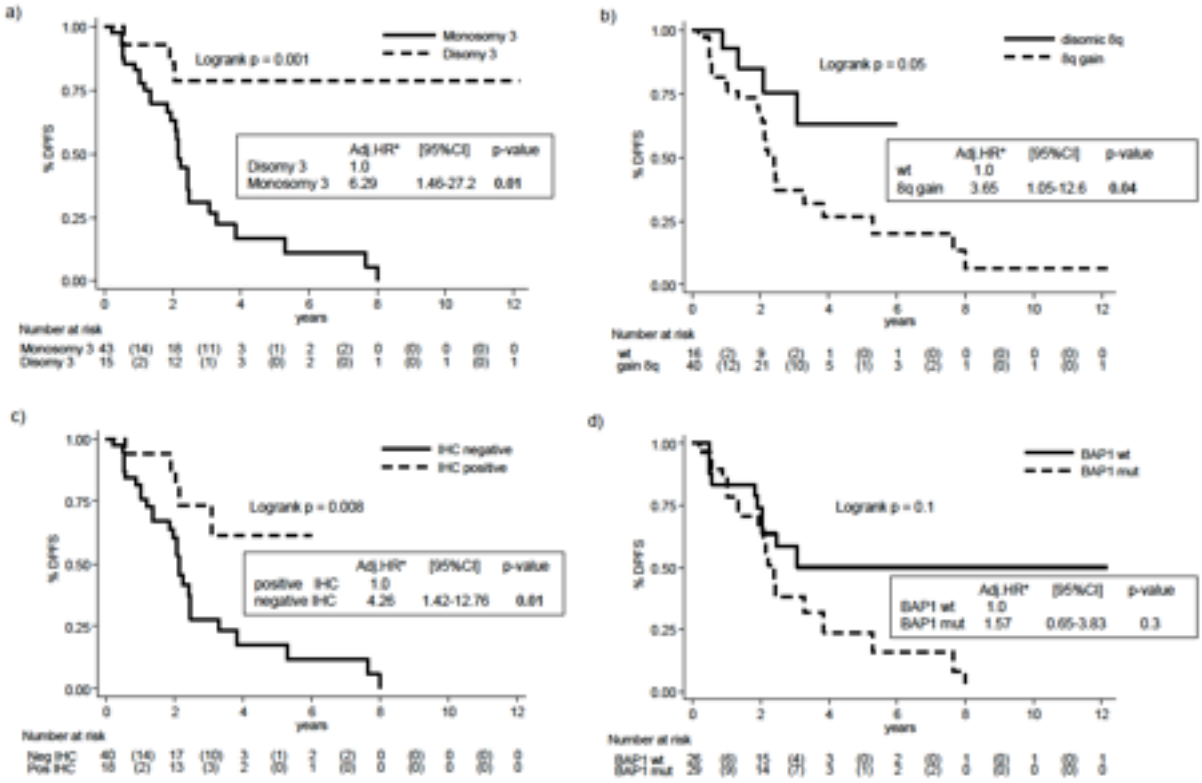

Distant Progression Free Survival (DPFS) curves and Hazard Ratios adjusted for age, sex and tumor stage (T) (Cox regression) (HR*) for:

a) chromosome 3 status (monosomy/disomy);

b) 8q status (disomic 8q/8q gain);

c) BAP1 IHC nuclear signal (positive/negative);

d) BAP1 mutation by Sanger sequencing (wt/mutated).

Figure 43. Kaplan-Meier DPFS curves and Hazard Ratios for chromosome 3 status (monosomy/disomy) and 8q status (disomic 8q/8q gain).

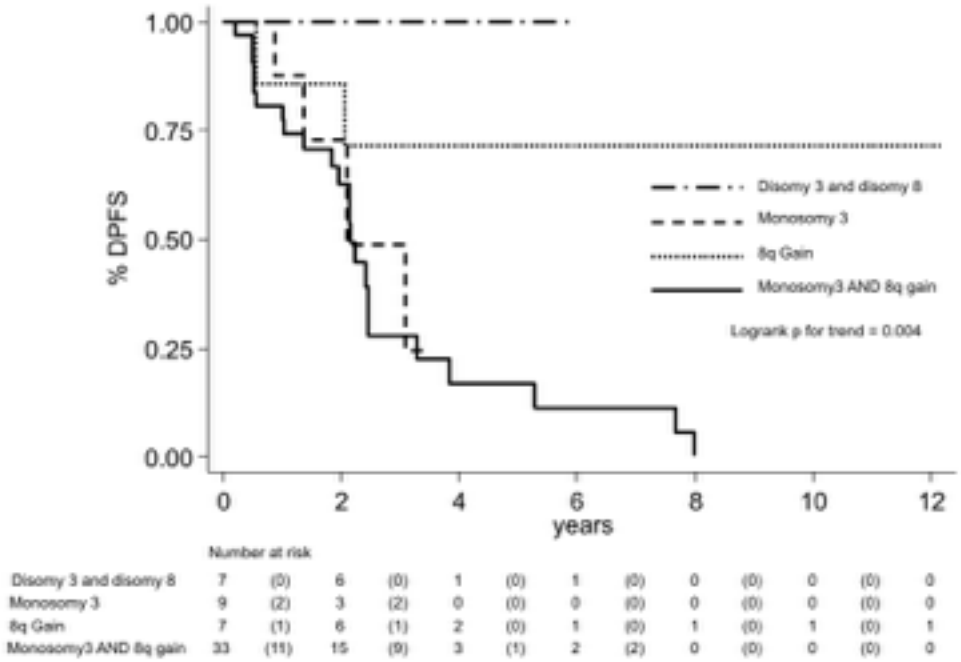

Number at risk

Disomy 3 and disomy 8	7	(0)	6	(0)	1	(0)	1	(0)	0	(0)	0	(0)	0
Monosomy 3	9	(2)	3	(2)	0	(0)	0	(0)	0	(0)	0	(0)	0
8q Gain	7	(1)	6	(1)	2	(0)	1	(0)	1	(0)	1	(0)	1
Monosomy3 AND 8q gain	33	(11)	15	(9)	3	(1)	2	(2)	0	(0)	0	(0)	0

DISCUSSION

In this study, we evaluated clinical, pathologic, and genetic features of a cohort of UM and we analyzed their associations with metastatic progression. Based on MLPA results, mutational analysis and BAP1 IHC we wanted to assess if there was a prognostic factor combination able to identify all metastatic cases.
In addition, we wanted to assess the specificity of BAP1 IHC for prognostic testing in comparison with the predictive value of the other genetic markers (i.e. monosomy 3, 8q gain, and BAP1 mutations).

Familial UM, defined as two or more family members diagnosed with UM, is estimated at less of 1% of all UM cases. BAP1 is the only gene known to contribute significant risk of UM, thus we investigated the presence, and the frequency, of BAP1 germline mutations in our UM samples blood.

Chromosomal aberrations, sequencing, and BAP1 expression

Chromosomal aberrations

Specific cytogenetic alterations are associated in UM to metastatic progression (Shields et al, 2017). According to previous results, monosomy 3 and 8q gain were found associated to metastatic UM, and 6p gain to UM with a good prognosis (Sisley et al, 1997; Patel et al, 2001; Damato et al, 2010; van den Bosch et al, 2012; Versluis et al, 2015; Bagger et al, 2017; Shields et al, 2017). Monosomy 3 together with 8q gain was found associated to metastatic disease, as already reported (Damato et al, 2010; Versluis et al, 2015). In our cases series, also monosomy 3 without 8q gain (n=9 subjects) was associated to metastases, in contrast with previous data derived from larger cohorts (Damato et al, 2010; Versluis M, et al, 2015). In addition to MLPA, MSA was used to identify cases with isodisomy 3, which carries the same prognostic significance as monosomy 3 but is not detected by MLPA, as well as by all the techniques that count the number of chromosomes, i.e. FISH and CGH (Onken et al, 2007) . In our UM case series, isodisomy 3 was found in 6% of total UM cases (9% of UM with monosomy 3), a frequency comparable to that reported in the few reports wherein two different prognostic tests have been performed on the

same tumor samples to identify isodisomy 3 (White et al, 1997; Singh et al, 2011).

Besides the 46 UM with monosomy 3, we found 5 samples with partial monosomy 3, 4 of which were metastatic. UM harboring partial monosomy 3 have already been reported by several authors, with discrepant evidences: Tschenysher et al (Tschentscher et al, 2001), and Abdel-Rahman et al (Abdel-Rahman et al, 2011), observed metastatic disease exclusively in UM with monosomy 3, while Scholes et al (Scholes et al, 2003) reported metastatic UM harboring partial monosomy 3.

A protective role of 6p gain towards metastatic progression has been supposed (Damato et al, 2010; Harbour et al, 2012). In agreement with these studies in our UM cohort 6p gain resulted associated to a good prognosis.

In our UM series MLPA showed loss of 6q and 8p with concomitant gain of 6p and 8q, suggesting the formation of an isochromosome i(6p) and i(8q), as already reported (Bastian et al, 1998, Aalto et al, 2011, Shields et al, 2017). However, mechanism(s) causing isochromosome formation are not yet known (Aalto et al, 2011). Recently, Yavuzyigitoglu et al (Yavuzyigitoglu et al, 2017) analyzed a large cohort of UM (277 UM samples) and described isocrhromosomes 6p and 8q (74%) only in samples harboring BAP1 mutations. For this reason the authors hypothesized that UM with specific mutations in BAP1,SF3B1 or EIF1AX mutations, are characterized by different mechanisms causing different types of chromosomal abnormalities. In contrast to Yavuzyigitoglu's data, we identified 3/5 i(6p) in UM harboring SF3B1 mutations, that are associated with late metastasis. This finding would suggest that there is a similar mechanism at the basis of chromosomal abnormalities in UM mutated in BAP1 or SF3B1 genes. We did not find any isochromosome in UM harboring EIF1AX mutations, confirming the hypothesis suggested by Yavuzyigitoglu of a different mechanism for chromosome aberration formation.

Sanger sequencing, BAP1 expression, and BAP1 MLPA

• GNAQ, GNA11, PLCB4, CYSLTR2 and PTK2B sequencing

In UM, GNAQ and GNA11 mutations have been found both in benign nevi and in all stages of UM, leading to suppose that they are early and crucial events in UM pathogenesis. Altogether, we found GNAQ or GNA11 mutations in 71.4% of samples, a lower frequency compared to previous studies reporting about 80-85% of GNAQ/11 mutated UM (Onken et al, 2008; van Raamsdonk et al, 2009; Harbour et al, 2010; Koopmans et al, 2013; Harbour et al, 2014; De Lange et al, 2015). The relatively small sample size could be at the basis of this difference. Recently, a very low GNAQ and GNA11 mutation rates have been observed in Greek patients (overall GNAQ/GNA11 mutation frequency 42%) and Chinese patients (overall GNAQ/GNA11 mutation frequency 38%) (Xy et al, 2014; Psinakis et al, 2017). Until now, the difference in the reported frequencies of GNAQ or GNA11 mutations among the various studies did not allows conclusions on inter-ethnic differences.

To further investigate the presence of other activating mutations able to induce MAPK pathway, we performed mutational analysis of PLCB4, CYSLTR2 and PTK2B genes in samples wild type for GNAQ or GNA11. Recently Johansson et al, and Moore et al identified novel mutations in PLCB4 and CYSLTR2 genes (Moore et al,2015; Johansson et al,2016). Another potential target of activating mutations is PTK2B, a. gene encoding a downstream protein of GPCr, whose expression level was evaluated in multiple myeloma and in glioblastoma cells (Lipinski et al, 2005; Zhang et al,2014).. Nevertheless, the putative oncogenic role of PTK2B in cancers has not been clarified yet.

Altogether, only 3/13 UM with wild type GNAQ and GNA11, showed an activating mutation in PLCB4, CYSLTR2 or PTK2B. One of these mutation was found in hotspot ...and the other two were identified in PTK2B: R936Q occurring in the FAT region, and S542I occurring in the kinase domain, and in PLCB4 1/13 UM sample harboring the mutation D630F. When we used PolyPhen-2 and SIFT to predict the possible impact of these aminoacid substitutions to the structure and function of Plcb4 and Ptk2b proteins we observed is a discrepancy between the prediction provided by the two tools, with a greater

tolerance of PolyPhen-2 than SIFT.

Considering that only 3 out of the 13 UM samples with GNAQ/GNA11 wild type harbored mutations in PTK2B or in PLCB4, it could be hypothesized that sporadic mutations could occur in other genes of the same pathway activated by GNAQ/GNA11 mutations.

- **SF3B1 and EIF1AX sequencing**

In our UM samples, SF3B1 mutations were identified in 10% of UM, a lower frequency compared to the mutation rate observed by Alsafadi et al (Alsafadi et al,2016). Recently, a mutational analysis performed in tumor DNA obtained from a large cohort of UM with a longer follow-up (20 years), showed an association between SF3B1 mutations and late metastases (Yavuzyigitoglu et al, 2016). As it could be expected, in our series Fisher's exact test did not show any association between SF3B1 mutations and metastatic risk (P=0.08): to evaluate the prognostic value of SF3B1 mutations, time-to-event analyses (i.e. Kaplan-Meier analyses), based on large cohort with a long follow-up, would be required (Yavuzyigitoglu et al, 2016).

EIF1AX mutations in UM were first described by Martin et al in tumors with disomy 3 (Martin et al,2013). Several authors (Martin et al,2013; Ewens et al, 2014; Yavuzyigitoglu et al,2016) agree with the hypothesis of correlation between EIF1AX mutations and a good prognosis, although few cases with monosomy 3 and EIF1AX mutation were reported (Ewens et al, 2014). In our UM series, we identified EIF1AX mutations in 8,2% of sequenced samples. Two out of 5 UM with EIF1AX mutation, had monosomy 3, finding already reported in the literature (Martin et al,2013). In contrast with previous studies (Martin et al, 2013; Ewens et al,2014; Yavuzyigitoglu et al,2016) EIF1AX mutations were not associated to a good prognosis, possible due to the small samples size. Also in this case, when we used PolyPhen-2 and SIFT, we could notice a remarkable discrepancy between the two prediction tools, with a general greater tolerance of PolyPhen-2 compared to SIFT.

- **BAP1 sequencing and BAP1 IHC**

The relationship between BAP1 loss and metastatic progression is reinforced by multiple independent studies (Harbour et al,2010; Luchini et al,2016). BAP1 is a tumor suppressor gene, involved in maintaining genome integrity through multiple mechanisms (Lee et al,2014; Zarrizi et al,2014; Ismail et al,2014). Until recently, it was thought that nuclear localization was required for all BAP1 functions. Recent experiments, however, showed a novel BAP1 cytoplasmic activity: wt BAP1 localizes at the endoplasmic reticulum, and has a role in promoting apoptosis via Ca2+ mitochondrial changes (Bononi et al, 2017). Moreover, it was shown that cells from individuals carrying heterozygous germline BAP1 mutations have a distinctive metabolic signature, consisting in impairment of mitochondrial respiration and increase of aerobic glycolysis leading to a Warburg effect (Bononi et al, 2017). Metastatic potential and prognosis in UM lacking BAP1 functions could be influenced also by these mechanisms, Warburg effect creating an environment that promotes tumor growth in hypoxia, and impaired apoptosis increasing the resistance to chemotherapy-induced apoptosis (Hsu et al, 2008; Cairns et al, 2011). BAP1 protein activity depends on the deubiquitinating domain and, for its nuclear activities, on nuclear localization signals. Missense mutations, which are mainly found in the UCH domain, can impair the catalytic domain (Harbour et al, 2014; Ji et al, 2014; Pan H et al, 2015). Frameshift mutations can give rise to abnormal mRNAs, subjected to nonsense-mediated RNA decay (Lykke-Andersen et al, 2015), or resulting in truncated proteins lacking the C-terminal nuclear localization signals or prone to rapid degradation (Ventii et al, 2008; Wang et al, 2016). Altogether, we found 31 BAP1 mutations in UM with monosomy/isodisomy 3. In 6 UM samples, Sanger sequencing identified heterozygous BAP1 mutations. All these samples were characterized by immune-cell infiltration, and in all of them BAP1 IHC clearly showed loss of nuclear immunosignal in UM cells, with infiltrating cells showing positive nuclear immunostaining. In these cases, a likely explanation for the observed BAP1 mutation heterozygosity could be the presence of wt BAP1 alleles from infiltrating cells, even if we cannot definitely exclude heterogeneity of BAP1 status in the tumor. Thirteen BAP1 mutations were in-frame mutations, 12 of those clustered in the region spanning exons 4 to 8 of the BAP1 gene, within

the UCH domain. In all but one case, the samples with BAP1 missense mutations were IHC negative: UM53, harboring in UCH domain the mutation H94R, predicted damaging by PolyPhen-2 and deleterious by SIFT, showed BAP1 nuclear signal. H94R could likely determine loss of UCH function while maintaining protein expression and nuclear localization. Polyphen-2 predicted as probably damaging/damaging all missense mutations. SIFT predicted as damaging all missense mutations with the exception of S697P, S63C and N78S, predicted as tolerated. We can observe a discrepancy between SIFT and Polyphen-2 prediction with a higher tolerance of SIFT.

However, it has to notice that all the 11 in-frame mutations had as consequence the loss of BAP1 protein expression, independently from functionality prediction by Polyphen2 and SIFT. These data are in agreement with previous reports, showing that the effect of missense mutations on BAP1 expression and localization is the loss of BAP1 IHC nuclear staining, and at times cytoplasmic accumulation of inactive mutated BAP1 (Ventii et al, 2008; Bhattacharya et al, 2015; Yavuzyigitoglu et al, 2016; Luchini et al, 2016). Until now, there is no a clear explanation for this phenomenon. Eighteen samples had truncating or read-through BAP1 mutations, and all showed the absence of BAP1 nuclear immunostaining. Previous studies showed that the consequence of out-of-frame mutations is the absence of BAP1 nuclear protein, with some exceptions: Koopmans (Koopmans et al, 2015) reported two hemizygous mutants harboring an out-of-frame deletion in exon 16 with a positive BAP1 staining, and Yavuzyigitoglu (Yavuzyigitoglu et al, 2016) described two UM cases (both with monosomy 3) expressing nuclear BAP1 protein despite the BAP1 nonsense mutations Q36*, and E406*, respectively. This latter finding is quite surprising, because both Q36* and E406* nonsense mutants are expected to have lost the epitope recognized by the antibody, and, in addition, they should have lost the nuclear localization signals.

Fisher's exact test showed statistically significant association between loss of BAP1 nuclear immunostaining and metastatic progression (P=0.005, Fisher's test), in agreement to previous studies (Shahet al, 2013; Koopmans et al, 2014; Szalai et al, 2017). In the literature, data about BAP1 mutations, Bap1 expression and/or Bap1 protein localization are not fully in agreement (Venti et al, 2008; Wiesner et al, 2012; Bhattacharya et al, 2015; Szalai et al, 2017). UM

cases lacking IHC BAP1 signal without BAP1 mutations were already reported (Harbour et al, 2010; Matatall et al, 2013; Yavuzyigitoglu et al, 2016; Koopmans et al, 2014), but until now no other mechanisms than mutations are known that could prevent BAP1 expression. DNA methylation, one of the key epigenetic mechanisms, was demonstrated not to be responsible for loss of BAP1 expression in cells with apparent “wt” BAP1 by Sanger sequencing (Ibragimova et al, 2013), neither considering promoter methylation or BAP1 gene body methylation (Nasu et al, 2015).

In our UM series, univariate analysis showed that chromosome 3 monosomy, 8q gain, BAP1 mutations, and loss of BAP1 nuclear immunostaining were all significantly associated with metastatic progression, in agreement with previous studies (Damato et al, 2010; Ewens et al, 2014; Koopmans et al, 2014; van de Nes et al, 2016; Szalai et al, 2017). Also Associations between imbalances/ mutations and DPFS were in agreement with previous reports (Ventii et al,2008; Patel et al, 2001; van Essen et al, 2014; Koopmans et al, 2014), with the exclusion of BAP1 mutation, which did not reach a statistically significant association. Various factors could have influenced the latter result, e.g. heterogeneity in the length of follow-up, or the relatively low statistical power which is a common bias of rare disease studies. Most importantly, however, in 11/43 (26%) UM with negative BAP1 IHC and no BAP1 mutations were found. Among the 11 cases with discrepancy between Sanger sequencing and IHC, 8 had monosomy 3 and 3 partial monosomy 3, 6/11 were metastatic (follow-up 6-39 months), 3/11 were non metastatic (follow-up 11-23 months), and 2 patients were lost to follow-up.

- **Analysis of UM cases with BAP1 wt and negative BAP1 IHC**

Van de Nes et al (van de Nes et al, 2016) showed hemizygous deletion of one or more BAP1 exons in a proportion of UM with monosomy 3, negative BAP1 IHC and BAP1 wt by Sanger sequencing, and Yoshikawa et al (Yoshikawa et al, 2016) demonstrated that the discrepancy between BAP1 IHC (negative) and BAP1 mutational status (wt) in malignant mesothelioma was due to BAP1 deletions, which were too large to be detected by Sanger sequencing. As already pointed out in Result section, in 4/7 UM cases BAP1-MLPA analysis could

identify deletion of one or more BAP1 exons (UM50, UM23, UM02, and UM18 failed). Altogether in 7 UM samples,

Two of these samples (UM40 and UM54) did not show any BAP1 mRNA signal after hybridization with RNAscope BAP1 probe, whereas one sample (UM46) showed BAP1 mRNA signal. One UM sample (UM10) with no BAP1 exon deletion, showed positive BAP1 mRNA signal. In one out of the two samples failed for BAP1-MLPA, we observed mRNA signal. In 2 UM cases (UM23, UM02), both BAP1-MLPA and RNAscope assay failed. Considering together the results obtained from BAP1-MLPA and from RNAscope assay, in 7 UM samples (UM46, UM10, UM02, and UM23) we did not have clarified the discrepancy between BAP1 wild type and negative BAP1 IHC, than further studies are required to understand if post-transcriptional mechanisms that may inhibit Bap1 protein expression in samples with BAP1 wild type occur.

Germline BAP1 mutations

*G*ermline BAP1 mutations were reported in less than 1% of UM patients in UK (Aoude et al, 2013; Soura et al, 2016) in association with a novel hereditary cancer syndrome, described as *BAP1* -TPDS.

Altogether, we found BAP1 germline mutations in 2/26 of examined samples

In UM58 case, we identified the missense mutation P338S, not detected in UM tumor tissue, where the mutation F168Sfs*19 has been observed. This evidence could be explained because during UM progression, the chromosome 3 harboring the germline mutation P338S was lost and the remaining allele developed the somatic mutation F168Sfs*16. In UM37 case we identified the synonymous mutation L452L, also found in UM. In addition, in UM sample we identified the mutation p.A95P. We could suppose that during tumor progression BAP1 wild type allele was lost and the remaining allele, already harboring the germline synonymous mutation L452L, developed the missense mutation A95P. In UM41 case we identified the frameshift mutation P110Sfs*4. The intronic variant c.1729+8 T>C in UM27 case was already reported in association with BAP1 tumor predisposition syndrome, and it has been described in ClinVar and refSNP with the ID rs150945583. This intronic variant has been described in ClinVar and Human Splicing Finder online software as benign, although ESEFinder, a tool of ALAMUT software, predicted a possible effect at nearest splice site.

There are some limitations of our mutational analysis. We have no personal and family history of the patients, therefore we cannot speculate if UM in patients harboring germline BAP1 mutation, was part of BAP1-TPDS or if it was a de novo event. This mutational analysis was performed in a limited number of samples than previous reports (Abdel-Rahaman et al,2013; Betti et al, 2016; O Shea et al 2016), thus our result did not has statistic significance: is our purpose to expand the number of samples analyzed for BAP1 germline mutations.

Conclusion

In our UM samples, we did not found a prognostic factor combination in common to all metastatic cases. Indeed, 4 out of 63 (6%) samples (samples UM13, UM17, UM60 and UM62) resulted with disomy 3, BAP1 wild-type and IHC positive (evaluated as good prognosis), developed liver metastasis. Among these four samples, only UM17 showed high instability with loss of four MLPA control probes. Among the metastatic UM, only one case (UM60) showed as unique imbalance the indicator of good prognosis 6p gain. It is known that rare UM with disomy 3 can develop metastases, but there is no evidence on possibly involved metastatic pathway(s). Damato et al, and Abdel-Rahman et al (Damato et al,2010; Abdel-Rahman et al 2011) reported metastatic disease occurring in UM with partial monosomy 3. Also Shields et al and Yonekawa et al reported unusual high frequency of metastasizing disomy 3 tumors (Shields et al, 2011; Yonekawa Y et al, 2014). A possible explanation given to justify this finding, was the use of different molecular techniques and different sampling methodologies. Indeed, the authors (Shields et al, 2011; Yonekawa Y et al, 2014) hypothesized that FNAB increase the chance to aspirate tissue with tumor heterogeneity.

Although many studies have reported quite large numbers of UM cases, those that have given a detailed mutational and cytogenetic analysis are indisputably fewer. In this view, this study gives a contribution in defining the genetic UM landscape.

Traditionally the various clinical and histopathologic tumor characteristics, are necessary for the assessment of prognosis for UM. The recently findings, established that for prognostication, loss of BAP1 protein expression, monosomy 3 and 8q gain represent the strongest, with important consequences for the implementation of a more intensive patient surveillance and adjuvant therapy. To date, no effective pharmacological therapies are available to treat UM and metastatic UM. Until recently, the possibility to use target cancer therapy has been hampered by the lack of known mutations, but now the knowledge is improving with the discovery of high frequency mutations in recurrent genes. Nonetheless, our work suggests that further studies are necessary to identify other driving mutations able to activate MAP kinase

pathways and to promote UM progression, important findings that could lead to better understand the UM pathogenesis.

The identification of mutations involved in UM pathogenesis could likely lead to better therapeutic strategies to treat UM and metastatic UM. The strong association between BAP1 mutations and metastatic risk, suggests that the pharmacological targeting of BAP1 mutations may be of therapeutic significance. In light of BAP1 role in histone modifications, HDAC inhibitors (histone deacetylases) were recently tested in UM cell lines but further studies to investigate the therapeutic potential of HDAC in tumors lacking BAP1 expression are required. Several adjuvant trials targeting the driver mutations identified in UM are registered at the clinical trials service of the National Institute of Health (clinicaltrials.gov). In particular, ClinicalTrials.gov lists 69 trials for metastatic UM.

In our study we assessed BAP1 status through sequencing analysis of 17 exons and near splice sites, and we evaluate BAP1 protein expression through BAP1 IHC. Sanger direct sequencing is an expensive and long- lasting technique and a big amount of DNA is necessary, not always available. Conversely, BAP1 IHC is a rapid and cost-effective method to evaluate BAP1 functional status. In our research we found a strong correlation between negative BAP1 IHC and metastatic disease risk, so in a future BAP1 immunoistochemistry analysis should be implemented in the routine histopathological examination of UM.

The validity of all these observations must be assessed in properly designed clinical trials. Further studies, concerning the identification and molecular characterization of mutations, involved in UM pathogenesis and tumor progression, could be helpful to define the more aggressive UM, taking advantages in patient care and clinical practice.

REFERENCES

- Aalto Y, Eriksson L, Seregard S, et al. Concomitant loss of chromosome 3 and whole arm losses and gains of chromosome 1, 6, or 8 in metastasizing primary uveal melanoma. Invest Ophthalmol Vis Sci. 2001 Feb;42(2):313-7;
- Abdel-Rahman MH, Christopher BN, Faramawi MF, et al. Frequency, molecular pathology and potential clinical significance of partial chromosome 3 aberrations in uveal melanoma. Mod Pathol. 2011 Jul;24(7):954-62;
- Abdel-Rahman MH, Pilarski R, Cebulla CM, et al. Germline BAP1 mutation predisposes to uveal melanoma, lung adenocarcinoma, meningioma, and other cancers. J Med Genet. 2011 Dec;48(12):856-9;
- Albino AP, Fountain JW. Molecular genetics of human malignant melanoma. Cancer Trat 1 Res 993 65: 201-255;
- Alsafadi S, Houy A, Battistella A, et al. Cancer-associated SF3B1 mutations affect alternative splicing by promoting alternative branchpoint usage. Nat Commun. 2016 Feb 4;7:10615;
- Amaro A, Gangemi R, Piaggio F, et al. The biology of uveal melanoma. Cancer Metastasis Rev. 2017 Mar;36(1):109-140;
- Aoude LG, Wadt K, Bojesen A et al. A BAP1 mutation in a Danish family predisposes to uveal melanoma and other cancers. PLoS One. 2013 Aug 19;8(8):e72144;
- Aoyama T, Mastrangelo MJ, Berd D, et al. Protracted survival after resection of metastatic uveal melanoma.Cancer. 2000 Oct 19)
- Atzpodien J, Terfloth K, Fluck M,et al. Cisplatin, gemcitabine and treosulfan is effective in chemotherapy-pretreated relapsed stage IV uveal melanoma patients. Cancer Chemother Pharmacol. 2008;62:685–688;
- Bastian BC, LeBoit PE, Hamm H, et al. Chromosomal gains and losses in primary cutaneous melanomas detected by comparative genomic hybridization. Cancer Res. 1998 May 15;58(10):2170-5;
- Battaglia A. The Importance of Multidisciplinary Approach in Early Detection of BAP1 Tumor Predisposition Syndrome: Clinical Management and Risk Assessment. Clin Med Insights Oncol.2014 Apr 28; 8:37-47;
- Bauer J, Kilic E, Vaarwater J, et al. Oncogenic GNAQ mutations are not correlated with disease-free survival in uveal melanoma. Br J Cancer. 2009 Sep 1;101(5):813-5.

- Bhatia S, Moon J, Margolin KA, et al. Phase II trial of sorafenib in combination with carboplatin and paclitaxel in patients with metastatic uveal melanoma: SWOG S0512. PLoS One. 2012;7:e48787;
- Bhattacharya S, Hanpude P, Maiti TK. Cancer associated missense mutations in BAP1 catalytic domain induce amyloidogenic aggregation: A new insight in enzymatic inactivation. Sci Rep. 2015 Dec 18;
- Biankin AV, Waddell N, Kassahn KS, et al. Pancreatic cancer genomes reveal aberrations in axon guidance pathway genes. Nature. 2012 Nov 15;491(7424):399-405;
- Bingham V, McIlreavey L, Greene C, et al. RNAscope in situ hybridization confirms mRNA integrity in formalin-fixed, paraffin-embedded cancer tissue samples. Oncotarget. 2017 Oct 16;8(55):93392-93403;
- Bishop KD, Olszewski AJ. Epidemiology and survival outcomes of ocular and mucosal melanomas: a population-based analysis. Int J Cancer. 2014 Jun 15;134(12):2961-71.
- Bononi A, Yang H, Giorgi C et al. Germline BAP1 mutations induce a Warburg effect. Cell Death Differ. 2017 Oct;24(10):1694-1704.
- Buder K, Gesierich A, Gelbrich G, et al. Systemic treatment of metastatic uveal melanoma: review of literature and future perspectives. Cancer Med. 2013;2:674–686;
- Cairns RA, Harris IS, Mak TW. Regulation of cancer cell metabolism. Nat Rev Cancer. 2011 Feb;11(2):85-95;
- Callender GR. Malignant melanotic tumors of the eye: a study of histologic types in 111 cases. Trans Am Acad Ophtalmol Otolaryngol.1931; 36:131-142;
- Carbone M, Ferris LK, Baumann F, et al. BAP1 cancer syndrome: malignant mesothelioma, uveal and cutaneous melanoma, and MBAITs. J Transl Med. 2012 Aug 30;10:179. doi:10.1186/1479-5876-10-179.
- Carbone M, Flores EG, Emi M et al. Combined Genetic and Genealogic Studies Uncover a Large BAP1 Cancer Syndrome Kindred Tracing Back Nine Generations to a Common Ancestor from the 1700s. PLoS Genet. 2015 Dec 18;11(12):e1005633;
- Carbone M, Yang H, Pass HI, et al. BAP1 and cancer. Nat Rev Cancer. 2013 Mar;13(3):153-9;

- Carvajal RD, Sosman JA, Quevedo JF, et al. Effect of selumetinib vs chemotherapy on progression-free survival in uveal melanoma: a randomized clinical trial. JAMA. 2014;311:2397–2405;
- Cassoux N, Rodrigues MJ, Plancher C, et al.Genome-wide profiling is a clinically relevant and affordable prognostic test in posterior uveal melanoma. Br J Ophthalmol. 2014 Jun;98(6):769-741;
- Chang AE, Karnell LH, Menck HR. The National Cancer Data Base report on cutaneous and noncutaneous melanoma: a summary of 84,836 cases from the past decade. The American College of Surgeons Commission on Cancer and the American Cancer Society. Cancer. 1998 Oct 15;83(8):1664-78;
- Chattopadhyay C, Kim DW, Gombos DS, et al. Uveal melanoma: From diagnosis to treatment and the science in between. Cancer. 2016 Aug 1; 1;122(15):2299-312;
- Clarke LE, Warf MB, Flake DD 2nd, et al. Clinical validation of a gene expression signature that differentiates benign nevi from malignant melanoma. J Cutan Pathol. 2015 Apr;42(4):244-52;
- Coupier I, Cousin PY, Hughes D, Legoix-Né P, Trehin A,et al. BAP1 and breast cancer risk. Fam Cancer. 2005;4(4):273-7;
- Coupland SE, Lake SL, Zeschnigk M, et al. Molecular pathology of uveal melanoma. Eye (Lond). 2012 Feb;27(2):230-42;
- Cross NA, Ganesh A, Parpia M, et al. Multiple locations on chromosome 3 are the targets of specific deletions in uveal melanoma. Eye. 2006 Apr;
- Damato B, Dopierala J, Klaasen A, et al. Multiplex ligation-dependent probe amplification of uveal melanoma: correlation with metastatic death. Invest Ophthalmol Vis Sci 2009; 50(7): 3048–3055;
- Damato B, Catherine Duke, Sarah E, et al. Cytogenetics of uveal melanoma: a 7-year clinical experience. Ophthalmology. 2007 Oct;114(10):1925-31;
- Damato B, Dopierala JA, Coupland SE. Genotypic profiling of 452 choroidal melanomas with multiplex ligation-dependent probe amplification. Clin Cancer Res 2010 Dec 15;16(24):6083-92;
- Damato B. Progress in the management of patients with uveal melanoma. The 2012 Ashton Lecture. Eye. 2012; 26(9): 1157–1172;
- Daou S, Hammond-Martel I, Mashtalir N, et al. The BAP1/ASXL2 Histone H2A Deubiquitinase Complex Regulates Cell Proliferation and Is Disrupted in Cancer. The Journal of Biological Chemistry. 2015;290(48):28643-28663;

- de la Cruz PO Jr, Specht CS, McLean IW: Lymphocitic infiltration in uveal malignant melanoma. Cancer 1990;65:112-115;
- De Lange MJ, van Pelt ST, Varsluis M, et al. Heterogeneity revealed by integrated genomic analysis uncovers a molecular switch in malignant uveal melanoma. Oncotarget. 2015 Nov 10; 6(35):37824-35;
- Diener-West M, Reynolds SM, Agugliaro DJ, et al Collaborative Ocular Melanoma Study Group. Development of metastatic disease after enrollment in the COMS trials for treatment of choroidal melanoma: Collaborative Ocular Melanoma Study Group Report No. 26. Arch Ophthalmol. 2005 Dec;123(12): 1639-43;
- Edge SE, Bryd DR, Compton CA, et al. Ophtalmic Oncology Task Force. Malignant Melanoma of the Uvea. AJCC Cancer Staging Manual, 7th ed Springer; 2010:547-559;
- Ehlers JP, Worley L, Onken MD, et al. Integrative genomic analysis of aneuploid in uveal melanoma. Clinic Cancer Res. 2008 1;14(1):115-22;
- Epping MT, Bernards R. A causal role for the human tumor antigen preferentially expressed antigen of melanoma in cancer. Cancer Res. 2006 Nov 15;66(22):10639-42;
- Epping MT, Wang L, Edel MJ, et al. The human tumor antigen PRAME is a dominant repressor of retinoic acid receptor signaling. Cell. 2005 Sep 23;122(6): 835-47;
- Ewens KG, Kanetsky PA, Richards-Yutz J, et al. Genomic profile of 320 uveal melanoma cases: chromosome 8p-loss and metastatic outcome. Invest Ophtalmol Vis Sci 2013; 54:5721-9;
- Ewens KG, Kanetsky PA, Richards-Yutz J,et al. Chromosome 3 status combined with BAP1 and EIF1AX mutation profile are associated with metastasis in uveal melanoma. Invest Ophthalmol Vis Sci. 2014 Jun 26;55(8): 5160-7;
- Feng X, Chen Q, Gutkind JS. Oncotargeting G proteins: The Hippo in the room. Oncotarget.2014 Nov 30;5(22):10997-9;
- Feng X, Degese MS, Iglesias-Bartolome R, et al. Hippo-independent activation of YAP by the GNAQ uveal melanoma oncogene through a trio-regulated rho GTPase signaling circuitry. Cancer Cell. 2014 Jun 16;25(6): 831-45;

- Field MG, Decatur CL, Kurtenbach S, et al. PRAME as an Independent Biomarker for Metastasis in Uveal Melanoma. Clin Cancer Res. 2016 Mar 1;22(5):1234-42;
- Field MG, Harbour JW. Recent developments in prognostic and predictive testing in uveal melanoma. Curr Opin Ophthalmol. 2014 May;25(3):234-9;
- Folberg R, Rummelt V, Parys-Van, et al. The prognostic value of tumor blood vessel morphology in primary uveal melanoma. Ophthalmology. 1993 Sep; 100(9):1389-98;
- Folberg R, Hendrix MJ, Maniotis AJ. Vasculogenic mimicry and tumor angiogenesis. Am J Pathol. 2000 Feb;156(2):361-81;
- Folkman J. Angiogenesis in cancer, vascular, rheumatoid and other diseases. Nature Med 1995;1:27-31;
- Fountain JW, Bale SJ, Housman DE, et al. Genetics of melanoma. Cancer Surv. 1990;9(4):645-71;
- Fredericks AM, Cygan KJ, Brown BA,et al. RNA-Binding Proteins: Splicing Factors and Disease. Biomolecules. 2015 May 13;5(2):893-909;
- Furney SJ, Pedersen M, Gentien D, et al. SF3B1 mutations are associated with alternative splicing in uveal melanoma. Cancer Discov. 2013 Oct;3(10): 1122-1129;
- Garinis GA, Paltrinos GP, Spanakis NE, et al. DNA Hypermethylation: When tumor suppressor genes go silent. Hum Genet 2002; 111:115-127;
- Golas MM, Sander B, Will CL, et al. Molecular architecture of the multiprotein splicing factor SF3b. Science. 2003 May 9; 300(5621):980-4;
- Griffin CA, Long PP, Schachat AP. Trisomy 6p in an ocular melanoma. Cancer Genet Cytogenet 1988; 32(1): 129–132;
- Guénard F, Labrie Y, Ouellette G, et al. INHERIT BRCAs. Genetic sequence variations of BRCA1-interacting genes AURKA, BAP1, BARD1 and DHX9 in French Canadian families with high risk of breast cancer. Journal of human genetics. 2009;54(3):152-161;
- Gupta MP, Lane AM, DeAngelis MM, et al. Clinical Characteristics of Uveal Melanoma in Patients With Germline BAP1 Mutations. JAMA Ophthalmol. 2015 Aug;133(8):881-7;
- Hanahan D, Weiberg RA. Hallmarks of cancer. The next generation. Cell 2011; 144(5):646-674;
- Hanahan D, Weiberg RA. The hallmarks of cancer. Cell 2000 ; 100(1): 5770;

- Harbour JW, Chao DL. A molecular revolution in uveal melanoma: implications for patient care and targeted therapy. Ophthalmology. 2014 Jun;121(6): 1281-8;
- Harbour JW, Onken MD, Roberson ED, et al. Frequent mutation of BAP1 in metastasizing uveal melanomas. Science. 2010 Dec 3;330(6009):1410-3;
- Harbour JW, Roberson EDO, Anbunathan H, et al. Recurrent mutations at codon 625 of the splicing factor SF3B1 in uveal melanoma. Nature genetics 2013;45(2):133-135;
- Harbour JW. A prognostic test to predict the risk of metastasis in uveal melanoma based on a 15-gene expression profile. Methods Mol Biol. 2014;1102:427-40;
- Harbour JW. The genetics of uveal melanoma: an emerging framework for targeted therapy. Pigment Cell Melanoma Res. 2012 Mar;25(2):171-8;
- Hausler T, Stang A, Anastassiou G, et al. Loss of heterozygosity of 1p in uveal melanomas with monosomy 3. Int J Cancer 2005; 116(6): 909–913;
- Helgadottir H, Höiom V. The genetics of uveal melanoma: current insights. The Application of Clinical Genetics. 2016;9:147-155;
- Horsman DE, White VA. Cytogenetic analysis of uveal melanoma. Consistent occurrence of monosomy 3 and trisomy 8q. Cancer 1993; 71(3): 811–819;
- Hsu PP, Sabatini DM. Cancer cell metabolism: Warburg and beyond. Cell. 2008 Sep 5;134(5):703-7;
- Hughes S, Damato BE, Giddings I, et al. Microarray comparative genomic hybridisation analysis of intraocular uveal melanomas identifies distinctive imbalances associated with loss of chromosome 3. Br J Cancer 2005; 93(10): 1191–1196;
- Ibragimova I, Maradeo ME, Dulaimi E, et al. Aberrant promoter hypermethylation of PBRM1, BAP1, SETD2, KDM6A and other chromatin-modifying gene is absent or rare in clear cell RCC. Epigenetics. 2013 May; 8(5):486-93;
- Inamdar GS, Madhunapantula SV, Robertson GP. Targeting the MAPK pathway in melanoma: why some approaches succeed and other fail. Biochem Pharmacol. 2010 Sep 1;80(5):624-37;
- Janssen CS, Sibbett R, Henriquez FL, et al. The T1799A point mutation is present in posterior uveal melanoma. Br J Cancer. 2008 N. 18;99(10):1673-7;

- Johansson P, Aoude LG, Wadt K, et al. Deep sequencing of uveal melanoma identifies a recurrent mutation in PLCB4. Oncotarget. 2016 Jan 26;
- Johnson CP, Kim IK, Esmaeli B, et al. Systematic genomic and translational efficiency studies of uveal melanoma. PLoS One. 2017 Jun 8;12(6):e0178189;
- Kadariya Y, Cheung M, Xu J, et al. Bap1 Is a Bona Fide Tumor Suppressor: Genetic Evidence from Mouse Models Carrying Heterozygous Germline Bap1 Mutations. Cancer Res. 2016 May 1;76(9):2836-44;
- Kilic E, Naus NC, Van Gils W, et al. Concurrent loss of chromosome arm 1p and chromosome 3 predicts a decreased disease-free survival in uveal melanoma patients. Invest Ophthalmol Vis Sci 2005 46, 2253-7;
- Koopmans AE, Vaarwater J, Paridaens D, et al. Patient survival in uveal melanoma is not affected by oncogenic mutations in GNAQ and GNA11. BR J Cancer. 2013 Jul 23; 109(2): 493-6;
- Koopmans AE, Verdijk RM, Brouwer RW, et al. Clinical significance of immunohistochemistry for detection of BAP1 mutations in uveal melanoma. Mod Pathol. 2014 Oct;27(10):1321-30;
- Ladanyi M, Zauderer MG, Krug LM, et al. New strategies in pleural mesothelioma: BAP1 and NF2 as novel targets for therapeutic development and risk assessment. Clin Cancer Res. 2012 Sep 1;18(17):4485-90;
- Landis CA, Masters SB, Spada A, et al. GTPase inhibiting mutations activate the ά chain of Gs and stimulate adenylyl cyclase in human pituitary tumors. Nature 1989; 340, 692-696;
- Lipinski CA, Tran NL, Menashi E, et al. The Tyrosine Kinase Pyk2 Promotes Migration and Invasion of Glioma Cells. Neoplasia 2005;7(5):435-445;
- Luchini C, Veronese N, Yachida S, et al. Different prognostic roles of tumor suppressor gene BAP1 in cancer: A systematic review with meta-analysis. Genes Chromosomes Cancer. 2016 Oct;55(10):741-9;
- Lyons J, Landis CA, Harsh G, et al. Two G protein oncogenes in human endocrine tumors. Science. 1990 Aug 10;249(4969):655-9;
- Lykke-Andersen S, Jensen TH. Nonsense-mediated mRNA decay: an intricate machinery that shapes transcriptomes. Nat Rev Mol Cell Biol. 2015 Nov; 16 (11): 665-677
- Maat W, Kilic E, Luyten GP, et al. Pyrophosphorolysis detects B-RAF mutations in primary uveal melanoma. Invest Ophthalmol Vis Sci. 2008 Jan; 49(1):23-7;

- Malcovati L., Papaemmanuil E, Bowen DT, et al. Clinical significance of SF3B1 mutations in myelodysplasic syndromes and myelodysplasic/ myeloproliferative neoplasm. Blood 2011; 118:6239-46: Mar;89(3):285-94;
- Mariani P, Piperno-Neumann S, Servois V, et al. Surgical management of liver metastases from uveal melanoma: 16 years' experience at the Institut Curie. Eur J Surg Oncol. 2009;35:1192–1197;
- Martin M, Maßhöfer L, Temming P, et al. Exome sequencing identifies recurrent somatic mutations in EIF1AX and SF3B1 in uveal melanoma with disomy 3. Nature genetics. 2013;45(8):933-936;
- Matatall KA, Agapova OA, Onken MD, et al. BAP1 deficiency causes loss of melanocytic cell identity in uveal melanoma. BMC Cancer. 2013 Aug 5;13:371;
- McLaughlin CC, Wu XC, Jemal A, et al. Incidence of non cutaneous melanomas in the U.S. Cancer. 2005 Mar 1;103(5):1000-7;
- McLean IW, Foster WD, Zimmerman LE, et al. Modifications of Callender's classification of uveal melanoma at the Armed Forces Institute of Pathology. Am J Ophthalmol. 1983 Oct;96(4):502-9;
- McLean. Tumors of the Eye and Ocular Adnexa .1995, AFIP Atlas of Tumor Pathology Third Series, Fascicle 12;
- McNamara M, Felix C, Davison EV, et al. Assessment of chromosome 3 copy number in ocular melanoma using fluorescence in situ hybridization. Cancer Genet Cytogenet 1997; 98(1): 4–8;
- Merbs SL, Sidransky D. Analysis of p16 (CDKN2/MTS-1/INK4A) alterations in primary sporadic uveal melanoma. Invest Ophthalmol Vis Sci. 1999 Mar; 40(3):779-83;
- Moore AR, Ceraudo E, Sher JJ, et al. Recurrent activating mutations of G-protein-coupled receptor CYSLTR2 in uveal melanoma. Nat Genet. 2016 Jun; 48(6):675-80;
- The Collaborative Ocular Melanoma Study Group COMS report no. 4. Mortality in patients with small choroidal melanoma. 1997 Jul; Arch Ophthalmol 115(7):886-93;
- Murali R, Wiesner T, Scolyer RA. Tumours associated with BAP1 mutations. Pathology. 2013 Feb; 45(2):116-26;
- Nasu M, Emi M, Pastorino S et al, High incidence of somatic BAP1 alterations in sporadic malignant mesothelioma. J Thorac Oncol. 2015 Apr;10(4):565-76;

- Ness C, Garred O, Eide NA, et al. Multicellular tumor spheroids of human uveal melanoma induce genes associated whit anoikis resistance, lipogenesis, and SSXs. Mol Vis. 2017 Oct 3; 23:680-694;
- Nichols EE, Richmond A, Daniels AB. Disparities in Uveal Melanoma: Patient Characteristics. Semin Ophthalmol. 2016;31(4):296-303;
- Nichols EE, Richmond A, Daniels AB. Tumor Characteristics, Genetics, Management, and the Risk of Metastasis in Uveal Melanoma. Semin Ophthalmol. 2016;31(4):304-9;
- Njauw CN, Kim I, Piris A, et al. Germline BAP1 inactivation is preferentially associated with metastatic ocular melanoma and cutaneous-ocular melanoma families. PLoS One. 2012;7(4):e35295;
- O'Hayre M, Degese MS, Gutkind JS. Novel insights into G protein and G protein-coupled receptor signaling in cancer. Curr Opin Cell Biol. 2014 Apr; 27:126-35;
- Ohta M, Berd D, Shimizu M, et al. Deletion mapping of chromosome region 9p21-p22 surrounding the CDKN2 locus in melanoma. Int J Cancer. 1996 Mar 15;65(6):762-7;
- Olsen DS, Savner EM, Mathew A, Zhang F, Krishnamoorthy T, et al. Domains of eIF1A that mediate binding to eIF2, eIF3 and eIF5B and promote ternary complex recruitment in vivo. EMBO J. 2003 Jan 15;22(2):193-204:
- Onken MD, Ehlers JP, Worley LA,et al. Functional gene expression analysis uncovers phenotypic switch in aggressive uveal melanomas. Cancer Res. 2006 May 1;66(9):4602-9;
- Onken MD, Worley LA, Char DH,et al. Collaborative Ocular Oncology Group report number 1: prospective validation of a multi-gene prognostic assay in uveal melanoma.Ophthalmology. 2012 Aug;119(8):1596-603;
- Onken MD, Worley LA, Dávila RM, et al. Prognostic testing in uveal melanoma by transcriptomic profiling of fine needle biopsy specimens. J Mol Diagn. 2006 Nov;8(5):567-73;
- Onken MD, Worley LA, Ehlers JP, et al. Gene expression profiling in uveal melanoma reveals two molecular classes and predicts metastatic death. Cancer Res.2005 Oct 15;64(20):7205-9;
- Onken MD, Worley LA, Long MD, et al. Oncogenic mutations in GNAQ occur early in uveal melanoma. Invest Ophthalmol Vis Sci. 2008 Dec;49(12): 5230-4;

- Onken MD, Worley LA, Person E, et al. Loss of heterozygosity of chromosome 3 detected with single nucleotide polymorphisms is superior to monosomy 3 for predicting metastasis in uveal melanoma. Clin Cancer Res. 2007 May 15;13(10):2923-7;
- Ophthalmic Oncology Task Force. Local Recurrence Significantly Increases the Risk of Metastatic Uveal Melanoma. Ophthalmology. 2016 Jan;123(1): 86-91;
- O'Shea SJ, Robles-Espinoza CD, McLellan L,et al. A population-based analysis of germline BAP1 mutations in melanoma. Hum Mol Genet. 2017 Feb 15;26(4):717-728;
- Pan H, Jia R, Zhang L, et al. BAP1 regulates cell cycle progression through E2F1 target genes and mediates transcriptional silencing via H2A monoubiquitination in uveal melanoma cells. Int J Biochem Cell Biol. 2015 Mar;60:176-84;
- Papadopoulos S, Benter T, Anastassiou G, et al. Assessment of genomic instability in breast cancer and uveal melanoma by random amplified polymorphic DNA analysis. Int J Cancer 2002 99, 193-200;
- Parrella P, Fazio VM, Gallo AP, et al. Fine mapping of chromosome 3 in uveal melanoma: identification of a minimal region of deletion on chromosomal arm 3p25.1-p25.2. Cancer Res. 2003 Dec 1;
- Parrella P, Sidransky D, Merbs SL. Allelotype of posterior uveal melanoma implications for a bifurcated tumor progression pathway. Cancer Res. 1999;
- Parrella P, Caballero OL, Sidransky D, et al. Detection of c-myc amplification in uveal melanoma by fluorescent in situ Hybridaization. Invest Ophtalmol Vis Sci 2001; 42,1679-1684;
- Patel KA, Edmondson ND, Talbot F et al. Prediction of prognosis in patients with uveal melanoma using fluorescence in situ hybridisation. Br J Ophthalmol. 2001 Dec;85(12):1440-4;
- Peña-Llopis S, Vega-Rubín-de-Celis S, Liao A, et al. BAP1 loss defines a new class of renal cell carcinoma. Nat Genet. 2012 Jun 10;44(7):751-9;
- Pilarski R, Cebulla CM, Massengill JB,et al. Expanding the clinical phenotype of hereditary BAP1 cancer predisposition syndrome, reporting three new cases. Genes Chromosomes Cancer. 2014 Feb;53(2):177-82;

- Pilarski R, Rai K, Cebulla C,et al. BAP1 Tumor Predisposition Syndrome. 2016 Oct 13 In: Adam MP, Ardinger HH, Pagon RA, Wallace SE, Bean LJH, Stephens K, Amemiya A, editors. GeneReviews®;
- Popova T, Hebert L, Jacquemin V, et al. Germline BAP1 mutations predispose to renal cell carcinomas. Am J Hum Genet. 2013 Jun 6;92(6):974-80;
- Prescher G, Bornfeld N, Friedrichs W, et al. Cytogenetics of twelve cases of uveal melanoma and patterns of nonrandom anomalies and isochromosome formation. Cancer Genet Cytogenet. 1996 Mar;80(1):40-6;
- Prescher G, Bornfeld N, Hirche H, et al. Prognostic implications of monosomy 3 in uveal melanoma. Lancet. 1996 May 4;347(9010):1222-5;
- Prescher G, Bornfeld N, Horsthemke B, et al. Chromosomal aberrations defining uveal melanoma of poor prognosis. Lancet 1992; 339(8794): 691–692;
- Psinakis F, Katseli A, Koutsandrea C, et al. Uveal Melanoma: GNAQ and GNA111 Mutations in a Greek Population. Anticancer Res. 2017 oct; 37(10): 5719-5726;
- Rai K, Pilarski R, Boru G, et al. Germline BAP1 alterations in familial uveal melanoma. Genes Chromosomes Cancer. 2017 Feb;56(2):168-174;
- Rai K, Pilarski R, Cebulla CM, et al. Comprehensive review of BAP1 tumor predisposition syndrome with report of two new cases. Clin Genet. 2016 Mar; 89(3):285-94;
- Romano E, Schwartz GK, Chapman PB,et al. Treatment implications of the emerging molecular classification system for melanoma. Lancet Oncol. 2011 Sep;12(9):913-22;
- Rowley, D. A new consistent chromosomal abnormality in chronic myelogenus leukemia identified by quinacrime fluorescence and Giemsa staining. Nature 1973 243: 290-293;
- Scholes AG, Damato BE, Nunn J, et al. Monosomy 3 in uveal melanoma: correlation with clinical and histologic predictors of survival.Invest Ophthalmol Vis Sci. 2003 Mar;44(3):1008-1;
- Shah AA, Bourne TD, Murali R. BAP1 protein loss by immunohistochemistry: a potentially useful tool for prognostic prediction in patients with uveal melanoma. Pathology. 2013 Dec;45(7):651-6;

- Shields CL, Ganguly A, Bianciotto CG, et al. Prognosis of uveal melanoma in 500 cases using genetic testing of fine-needle aspiration biopsy specimens. Ophthalmology. 2011 Feb;118(2):396-401;
- Shields CL, Kaliki S, Furuta M, et al. American Joint Committee on Cancer Classification of Uveal Melanoma (Anatomic Stage) Predicts Prognosis in 7,731 Patients: The 2013 Zimmerman Lecture. Ophthalmology. 2015 Jun; 122(6):1180-6;
- Shields CL, Kaliki S, Furuta M, Fulco E, Alarcon C, Shields JA. American Joint Committee on Cancer classification of posterior uveal melanoma (tumor size category) predicts prognosis in 7731 patients. Ophthalmology. 2013 Oct; 120(10):2066-71;
- Shields CL, Say EAT, Hasanreisoglu M, et al. Cytogenetic Abnormalities in Uveal Melanoma Based on Tumor Features and Size in 1059Patients: The 2017 W. Richard Green Lecture. Ophthalmology.;
- Shoushtari AN, Carvajal RD. GNAQ and GNA11 mutations in uveal melanoma.Melanoma Res. 2014 Dec;24(6):525-34;
- Simpson ER, Gallie BL, Saakyan S, et al. AJCC Ophthalmic Oncology Task Force. International Validation of the American Joint Committee on Cancer's 7th Edition Classification of Uveal Melanoma. JAMA Ophthalmol. 2015 Apr; 133(4):376-83;
- Singh, A.D., Croce, C.M., Wary,K.K., et al. Familial Uveal Melanoma: Absence of Germline mutations involving the Cyclin dependent Kinase-4 inhibitor gene. Ophtalmic genet. 17,39-40 1996;
- Singh AD, Turell ME, Topham AK. Uveal melanoma: trends in incidence, treatment, and survival. Ophthalmology. 2011 Sep;118(9):1881-5;
- Singh AD. Uveal melanoma: implications of tumor doubling time. Ophthalmology. 2001 May;108(5):829-31.
- SinghAD, Borden EC. Metastatic Uveal Melanoma. Ophtalmol Clin North Am. 2005;18:143-140;
- Sisley K, Rennie IG, Parsons MA, et al. Abnormalities of chromosome 3 and 8 in posterior uveal melanoma correlate with prognosis; Genes Chromosomes Cancer. 1997 May;19(1):22-8;
- Sisley K, Parsons MA, Garnham J, et al. Association of specific chromosome alterations with tumor phenotype in posterior uveal melanoma. Br J Cancer. 2000 Jan;82(2):330-8;

- Soufir N, Bressac-de Paillerets B, Desjardins L, et al. Individuals with presumably hereditary uveal melanoma do not harbour germline mutations in the coding regions of either the P16INK4A, P14ARF or cdk4 genes. Br J Cancer. 2000 Feb;82(4):818-22;
- Soura E, Eliades P, Shannon K, et al. Hereditary Melanoma: Update on Syndromes and Management - Emerging melanoma cancer complexes and genetic counseling. Journal of the American Academy of Dermatology. 2016;74(3):411-420;
- Spencer W.H. Ophthalmic Pathology, an Atlas-Textbook. 4th Edition, Saunders;

Szalai E, Wells JR, Ward L, et al. Uveal Melanoma Nuclear BRCA1-Associated Protein-1 Immunoreactivity Is an Indicator of Metastasis. Ophthalmology. 2017 Aug 17. pii: S0161-6420(17)31332-5;

- Tarlan B, Kıratlı H. Uveal Melanoma: Current Trends in Diagnosis and Management. Turkish Journal of Ophthalmology. 2016;46(3):123-137;

Te Raa GD, Derks IA, Navrkalova V, et al. The impact of SF3B1 mutations in CLL on the DNA-damage response. Leukemia. 2015 May;29(5):1133-42;

- Testa JR, Cheung M, Pei J, et al. Germline BAP1 mutations predispose to malignant mesothelioma. Nature genetics. 2011;43(10):1022-1025;
- The Cancer genome Atlas Network. Comprehensive molecular portraits of human breast tumor. Nature 2012;490:61-70;
- Thomson FH, Emerson J, Olson S, et al. Cytogeentics of 158 patients with regional or disseminated melanoma Subset analysis of near-diploid and simple karyotypes. Cancer Genet Cytogenet 1995 83:93-104;
- Trolet J, Hupé P, Huon I,et al. Genomic profiling and identification of high-risk uveal melanoma by array CGH analysis of primary tumors and liver metastases. Invest Ophthalmol Vis Sci. 2009 Jun;50(6):2572-80;

Tschentscher F, Hüsing J, Hölter T, Kruse E, Dresen IG, et al. Tumor classification based on gene expression profiling shows that uveal melanomas with and without monosomy 3 represent two distinct entities. Cancer Res. 2003 May 15;63(10):2578-84;

- Tschentscher F, Prescher G, Horsman DE, White VA, Rieder H,et al. Partial deletions of the long and short arm of chromosome 3 point to two tumor suppressor genes in uveal melanoma. Cancer Res. 2001 Apr 15;61(8): 3439-42.

- Tschentscher F, Prescher G, Zeschnigk M, et al. Identification of chromosomes 3, 6, and 8 aberrations in uveal melanoma by microsatellite analysis in comparison to comparative genomic hybridization. Cancer Genet Cytogenet 2000; 122(1): 13-17;
- Turunen JA, Markkinen S, Wilska R, et al. BAP1 Germline Mutations in Finnish Patients with Uveal Melanoma. Ophthalmology. 2016 May;123(5): 1112-7;
- Van Beek JG, Rooprnans AE, Vaarwater J, et al. The prognostic value of extraocular extension in relation to monosomy 3 and gain of chromosome 8q in uveal melanoma. Invest Ophtalmol Vis Sci 2014; 55:1284-91;
- van de Nes JA, Nelles J, Kreis S, et al. Comparing the Prognostic Value of BAP1 Mutation Pattern, Chromosome 3 Status, and BAP1 Immunohistochemistry in Uveal Melanoma. Am J Surg Pathol. 2016 Jun;40(6): 796-805;
- van den Bosh T, Van Beek JG, Vaarwater J, et al. Higher percentage of FISH-determined monosomy 3 and 8q amplification in uveal melanoma cells relate to poor patient prognosis. Invest Ophtalmol Vis Sci 2012; 53:2668-74;
- van Essen TH, van Pelt SI, Versluis M, et al. Prognostic parameters in uveal melanoma and their association with BAP1 expression. Br J Ophthalmol. 2014 Dec;98(12):1738-43;
- van Raamsdonk CD, Bezrookove V, Green G, Bauer J, Gaugler L, et al. Frequent somatic mutations of GNAQ in uveal melanoma and blue naevi. Nature. 2009 Jan 29;457(7229):599-602;
- Van Gils W, Lodder EM, Mensink HW, Kiliç E, Naus NC, et al. Gene expression profiling in uveal melanoma: two regions on 3p related to prognosis. Invest Ophthalmol Vis Sci. 2008 Oct;49(10):4254-62;
- Ventii KH, Devi NS, Friedrich KL, et al. BRCA1-associated protein-1 is a tumor suppressor that requires deubiquitinating activity and nuclear localization. Cancer Res. 2008 Sept 1;68(17):6953-62;
- Versluis M, de Lange MJ, van Pelt SI et al. Digital PCR validates 8q dosage as prognostic tool in uveal melanoma. PLoS One. 2015 Mar 12;10(3):e0116371
- Virgili G, Gatta G, Ciccolallo L, et al, EUROCARE Working Group. Incidence of uveal melanoma in Europe. Ophthalmology. 2007 Dec;114(12):2309-15;

- Vit VV. Prognostic role of morphologic characteristics of the immune response in human melanomas of various cellular types. Arkh Pathol 1983;45:25-30;
- Wang F, Flanagan J, Su N, et al. RNAscope: A Novel In Situ RNA Analysis Platform for Formalin-fixed Paraffin-embedded Tissues.J of Mol Diagnostics 2012; 14(1):22-29;
- Wang L, Lawrence MS, Wan Y, et al. SF3B1 and other novel cancer genes in chronic lymphocytic leukemia. N Engl J Med 2011 Dec 29;365(26):2497-506;
- Weis E, Shah CP, Lajous M, et al. The association between host susceptibility factors and uveal melanoma: a meta-analysis. Arch Ophthalmol.2006 Jan; 124(1):54-60;
- White VA, Chambers JD, Courtright PD et al. Correlation of cytogenetic abnormalities with the outcome of patients with uveal melanoma. Cancer. 1998 Jul 15;83(2):354-9;
- Wiesner T, Murali R, Fried I, et al. distinct subset of atypical Spitz tumors is characterized by BRAF mutation and loss of BAP1 expression. Am J Surg Pathol. 2012 Jun;36(6):818-30;
- Wiesner T, Obenauf AC, Murali R, et al. Germline mutations in BAP1 predispose to melanocytic tumors. Nat Genet. 2011 Aug 28;43(10):1018-21;
- Xu X, Wei WB, Li B, Gao F, et al. Oncogenic and GNA11 mutations in uveal melanoma in Chinese. PloS One. 2014 Oct 3; 9(10):e109699.
- Yavuzyigitoglu S, Drabarek W, Smit KN et al. Rotterdam Ocular Melanoma Study Group. Correlation of Gene Mutation Status with Copy Number Profile in Uveal Melanoma. Ophthalmology. 2017 Apr;124(4):573-575;
- Yavuzyigitoglu S, Koopmans AE, Verdijk RM, et al. Rotterdam Ocular Melanoma Study Group. Uveal Melanomas with SF3B1 Mutations: A Distinct Subclass Associated with Late-Onset Metastases. Ophthalmology. 2016 May; 123(5):1118-28;
- Yonekawa Y, Kim IK, Gragoudas ES, et al. Aggressive skull base metastasis from uveal melanoma: a clinicpathologic study.Eur J Ophthalmol. 2014 Sep-Oct;24(5):811-3;
- Yoshida K, Sanada M, Shiraishi Y, et al. Frequent pathway mutations of splicing machinery in myelodysplasia. Nature. 2011 Sep 11;478(7367):64-9;
- Yoshikawa Y, Emi M, Hashimoto-Tamaoki T et al. High-density array-CGH with targeted NGS unmask multiple noncontiguous minute deletions on

chromosome 3p21 in mesothelioma. Proc Natl Acad Sci U S A. 2016 Nov 22;113(47):13432-13437;

- Yu FX, Luo J, Mo JS, et al. Mutant Gq/11promote uveal melanoma tumorigenesis by activating YAP. Cancer Cell. 2014;
- Zaidi MR, Ksander BR, Merlino G, et al. Hippo-independent activation of YAP by the GNAQ uveal melanoma oncogene through a trio-regulated rho GTPase signaling circuitry. Cancer Cell. 2014 Jun 16;25(6):831-45;
- Zhang Y, Moschetta M, Huynh D, et al. Pyk2 promotes tumor progression in multiple myeloma. Blood. 2014 Oct 23;
- Zloto O, Pe'er J, Frenkel S. Gender differences in clinical presentation and prognosis of uveal melanoma. Invest Ophthalmol Vis Sci. 2013 Jan 23;54(1): 652-6.